SINTEF

TR A7474- Unrestricted

Report

A Linear State-Space Model of an Offshore Wind Turbine, Implemented in the STAS Wind Power Plant Analysis Program

Author(s)
Karl O. Merz

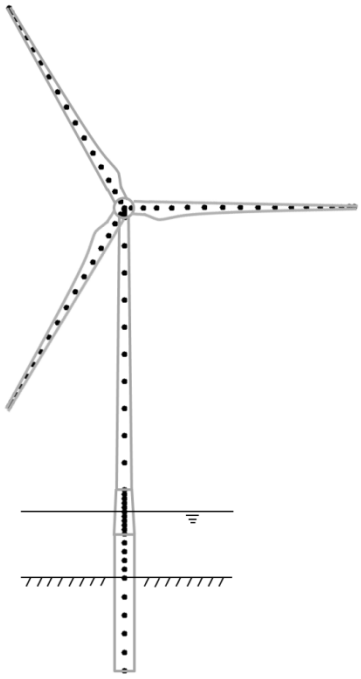

SINTEF Energy Research
Power Conversion and Transmission
2015-03-17

SINTEF Energi AS
SINTEF Energy Research
Address:
Sem Sælands vei 11
7034 Trondheim
NORWAY
Telephone:+47 73597200

energy.research@sintef.no
www.sintef.no/energi
Enterprise /VAT No:
NO 939 350 675 MVA

KEYWORDS:
wind turbine
wind farm
wind power plant
state space
offshore
aerodynamics
structures

Report

A Linear State-Space Model of an Offshore Wind Turbine, Implemented in the STAS Wind Power Plant Analysis Program

VERSION
1.0

DATE
2015-03-17

AUTHOR(S)
Karl O. Merz

CLIENT(S)
NOWITECH

CLIENT'S REF.
DC.2-2

PROJECT NO.
502000059-10

NUMBER OF PAGES/APPENDICES:
68 + Appendices

ABSTRACT

A set of Matlab/Octave scripts have been developed, which output state matrices describing the linearized aeroelastic dynamics of an offshore wind turbine. The aerodynamic model is based on momentum balance, and includes time-lag models for dynamic inflow, circulation lag, and dynamic stall. The structural model is a multibody formulation, with modal reduction applied to the foundation/tower, nacelle, driveshaft, and each of three blades. At present the model is set up for a monopile foundation, although the methods are also applicable to other types of foundations. The seabed properties are represented by springs and dampers distributed along the foundation. Hydrodynamic added mass is included. The model has been verified by comparison of natural frequencies, damping ratios, and transfer functions against results obtained using other programs.

PREPARED BY
Karl O. Merz

SIGNATURE

CHECKED BY
Harald G. Svendsen

SIGNATURE

APPROVED BY
Knut Samdal

SIGNATURE

REPORT NO.	ISBN	CLASSIFICATION	CLASSIFICATION THIS PAGE
TR A7474	978-82-594-3618-4	Unrestricted	Unrestricted

Document history

VERSION	DATE	VERSION DESCRIPTION
1.0	2015-03-17	Original document

SINTEF

Table of contents

1 Introduction

STAS (State Space Analysis of Offshore Wind Power Plants) is a program for the analysis of offshore wind power plants as a unified, linear state space. The program consists of modules which generate portions of the state space, which are then linked (using Equation 1.4) to form the assembled model. This report describes the module which generates state matrices describing the aeroelastic dynamics of the individual wind turbines in the plant. Although the resulting state matrices are intended for use as part of the STAS program, they can also be used independently, for aeroelastic stability, control design, or preliminary estimates of design loads.

The model is representative of the state-of the art in wind turbine analysis. The blade-element momentum method is used for the aerodynamics, and the structures are represented by finite element beams. The equations are linearized about a steady-state operating point, which is specified as input. The module outputs the state matrices describing fluctuations about the operating point. As these fluctuations are modelled as linear, the model is not valid far from the steady-state operating point. In general, it can be expected that the linearized model will provide reasonable estimates of the stochastic response of the wind turbine to normal levels of turbulence $(\sigma_u / u \approx 0.1)$, but not extreme loads.

Creation of a linear state-space model is motivated by three things. First, such linear models are useful in control system design. It is typical to use highly simplified models when designing and tuning a control system. However, if one proposes to use additional sensors, like strain gauges or accelerometers, as control inputs, then it is important to have a good model for the data obtained from these sensors. Even high-frequency dynamics can impact the relative phase between the excitation and control response, which is important for active damping, so it is useful to have a full linear model of the wind turbine. Such a model may also be useful in optimal control algorithms.

The second reason to use a linear model is the speed of frequency-domain calculations. For a stochastic estimate of lifetime loads, a calculation in the frequency domain is orders of magnitude faster than a corresponding calculation in the time domain.

The third reason is that frequency-domain estimates of stochastic loads do not involve random numbers. They are perfectly repeatable functions of the design parameters, and can be made numerically smooth, for use in gradient-based optimization algorithms.

1.1 A Linear State-Space Model of a Wind Turbine

A linear state-space model can be written in the standard form:

$$\begin{aligned} \frac{d\mathbf{x}}{dt} &= \mathbf{A}\mathbf{x} + \mathbf{B}\mathbf{u} \\ \mathbf{y} &= \mathbf{C}\mathbf{x} + \mathbf{D}\mathbf{u}, \end{aligned} \tag{1.1}$$

where **x** is a vector of system states, **u** is a vector of inputs, and **y** is a vector of outputs. It is evident from the expression $\mathbf{y} = \mathbf{C}\mathbf{x} + \mathbf{D}\mathbf{u}$ that the outputs can be chosen as any system variable that can be written as a (linearizable) function of states and inputs.

In the present model of a wind turbine it is convenient to work with a different form of the state equations:

$$\begin{aligned} \mathbf{L}\frac{d\mathbf{x}}{dt} &= \mathbf{A}\mathbf{x} + \mathbf{B}\mathbf{u} \\ \mathbf{y} &= \mathbf{C}\mathbf{x} + \mathbf{D}\mathbf{u}, \end{aligned} \tag{1.2}$$

where we now permit a square matrix multiplying the time derivative of the state vector. The systems (1.1) and (1.2) are equivalent, and the matrix **L** can be inverted to recover (1.1). Computationally, however, this is undesireable, as **L** is a sparse matrix, while its inverse may be full.

1.2 A Linear State-Space Model as a Collection of Linked Modules

It is not convenient to write the state equations for the system directly in the form of Equation 1.2. It is much preferable to isolate parts of the calculation, and write their behavior in the standard form using local, rather than global, inputs and outputs.

Let the system be represented as a collection of linked modules, each of which has a local state-space representation, with local inputs, outputs, and states. Let every link between two modules be an element of the global output vector **y**. Now, isolating each module in turn, it is possible to write:

$$\begin{aligned} \mathbf{L}\frac{d\mathbf{x}}{dt} &= \tilde{\mathbf{A}}\mathbf{x} + \mathbf{B}_u\mathbf{u} + \mathbf{B}_y\mathbf{y} \\ \mathbf{y} &= \tilde{\mathbf{C}}\mathbf{x} + \mathbf{D}_u\mathbf{u} + \mathbf{D}_y\mathbf{y}\,. \end{aligned} \tag{1.3}$$

Here **u** still represents the vector of global inputs. The **y** on the left-hand side of the equation $\mathbf{y} = \tilde{\mathbf{C}}\mathbf{x} + \mathbf{D}_u\mathbf{u} + \mathbf{D}_y\mathbf{y}$ contains the rows of equations associated with the local outputs from the module. The **y**'s on the right-hand side, $\mathbf{B}_y\mathbf{y}$ and $\mathbf{D}_y\mathbf{y}$, contain entries associated with local inputs. Each local input is, by definition, a local output from one of the other modules. Note that the diagonals of $\mathbf{D}_y$ are zero. An appropriately constructed block diagram, in the present context, will not have the output of a module fed directly back to the input of the same module.

The rows of state and output equations for all the modules are collected into a global state-space, still in the form of Equation 1.2. This can then be manipulated to eliminate **y** from the right-hand side:

$$\begin{aligned} \mathbf{L}\frac{d\mathbf{x}}{dt} &= [\tilde{\mathbf{A}} + \mathbf{B}_y(\mathbf{I} - \mathbf{D}_y)^{-1}\tilde{\mathbf{C}}]\mathbf{x} + [\mathbf{B}_u + \mathbf{B}_y(\mathbf{I} - \mathbf{D}_y)^{-1}\mathbf{D}_u]\mathbf{u} \\ \mathbf{y} &= (\mathbf{I} - \mathbf{D}_y)^{-1}\tilde{\mathbf{C}}\mathbf{x} + (\mathbf{I} - \mathbf{D}_y)^{-1}\mathbf{D}_u\mathbf{u}\,. \end{aligned} \tag{1.4}$$

Equation 1.4 is now in the linear state-space form of Equation 1.2. All links between modules are accounted for by a series of automated matrix operations.

The procedure for generating a global, linear, state-space representation is thus as follows. The system is broken into modules, each of which represents a given operation or physical process. For each module, governing equations, which may be nonlinear, are derived in state-space form. Using perturbation theory, the first-order terms are collected, and higher-order terms discarded. Discriminating between global and local inputs, the linear equations are written in the form of Equation 1.3; this is manipulated into standard form, as shown in Equation 1.4.

1.3 Linear Analysis of Wind Turbines

Simplified, linear models of wind turbines are frequently employed in the analysis of control systems and electrical systems. For instance, for electrical system studies, Ellis *et al*. [9] recommend a two-mass model – one rotational inertia for the rotor and one for the generator – described by a linear differential equation. Leithead and Connor [19] describe a linear model for use in control system design.

More advanced linearized models are used to analyze the aeroelastic frequency, damping, and stability properties of wind turbines. Sørensen *et al*. ([28],[29]) describe a frequency-domain method which is in many respects identical to the present one, although the derivation is based on transfer functions. The structural model and the aerodynamics are simplified with respect to the present program. The methods described by Hansen ([10],[11]), and developed into the HAWCStab2 program, extend the work of Sørensen to include a more advanced representation of the aerodynamics. In addition, aeroelastic analysis software such as Bladed and FAST provide the ability to linearize the model about a chosen operating point, giving azimuth-dependent state matrices.

There is a history of using linear methods to estimate design loads. This is one of the stated purposes of Sørensen's method [28]. Burton *et al*. [5] provide a method for the estimation of the stochastic response of a wind turbine blade, based on a linearized aerodynamic and structural model. The TURBU Offshore software, as described by van Engelen and Braam [30], employs frequency-domain analysis, and is intended for rapid design load estimation. For some stochastic load cases, frequency-domain methods may provide reasonable estimates of extreme loads. Merz ([20],[21]) describes methods for extreme load prediction, and comparisons against nonlinear simulations.

The present model is similar to that implemented in the HAWCStab2 and TURBU programs, and is expected to give similar results, as demonstrated in Section 5.2.2. The model has been developed in Matlab/Octave, as part of the STAS wind power plant analysis program, for ease of integration with existing electrical system models.

1.4 Notation and Coordinate Systems

Vectors and matrices are denoted with a bold font, for instance the state vector **x** and matrix **A**. When a vector or matrix has a certain coordinate system as a basis, then this is indicated by the use of a superscript. It may be important to keep track of two coordinate systems, one the basis in which the components of a vector are expressed, and another relative to which the vector is measured. In this case the basis is indicated by a superscript, and the relative is indicated by a slash in the subscript. Thus the position of a node **r** – that is, the length of the vector – might be measured relative to the global coordinate system, but the components expressed in a local body coordinate system; this would be written as $\mathbf{r}_{/g}^{B}$.

Subscripts are frequently used in other contexts as well. When a spatial vector has a subscript, for instance the induced velocity $\mathbf{V}_i$, then one of the spatial components is indicated by an additional subscript outside a parentheses; so the Z^r component of the induced velocity, a scalar, would be written $(\mathbf{V}_i^r)_Z$. Subscripts never denote derivatives.

The structural and aerodynamic analyses employ a variety of coordinate systems. Most of these are sketched in Figure 1. For clarity, the following description is given as if the structure were rigid. The formulation of structural displacements in Section 3 allows for small elastic rotations which may incrementally misalign the various coordinate systems.

The global coordinate system is located at the base of the tower, or equivalently the top of the transition piece. The X^g axis is parallel with the undisturbed ocean surface and indicates the direction of zero yaw angle; at zero yaw, the X^g axis points downwind. The Z^g axis is normal to the undisturbed ocean surface and typically passes through the center of the undeformed tower.

The yaw coordinate system indicates the position of the yaw bearing. At zero yaw it is aligned with the global coordinate system. Positive yaw angle involves a rotation about the $Z^y = Z^g$ axis.

The nacelle coordinate system is aligned with the axis of rotation of the driveshaft. The Z^n axis points in the direction of the X^y axis, except that it is rotated about the Y^y axis by the driveshaft tilt angle δ: positive tilt angle raises the rotor hub. Note that the *yaw* coordinate system is the reference coordinate system for the nacelle structure. The "nacelle" coordinate system serves as an intermediate frame against which driveshaft rotation is measured.

Thus, the driveshaft coordinate system is rotated, with respect to the nacelle coordinate system, by the azimuth angle ψ about the $Z^d = Z^n$ axis.

The rotorplane coordinate system is used in the aerodynamic analysis. It is aligned with the nacelle coordinate system, but has its origin at the center of the rotor hub. Quantities expressed in rotorplane coordinates have in general an "axial" component, in the Z^r direction, and a "tangential" component, which is tangent to a particular radius, for instance

$$(\mathbf{V}_i^r)_t := -(\mathbf{V}_i^r)_X \sin\psi_b + (\mathbf{V}_i^r)_Y \cos\psi_b . \qquad (1.5)$$

This decomposition of the coordinates is convenient, because the spanwise component of relative velocity is neglected when computing aerodynamic forces.

The remaining coordinate systems occur in triplets, one associated with each blade. The hub coordinate systems is not shown in Figure 1. Its origin is the same as the rotorplane coordinate system, at the center of the rotor hub, and the X^h axis points from the axis of rotation to the pitch bearing. The hub coordinate system is aligned with the driveshaft coordinate system for Blade 1, and is rotated about the $Z^h = Z^d$ axis by the blade offset angle of $2\pi/3$ for Blade 2 and $4\pi/3$ for Blade 3.

The blade coordinate system is located at the pitch bearing. It is rotated, with respect to the hub coordinate systesm, about the $Y^h = Y^b$ axis by the blade cone angle ϕ. (The blade cone angle is not shown in Figure 1.)

The blade pitch coordinate system is offset from the hub coordinates system by rotation about the $X^b = X^p$ axis by the *negative* of the pitch angle. The negative sign is required such that, by convention, positive pitch rotates the leading edge of the blades into the wind.

There are additional coordinate systems associated with each blade element in the aerodynamic analysis. These are shown in Figure 2. The section coordinate system is offset from the pitch coordinate system by rotation about the $X^p = X^s$ axis by the *negative* of the blade aerodynamic twist angle. The airfoil coordinate system is the traditional one used to represent lift and drag, or normal and chordwise, forces. The origin is one quarter-chord aft from the leading edge, and the X^a axis lies along the chordline.

Structural finite elements also have an associated section coordinate system. This is described in Section 3.

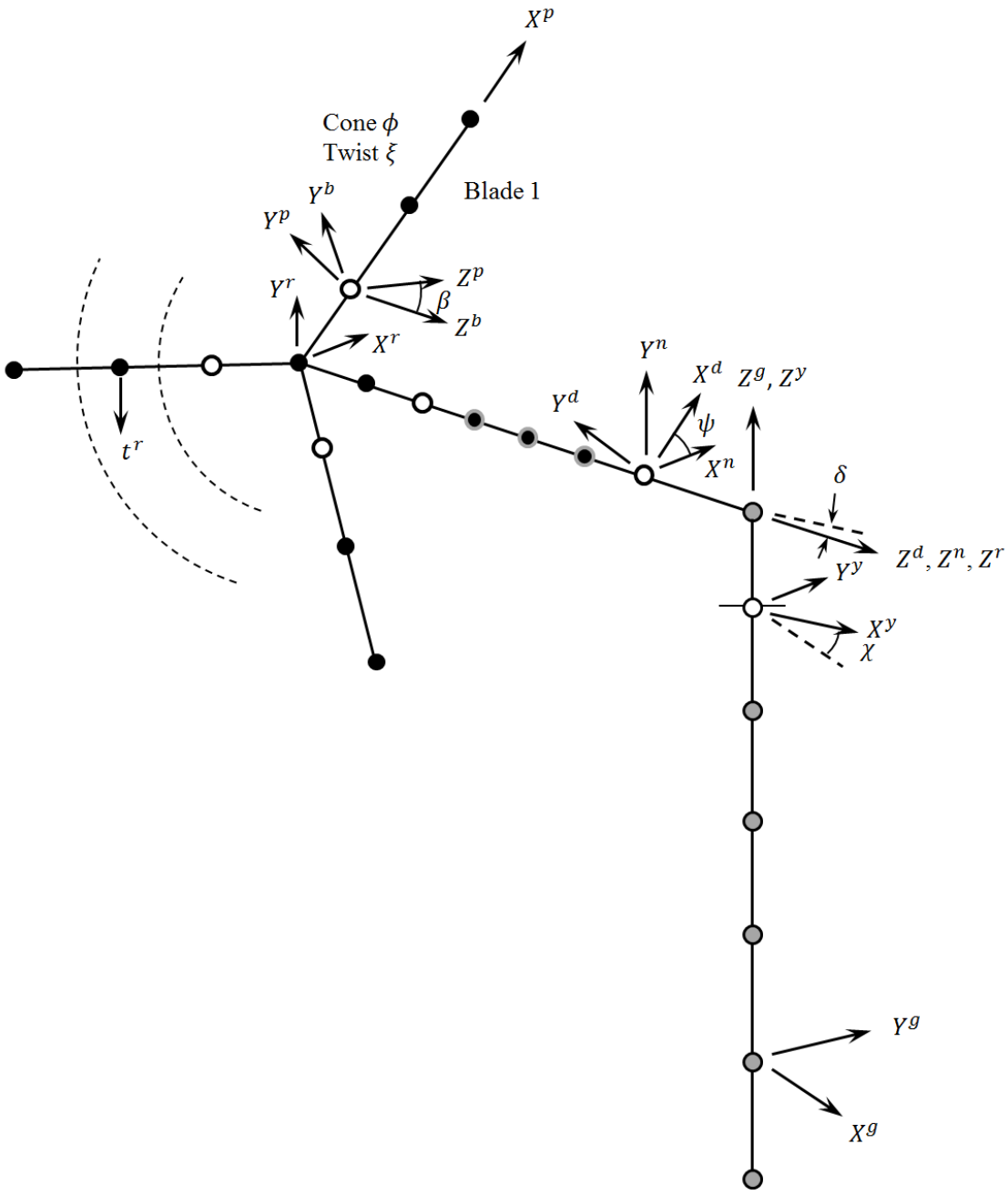

Figure 1: Important coordinate systems and angles used in the wind turbine model. The wind turbine structures are represented by beam finite elements. Rotating nodes are shown by black dots, and fixed nodes by gray dots. White dots show joints. All joints restrain 5 degrees-of-freedom, allowing one rotational degree-of-freedom, with the exception of the front driveshaft bearing, which restrains only X^n and Y^n displacements.

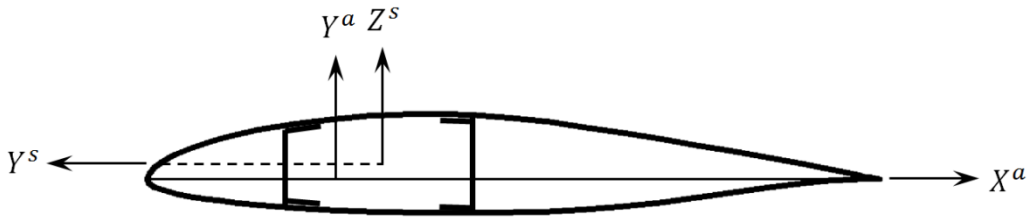

Figure 2: Coordinate systems associated with each airfoil section. The aerodynamic coordinate system passes through a point 0.25*c* aft of the leading edge, where *c* is the chord length. The section coordinate system passes through the blade pitch axis.

1.5 Maps of the State and Output Vectors

Table I lists the state, input, and output vectors, along with the dimension of each set of variables. The states include the position and velocity of the structure, transformed into mode shape amplitudes; intermediate variables associated with dynamic inflow; the induced velocity; the effective angle-of-attack, including the effects of circulation lag and dynamic stall; and intermediate variables associated with circulation lag. Inputs are axial and tangential components of turbulence at each blade element, and a vector of nodal forces. Outputs are the position and velocity of the structural degrees-of-freedom, in body coordinates; the velocity of the structural nodes relative to the global coordinate system; the velocity of the blade nodes, relative to the global coordinate system, and expressed in terms of rotorplane coordinates; the quasi-steady induced velocity; the quasi-steady angle-of-attack; the effective angle-of-attack including circulation lag; lift and drag coefficients; lift and drag forces; aerodynamic forces expressed in rotorplane coordinates, section coordinates, and blade pitch coordinates; and finally aerodynamic nodal forces. N_{DOF} is the number of structural degrees-of-freedom of the unconstrained bodies, N_{rDOF} is the number of reduced modal degrees-of-freedom including constraints, N_b is the number of blades (always 3 in the present implementation of the code), N_{eb} is the number of aerodynamic elements per blade

Table I: A list of states, inputs, and outputs

States		Inputs		Outputs	
$\Delta\hat{\mathbf{q}}^B$	N_{rDOF}	(u_z, u_t)	$2N_bN_{eb}$	$\Delta\mathbf{q}^B$	N_{DOF}
$d\Delta\hat{\mathbf{q}}^B/dt$	N_{rDOF}	$\Delta\mathbf{F}^B$	N_{DOF}	$\Delta\mathbf{q}^B/dt$	N_{DOF}
(s_z, s_t)	$2N_bN_{eb}$			$d\Delta\mathbf{x}^g_{/g}/dt$	N_{DOF}
$\mathbf{v}_i^r$	$2N_bN_{eb}$			$d\mathbf{w}^r_{/g}/dt$	$2N_bN_{eb}$
α	N_bN_{eb}			$\mathbf{v}_{iq}^r$	$2N_bN_{eb}$
(a_1, a_2)	$2N_bN_{eb}$			α_q	N_bN_{eb}
				α_T	N_bN_{eb}
				(c_L, c_D)	$2N_bN_{eb}$
				(f_L, f_D)	$2N_bN_{eb}$
				$\mathbf{f}_a^r$	$2N_bN_{eb}$
				$\mathbf{f}_a^s$	$6N_bN_{eb}$
				$\mathbf{f}_a^p$	$6N_bN_{eb}$
				$\Delta\mathbf{F}^B$	N_{DOF}

2 Aerodynamics

The aerodynamic model is based upon the blade-element momentum method. The model includes Prandtl's tip loss function, dynamic inflow, circulation lag, and dynamic stall.

The modules can be organized as follows. Momentum balance and dynamic inflow are used to compute induced velocities $\mathbf{v}_i^r$. The induced velocities are used in the calculation of the instantaneous angle-of-attack α_q on each airfoil. The change in circulation (lift) of the airfoil is modelled as a time-lag on the instantaneous angle-of-attack, and dynamic stall is a time-lag on the circulation, resulting in modified lift and drag coefficients c_L and c_D. The lift and drag forces f_L and f_D follow from the coefficients, together with the local velocity magnitude. Coordinate transforms convert lift and drag forces into rotor coordinates ($\mathbf{f}_a^r$, needed for momentum balance) and pitch coordinates ($\mathbf{f}_a^p$, needed for the structural model).

2.1 Momentum Balance

Momentum balance is used to determine the induced velocities at the rotor plane. The momentum balance equation is

$$\mathbf{F}_a^r = -2\rho A f \left|\mathbf{V}_0^r + f\mathbf{n}\left(\mathbf{n}\cdot\mathbf{V}_i^r\right)\right|\mathbf{V}_i^r, \tag{2.1}$$

where $\mathbf{F}_a^r$ is the normal (axial) and in-plane (tangential) force on the blade element, $\mathbf{V}_0^r$ is the wind velocity vector at the location of the airfoil, $\mathbf{V}_i^r$ is the induced velocity vector, $\mathbf{n}$ is the normal to the rotorplane, f is Prandtl's tip-loss function, A is the portion of the rotor swept area associated with the blade element, and ρ is the air density. In terms of perturbed and steady-state variables, and including a *q* subscript to indicate that here the induced velocity is the quasi-steady (as opposed to dynamic inflow) value,

$$\left(\mathbf{V}_{iq0}^r + \mathbf{v}_{iq}^r\right)\sqrt{\left\{V_\infty + u_z + f\left[(\mathbf{V}_{iq0}^r)_Z + (\mathbf{v}_{iq}^r)_Z\right]\right\}^2 + u_t^2} = -\frac{1}{2\rho A f}\left(\mathbf{F}_{a0}^r + \mathbf{f}_a^r\right). \tag{2.2}$$

Here $\mathbf{v}_{iq}^r$ is a local output and u_z, u_t, and $\mathbf{f}_a^r$ are local inputs. Globally, $\mathbf{v}_{iq}^r$ and $\mathbf{f}_a^r$ are intermediate variables, part of the vector **y**, while u_z and u_t are global inputs, part of the vector **u**. Linearizing Equation 2.2 gives

$$(\mathbf{v}_{iq}^r)_Z = -\frac{(\mathbf{V}_{iq0}^r)_Z}{V_\infty + 2f(\mathbf{V}_{iq0}^r)_Z}u_z - \frac{1}{2\rho A f\left[V_\infty + 2f(\mathbf{V}_{iq0}^r)_Z\right]}(\mathbf{f}_a^r)_Z \tag{2.3}$$

$$\begin{aligned}(\mathbf{v}_{iq}^r)_t = {} & \frac{(\mathbf{V}_{iq0}^r)_t}{V_\infty + f(\mathbf{V}_{iq0}^r)_Z}\left[\frac{f(\mathbf{V}_{iq0}^r)_Z}{V_\infty + 2f(\mathbf{V}_{iq0}^r)_Z} - 1\right]u_z \\ & + \frac{f(\mathbf{V}_{iq0}^r)_t}{2\rho A f\left[V_\infty + 2f(\mathbf{V}_{iq0}^r)_Z\right]\left[V_\infty + f(\mathbf{V}_{iq0}^r)_Z\right]}(\mathbf{f}_a^r)_Z \\ & - \frac{1}{2\rho A f\left[V_\infty + f(\mathbf{V}_{iq0}^r)_Z\right]}(\mathbf{f}_a^r)_t.\end{aligned} \tag{2.4}$$

This is consistent with the modular state space form $\mathbf{y} = \mathbf{D}_u\mathbf{u} + \mathbf{D}_y\mathbf{y}$. Note that the tip-loss function *f* is assumed to be constant.

2.2 Dynamic Inflow

Dynamic inflow is modelled by the time-lag function of Øye, as described by Hansen [14]. The equations are

$$\frac{d\hat{\mathbf{v}}_i^r}{dt} = -\frac{1}{\tau_1}\hat{\mathbf{v}}_i^r + \frac{1}{\tau_1}\mathbf{v}_{iq}^r + 0.6\frac{d\mathbf{v}_{iq}^r}{dt} \tag{2.5}$$

$$\frac{d\mathbf{v}_i^r}{dt} = -\frac{1}{\tau_2}\mathbf{v}_i^r + \frac{1}{\tau_2}\hat{\mathbf{v}}_i^r. \tag{2.6}$$

This form of the equations is not ideal because $d\mathbf{v}_{iq}^r/dt$ is directly proportional to the global input u_z. This would lead to imaginary terms, proportional to $i\omega$, in the $\mathbf{B}_y$ matrix, which would complicate calculation of transfer functions. We introduce a variable

$$\mathbf{s} = \hat{\mathbf{v}}_i^r - 0.6\mathbf{v}_{iq}^r; \tag{2.7}$$

then Equations 2.5 and 2.6 can be written

$$\frac{d\mathbf{s}}{dt} = -\frac{1}{\tau_1}\mathbf{s} + \frac{0.4}{\tau_1}\mathbf{v}_{iq}^r \tag{2.8}$$

and

$$\frac{d\mathbf{v}_i^r}{dt} = -\frac{1}{\tau_2}\mathbf{v}_i^r + \frac{1}{\tau_2}\mathbf{s} + \frac{0.6}{\tau_2}\mathbf{v}_{iq}^r . \tag{2.9}$$

These are linear differential equations, and fit directly into a state-space representation $d\mathbf{x}/dt = \tilde{\mathbf{A}}\mathbf{x} + \mathbf{B}_y\mathbf{y}$.

The time constants are computed as [14]

$$\tau_1 = \frac{1.1}{1-1.3a}\left(\frac{D}{2V_\infty}\right); \qquad a = \frac{\sqrt{(V_{i0}^r)_Z^2 + (V_{i0}^r)_t^2}}{V_\infty} \tag{2.10}$$

and

$$\tau_2 = \left[0.39 - 0.26\left(\frac{2r}{D}\right)^2\right]\tau_1 . \tag{2.11}$$

The time constants are evaluated at the steady-state values, and are not updated with fluctuations in the induction factor *a*.

2.3 Instantaneous Angle-of-Attack

The instantaneous angle-of-attack can be determined from the state of flow local to the rotorplane.[1] It is most convenient to work in rotorplane coordinates. Figure 3 shows the cross-section of a blade, together with the flow components that form the local velocity vector **V**.

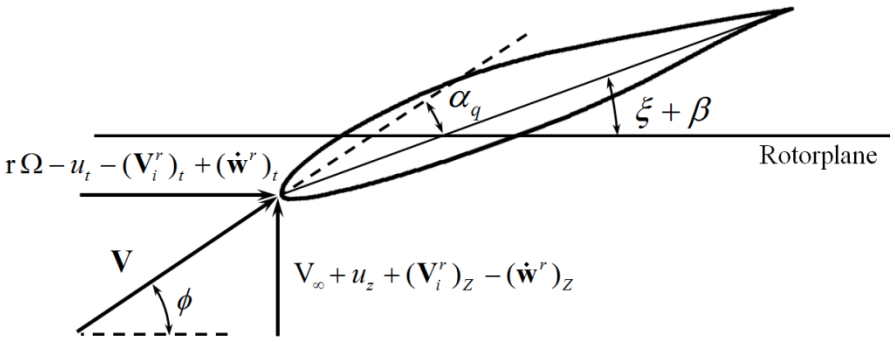

Figure 3: Velocity triangle of local flow at the airfoil

From the velocity triangle in Figure 3, it follows that

$$\tan\left(\alpha_{q0} + \alpha_q + \beta_0 + \beta + \xi_0 - (\boldsymbol{\theta}^s)_X\right) = \frac{V_\infty + u_z + (\mathbf{V}_{i0}^r)_Z + (\mathbf{v}_i^r)_Z - (\dot{\mathbf{w}}^r)_Z}{r\Omega_0 + r\Omega - u_t - (\mathbf{V}_{i0}^r)_t - (\mathbf{v}_i^r)_t + (\dot{\mathbf{w}}^r)_t}, \tag{2.12}$$

such that

$$\alpha_q = -\alpha_{q0} - \beta_0 - \beta - \xi_0 + (\boldsymbol{\theta}^s)_X + \tan^{-1}\left(\frac{V_\infty + u_z + (\mathbf{V}_{i0}^r)_Z + (\mathbf{v}_i^r)_Z - (\dot{\mathbf{w}}^r)_Z}{r\Omega_0 + r\Omega - u_t - (\mathbf{V}_{i0}^r)_t - (\mathbf{v}_i^r)_t + (\dot{\mathbf{w}}^r)_t}\right). \tag{2.13}$$

The $\tan^{-1}$ function is linearized as

[1] The instantaneous angle-of-attack is also referred to as the quasi-steady angle-of-attack, hence the "*q*" subscript. The "quasi-steady" aspect does not refer to the incoming flow, which is variable, but rather the dynamic stall analysis of Section 2.4.

$$g_0 + \left.\frac{dg}{d(\mathbf{v}_i^r)_Z}\right|_0 (\mathbf{v}_i^r)_Z + \left.\frac{dg}{d(\mathbf{v}_i^r)_t}\right|_0 (\mathbf{v}_i^r)_t + \left.\frac{dg}{d(\dot{\mathbf{w}}^r)_z}\right|_0 (\dot{\mathbf{w}}^r)_z + \left.\frac{dg}{d(\dot{\mathbf{w}}^r)_t}\right|_0 (\dot{\mathbf{w}}^r)_t + \left.\frac{dg}{d\Omega}\right|_0 \Omega + \left.\frac{dg}{du_z}\right|_0 u_z + \left.\frac{dg}{du_t}\right|_0 u_t, \tag{2.14}$$

with

$$g_0 = \tan^{-1}\frac{V_\infty + (\mathbf{V}_{i0}^r)_Z}{r\Omega_0 - (\mathbf{V}_{i0}^r)_t}, \tag{2.15}$$

$$\left.\frac{dg}{d(\mathbf{v}_i^r)_Z}\right|_0 = \left.\frac{dg}{du_z}\right|_0 = \frac{r\Omega_0 - (\mathbf{V}_{i0}^r)_t}{[V_\infty + (\mathbf{V}_{i0}^r)_Z]^2 + [r\Omega_0 - (\mathbf{V}_{i0}^r)_t]^2}, \tag{2.16}$$

$$\left.\frac{dg}{d(\dot{\mathbf{w}}^r)_Z}\right|_0 = -\frac{r\Omega_0 - (\mathbf{V}_{i0}^r)_t}{[V_\infty + (\mathbf{V}_{i0}^r)_Z]^2 + [r\Omega_0 - (\mathbf{V}_{i0}^r)_t]^2}, \tag{2.17}$$

$$\left.\frac{dg}{d(\mathbf{v}_i^r)_t}\right|_0 = \left.\frac{dg}{du_t}\right|_0 = \frac{V_\infty + (\mathbf{V}_{i0}^r)_Z}{[V_\infty + (\mathbf{V}_{i0}^r)_Z]^2 + [r\Omega_0 - (\mathbf{V}_{i0}^r)_t]^2}, \tag{2.18}$$

$$\left.\frac{dg}{d(\dot{\mathbf{w}}^r)_t}\right|_0 = -\frac{V_\infty + (\mathbf{V}_{i0}^r)_Z}{[V_\infty + (\mathbf{V}_{i0}^r)_Z]^2 + [r\Omega_0 - (\mathbf{V}_{i0}^r)_t]^2}, \tag{2.19}$$

and

$$\left.\frac{dg}{d\Omega}\right|_0 = -r\frac{V_\infty + (\mathbf{V}_{i0}^r)_Z}{[V_\infty + (\mathbf{V}_{i0}^r)_Z]^2 + [r\Omega_0 - (\mathbf{V}_{i0}^r)_t]^2}. \tag{2.20}$$

This linearization puts Equation 2.13 in the form $\mathbf{y} = \mathbf{C}\mathbf{x} + \mathbf{D}_u\mathbf{u}$.

2.4 Circulation Lag and Dynamic Stall

When the flow conditions relative to an airfoil change dynamically, the response of the airfoil is not instantaneous. Rather, the response is subject to a time-lag with respect to the excitation. Sønderby and Hansen ([26],[27]) have demonstrated that if these transient effects are not modelled, then the response of the wind turbine to aerodynamic or blade pitch perturbations is nonetheless accurately predicted at low windspeeds. However, near the cutout windspeed, the computed response may be in error in a frequency band that, in the case of a large utility-scale wind turbine, are in the range of the second modes of vibration of the blades and support structure, and the free-free mode of the drivetrain.

The simplest engineering methods used to account for the unsteady aerodynamics are easy to implement, and so are included in the STAS program. The downside is that then the aerodynamic portion of the model accounts for the majority of states; the sizes of the system matrices are increased. Sønderby [26] has developed modal decomposition techniques to reduce the number of aerodynamic states, without a loss in accuracy. Such methods are not yet implemented here, but would be desirable.

The unsteady aerodynamic models account for circulation lag, the time it takes to convect shed vorticity away from the airfoil; and dynamic stall, the time needed for the point of flow

separation, along the low-pressure surface of a stalled airfoil, to change position. Circulation lag is present and most pronounced under attached-flow conditions, while dynamic stall is active only under stalled flow conditions.

Circulation lag is modelled by the method suggested by Leishman [18], also adopted by Hansen *et al*. [12]. For each airfoil, a state-space is defined, with input being the quasi-steady angle-of-attack α_q, and output the "Theodorsen" angle-of-attack α_T.

$$\frac{d}{dt}\begin{bmatrix} a_1 \\ a_2 \end{bmatrix} = \begin{bmatrix} 0 & 1 \\ -b_1 b_2 \left(\frac{2V}{c}\right)^2 & -(b_1+b_2)\left(\frac{2V}{c}\right) \end{bmatrix}\begin{bmatrix} a_1 \\ a_2 \end{bmatrix} + \begin{bmatrix} 0 \\ 1 \end{bmatrix}\alpha_q \tag{2.21}$$

$$\alpha_T = \begin{bmatrix} (A_1+A_2)b_1 b_2 \left(\frac{2V}{c}\right)^2 & (A_1 b_1 + A_2 b_2)\left(\frac{2V}{c}\right) \end{bmatrix}\begin{bmatrix} a_1 \\ a_2 \end{bmatrix} + (1-A_1-A_2)\alpha_q \tag{2.22}$$

Constant parameters are

$$A_1 = 0.165,\ A_2 = 0.335,\ b_1 = 0.0455, \text{ and } b_2 = 0.3.$$

For dynamic stall, the linear model of Merz [20] is used. This has the same mathematical form as the model of Øye [22], when the latter is linearized. Dynamic stall is represented as a first-order time-lag on the effective angle-of-attack,

$$\frac{d\alpha}{dt} = -\frac{1}{\tau}\alpha + \frac{1}{\tau}\alpha_q. \tag{2.23}$$

A value of $\tau = 4.3c/V$ is recommended, based upon comparisons with measurements on various airfoils [20]. The lift force then responds as

$$c_L = (\gamma_q - \gamma_{\max})|_0\ \alpha + \gamma_{\max}\alpha_q, \tag{2.24}$$

where

$$\gamma_{\max} = \max\{\, C_{L0}/(\alpha_0 - \alpha_z), |\gamma_q| \,\}. \tag{2.25}$$

Equations 2.21 and 2.22 are of the forms $d\mathbf{x}/dt = \mathbf{A}\mathbf{x} + \mathbf{B}_y\mathbf{y}$ and $\mathbf{y} = \mathbf{C}\mathbf{x} + \mathbf{D}_y\mathbf{y}$, respectively.

Dynamic stall has a minimal effect on the drag coefficient; this is therefore given its instantaneous value

$$c_D = \left.\frac{dC_D}{d\alpha_q}\right|_0 \alpha_q. \tag{2.26}$$

The moment coefficient is neglected, as its value is small and nearly constant over the expected range of angles-of-attack for a pitch-regulated wind turbine. From the perspective of the structure, torsional moments are assumed to be dominated by the offset between the lift force, at approximately $c/4$ from the leading edge (for zero moment coefficient), and the structural centroid.

2.5 Lift and Drag Forces

Lift and drag forces follow from the respective coefficients, as

$$\mathrm{F}_{L0} + f_L = (C_{L0} + c_L)\frac{1}{2}\rho c L|\mathbf{V}|^2 \tag{2.27}$$

and

$$\mathrm{F}_{D0} + f_D = \left(C_{D0} + c_D\right)\frac{1}{2}\rho c L\left|\mathbf{V}\right|^2, \tag{2.28}$$

with

$$\left|\mathbf{V}\right|^2 = \left[V_\infty + u_z + (\mathbf{V}_i^r)_Z - (\dot{\mathbf{w}}^r)_Z\right]^2 + \left[r(\Omega_0 + \Omega) - u_t - (\mathbf{V}_i^r)_t + (\dot{\mathbf{w}}^r)_t\right]^2. \tag{2.29}$$

The right-hand side of Equation 2.29 is linearized as

$$\begin{aligned} & g_0 + \left.\frac{\partial g}{\partial \Omega}\right|_0 \Omega + \left.\frac{\partial g}{\partial (\mathbf{v}_i^r)_Z}\right|_0 (\mathbf{v}_i^r)_Z + \left.\frac{\partial g}{\partial (\mathbf{v}_i^r)_t}\right|_0 (\mathbf{v}_i^r)_t \\ & + \left.\frac{\partial g}{\partial (\dot{\mathbf{w}}^r)_Z}\right|_0 (\dot{\mathbf{w}}^r)_Z + \left.\frac{\partial g}{\partial (\dot{\mathbf{w}}^r)_t}\right|_0 (\dot{\mathbf{w}}^r)_t + \left.\frac{\partial g}{\partial u_z}\right|_0 u_z + \left.\frac{\partial g}{\partial u_t}\right|_0 u_t + \left.\frac{\partial g}{\partial c_L}\right|_0 c_L, \end{aligned} \tag{2.30}$$

with

$$g_0 = F_{L0} = C_{L0}\frac{1}{2}\rho c L\left|\mathbf{V}_0\right|^2, \tag{2.31}$$

$$\left.\frac{\partial g}{\partial \Omega}\right|_0 = C_{L0}\rho c L r\left[r\Omega_0 - (\mathbf{V}_{i0}^r)_t\right], \tag{2.32}$$

$$\left.\frac{\partial g}{\partial u_z}\right|_0 = \left.\frac{\partial g}{\partial (\mathbf{v}_i^r)_Z}\right|_0 = C_{L0}\rho c L\left[V_\infty + (\mathbf{V}_{i0}^r)_Z\right], \tag{2.33}$$

$$\left.\frac{\partial g}{\partial u_t}\right|_0 = \left.\frac{\partial g}{\partial (\mathbf{v}_i^r)_t}\right|_0 = -C_{L0}\rho c L\left[r\Omega_0 - (\mathbf{V}_{i0}^r)_t\right], \tag{2.34}$$

$$\left.\frac{\partial g}{\partial (\dot{\mathbf{w}}^r)_Z}\right|_0 = -C_{L0}\rho c L\left[V_\infty + (\mathbf{V}_{i0}^r)_Z\right], \tag{2.35}$$

$$\left.\frac{\partial g}{\partial (\dot{\mathbf{w}}^r)_t}\right|_0 = C_{L0}\rho c L\left[r\Omega_0 - (\mathbf{V}_{i0}^r)_t\right], \tag{2.36}$$

and

$$\left.\frac{\partial g}{\partial c_L}\right|_0 = \frac{1}{2}\rho c L\left(\left[V_\infty + (\mathbf{V}_{i0}^r)_Z\right]^2 + \left[r\Omega_0 - (\mathbf{V}_{i0}^r)_t\right]^2\right). \tag{2.37}$$

The expressions for the drag force are identical, except for the substitution of C_D for C_L. With this linearization, Equations 2.27 and 2.28 are of the form $\mathbf{y} = \mathbf{C}\mathbf{x} + \mathbf{D}_u\mathbf{u} + \mathbf{D}_y\mathbf{y}$.

2.6 Aerodynamic Forces

Lift and drag forces are respectively perpendicular and parallel to the vector **V** in Figure 3. Momentum balance (Section 2.1) requires these forces in rotorplane coordinates, and structural dynamics (Section 3) requires these forces in blade pitch coordinates. The transform to rotorplane coordinates is

$$\mathbf{F}_a^r := \begin{bmatrix} (\mathbf{F}_{a0}^r)_Z + (\mathbf{f}_a^r)_Z \\ (\mathbf{F}_{a0}^r)_t + (\mathbf{f}_a^r)_t \end{bmatrix} = \begin{bmatrix} \cos\phi & \sin\phi \\ \sin\phi & -\cos\phi \end{bmatrix} \begin{bmatrix} F_{L0} + f_L \\ F_{D0} + f_D \end{bmatrix}, \tag{2.38}$$

with

$$\phi = \alpha_{q0} + \alpha_q + \beta_0 + \beta + \xi_0 - (\boldsymbol{\theta}^s)_X ; \quad \phi_0 = \alpha_{q0} + \beta_0 + \xi_0 . \tag{2.39}$$

The trigonometric functions are linearized using

$$\frac{\partial}{\partial \alpha_q} \cos\phi \Big|_0 = \frac{\partial}{\partial \beta} \cos\phi \Big|_0 = -\sin\phi_0 , \tag{2.40}$$

$$\frac{\partial}{\partial (\boldsymbol{\theta}^s)_X} \cos\phi \Big|_0 = \sin\phi_0 , \tag{2.41}$$

$$\frac{\partial}{\partial \alpha_q} \sin\phi \Big|_0 = \frac{\partial}{\partial \beta} \sin\phi \Big|_0 = \cos\phi_0 , \tag{2.42}$$

and

$$\frac{\partial}{\partial (\boldsymbol{\theta}^s)_X} \sin\phi \Big|_0 = -\cos\phi_0 . \tag{2.43}$$

The result is

$$\begin{aligned} \begin{bmatrix} (\mathbf{f}_a^r)_Z \\ (\mathbf{f}_a^r)_t \end{bmatrix} &= \begin{bmatrix} -\sin\phi_0 & \cos\phi_0 \\ \cos\phi_0 & \sin\phi_0 \end{bmatrix} \begin{bmatrix} F_{L0} \\ F_{D0} \end{bmatrix} \left(\beta - (\boldsymbol{\theta}^s)_X \right) \\ &+ \begin{bmatrix} -\sin\phi_0 & \cos\phi_0 \\ \cos\phi_0 & \sin\phi_0 \end{bmatrix} \begin{bmatrix} F_{L0} \\ F_{D0} \end{bmatrix} \alpha_q + \begin{bmatrix} \cos\phi_0 & \sin\phi_0 \\ \sin\phi_0 & -\cos\phi_0 \end{bmatrix} \begin{bmatrix} f_L \\ f_D \end{bmatrix}, \end{aligned} \tag{2.44}$$

which is of the form $\mathbf{y} = \mathbf{C}\mathbf{x} + \mathbf{D}_y \mathbf{y}$.

The transform to section coordinates is

$$\mathbf{F}_a^s := \begin{bmatrix} (\mathbf{F}_{a0}^s)_X + (\mathbf{f}_a^s)_X \\ (\mathbf{F}_{a0}^s)_Y + (\mathbf{f}_a^s)_Y \\ (\mathbf{F}_{a0}^s)_Z + (\mathbf{f}_a^s)_Z \\ (\mathbf{M}_{a0}^s)_X + (\mathbf{m}_a^s)_X \\ (\mathbf{M}_{a0}^s)_Y + (\mathbf{m}_a^s)_Y \\ (\mathbf{M}_{a0}^s)_Z + (\mathbf{m}_a^s)_Z \end{bmatrix} = \begin{bmatrix} 0 & 0 \\ \sin\left(\alpha_{q0} + \alpha_q\right) & -\cos\left(\alpha_{q0} + \alpha_q\right) \\ \cos\left(\alpha_{q0} + \alpha_q\right) & \sin\left(\alpha_{q0} + \alpha_q\right) \\ \varepsilon \cos\left(\alpha_{q0} + \alpha_q\right) & 0 \\ 0 & 0 \\ 0 & 0 \end{bmatrix} \begin{bmatrix} F_{L0} + f_L \\ F_{D0} + f_D \end{bmatrix}, \tag{2.45}$$

where ε is the offset from the aerodynamic center to the structural centroid; referring to Figure 2, this is the distance, along the X^a axis, from the Y^a to the Z^s axes. Linearizing, the result is

$$\begin{bmatrix} (\mathbf{f}_a^s)_X \\ (\mathbf{f}_a^s)_Y \\ (\mathbf{f}_a^s)_Z \\ (\mathbf{m}_a^s)_X \\ (\mathbf{m}_a^s)_Y \\ (\mathbf{m}_a^s)_Z \end{bmatrix} = \begin{bmatrix} 0 & 0 \\ \cos\alpha_{q0} & \sin\alpha_{q0} \\ -\sin\alpha_{q0} & \cos\alpha_{q0} \\ -\varepsilon\sin\alpha_{q0} & 0 \\ 0 & 0 \\ 0 & 0 \end{bmatrix} \begin{bmatrix} F_{L0} \\ F_{D0} \end{bmatrix} \alpha_q + \begin{bmatrix} 0 & 0 \\ \sin\alpha_{q0} & -\cos\alpha_{q0} \\ \cos\alpha_{q0} & \sin\alpha_{q0} \\ \varepsilon\cos\alpha_{q0} & 0 \\ 0 & 0 \\ 0 & 0 \end{bmatrix} \begin{bmatrix} f_L \\ f_D \end{bmatrix}. \tag{2.46}$$

This is of the form $\mathbf{y} = \mathbf{D}_y \mathbf{y}$.

The transform to pitch coordinates is

$$\mathbf{T}_s^p = \begin{bmatrix} 1 & 0 & 0 \\ 0 & \cos\xi & \sin\xi \\ 0 & -\sin\xi & \cos\xi \end{bmatrix}, \tag{2.47}$$

such that

$$\mathbf{f}_a^p = -\left.\frac{\partial \mathbf{T}_s^p}{\partial \xi}\right|_0 \mathbf{F}_{a0}^s(\boldsymbol{\theta}^p)_X + \mathbf{T}_{s0}^p \mathbf{f}_a^s, \tag{2.48}$$

or, expanding the terms,

$$\begin{aligned} \begin{bmatrix} (\mathbf{f}_a^p)_X \\ (\mathbf{f}_a^p)_Y \\ (\mathbf{f}_a^p)_Z \\ (\mathbf{m}_a^p)_X \\ (\mathbf{m}_a^p)_Y \\ (\mathbf{m}_a^p)_Z \end{bmatrix} = &- \begin{bmatrix} 0 & 0 & 0 & 0 & 0 & 0 \\ 0 & -\sin\xi_0 & \cos\xi_0 & 0 & 0 & 0 \\ 0 & -\cos\xi_0 & -\sin\xi_0 & 0 & 0 & 0 \\ 0 & 0 & 0 & 0 & 0 & 0 \\ 0 & 0 & 0 & 0 & -\sin\xi_0 & \cos\xi_0 \\ 0 & 0 & 0 & 0 & -\cos\xi_0 & -\sin\xi_0 \end{bmatrix} \begin{bmatrix} (\mathbf{F}_{a0}^s)_X \\ (\mathbf{F}_{a0}^s)_Y \\ (\mathbf{F}_{a0}^s)_Z \\ (\mathbf{M}_{a0}^s)_X \\ (\mathbf{M}_{a0}^s)_Y \\ (\mathbf{M}_{a0}^s)_Z \end{bmatrix} (\boldsymbol{\theta}^s)_X \\ &+ \begin{bmatrix} 1 & 0 & 0 & 0 & 0 & 0 \\ 0 & \cos\xi_0 & \sin\xi_0 & 0 & 0 & 0 \\ 0 & -\sin\xi_0 & \cos\xi_0 & 0 & 0 & 0 \\ 0 & 0 & 0 & 1 & 0 & 0 \\ 0 & 0 & 0 & 0 & \cos\xi_0 & \sin\xi_0 \\ 0 & 0 & 0 & 0 & -\sin\xi_0 & \cos\xi_0 \end{bmatrix} \begin{bmatrix} (\mathbf{f}_a^s)_X \\ (\mathbf{f}_a^s)_Y \\ (\mathbf{f}_a^s)_Z \\ (\mathbf{m}_a^s)_X \\ (\mathbf{m}_a^s)_Y \\ (\mathbf{m}_a^s)_Z \end{bmatrix}. \end{aligned} \tag{2.49}$$

3 Structures

The structures of the wind turbine are represented by beam finite elements. The elastic deflections are assumed to be small. Large rigid-body rotations are permitted at the yaw bearing, the driveshaft and rotor, and the pitch bearings. These latter degrees-of-freedom will be referred to as the joints of the structure.

Figure 4 through Figure 7 show sketches of the structural components together with the finite-element model. The structural components are linked at the joints to form the entire wind turbine. Links are described by constraint equations, which associate the degrees-of-freedom of the structures on each side of the joints. The constraint equations are used to eliminate dependent degrees-of-freedom from the model.

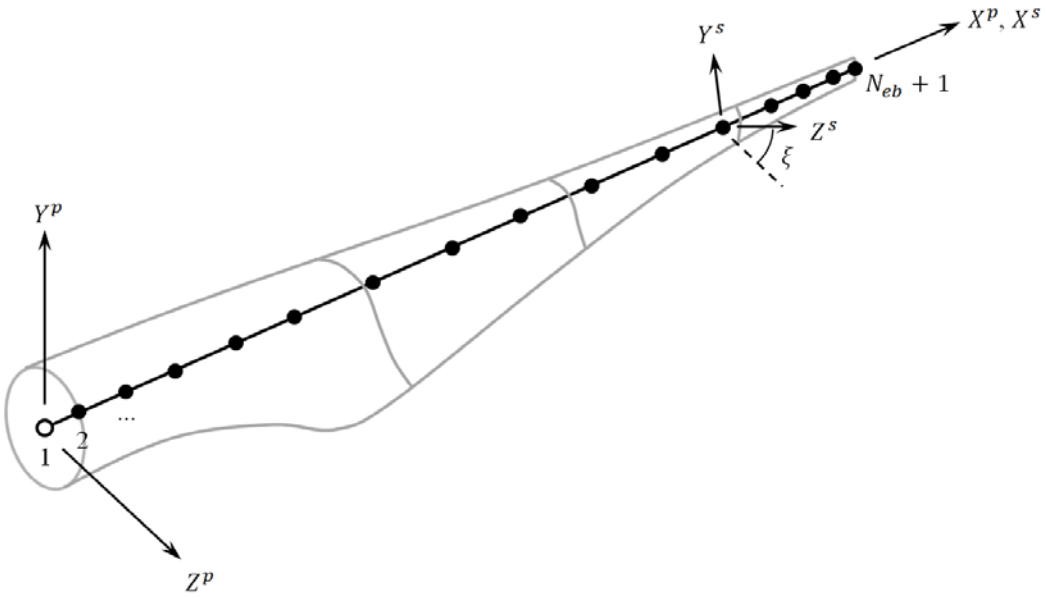

Figure 4: Blade nodes and coordinate systems.

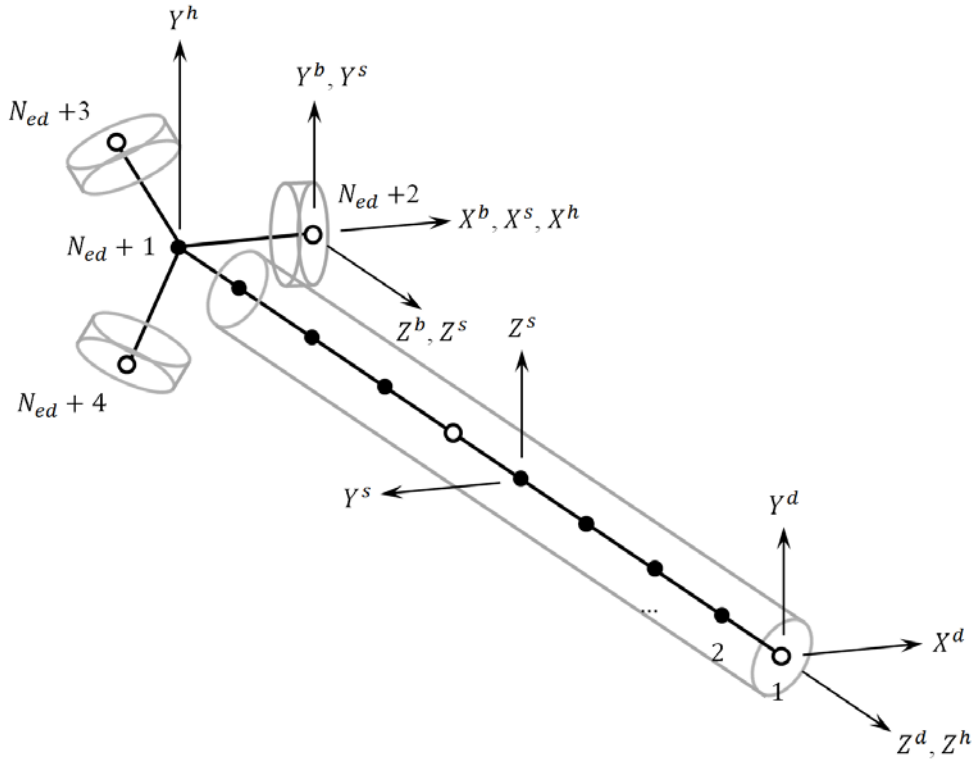

Figure 5: Driveshaft nodes and coordinate systems (sketched with zero blade cone angle).

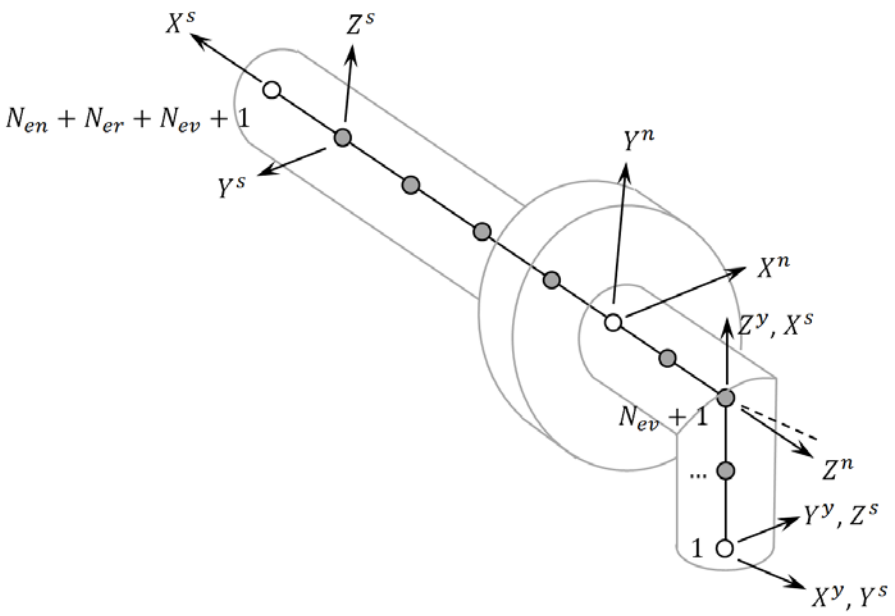

Figure 6: Nacelle nodes and coordinate systems.

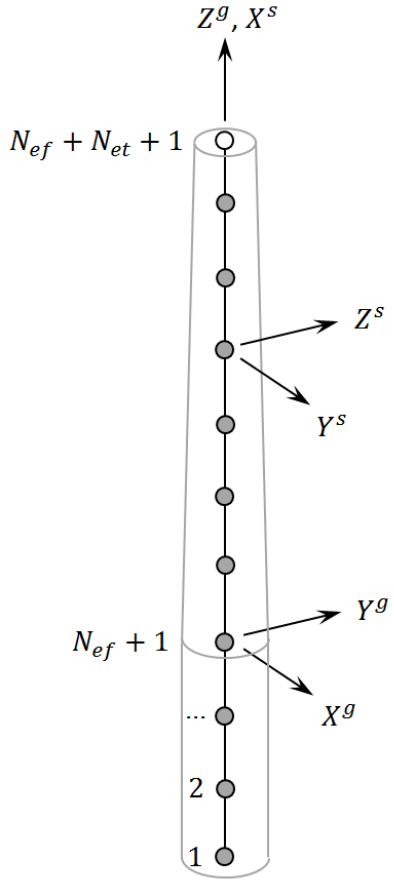

Figure 7: Tower and foundation nodes and coordinate systems.

Figure 8 shows the length dimensions which are used to define the turbine structure. Joints are shown by white dots. By default, the global coordinate system has its origin at the base of the tower, at the top of the transition piece between the tower and foundation. On land, this would

typically be at ground level. Offshore, however, this might not be the same as either the seabed or undisturbed ocean surface elevation. The location of the origin can be moved by suitable redefinition of L_f and L_t in the input file.

Note that the nacelle and driveshaft structures overlap between the rear and front bearings.

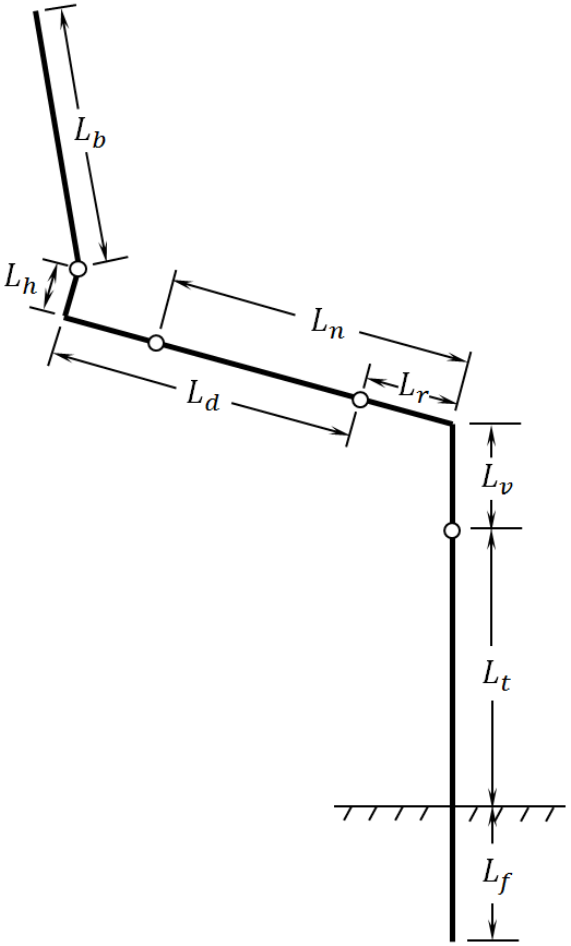

Figure 8: Dimensions of the turbine structures. Only one blade is shown.

3.1 Element Mass, Stiffness, and Damping Matrices

The element mass and stiffness matrices are developed according to standard finite-element beam theory. Some comments are required, however, related to the modelling of airfoil profiles and foundation elements in the sea floor. The implementation of structural damping is not straightforward, and this is discussed in more detail.

3.1.1 Element Mass Matrix

For cross-sections with no coupling between degrees-of-freedom, the element mass matrix is

$$\begin{bmatrix}
2C_a & 0 & 0 & 0 & 0 & 0 & C_a & 0 & 0 & 0 & 0 & 0 \\
0 & 156C_b & 0 & 0 & 0 & 22LC_b & 0 & 54C_b & 0 & 0 & 0 & -13LC_b \\
0 & 0 & 156C_b & 0 & -22LC_b & 0 & 0 & 0 & 54C_b & 0 & 13LC_b & 0 \\
0 & 0 & 0 & 2C_r & 0 & 0 & 0 & 0 & 0 & C_r & 0 & 0 \\
0 & 0 & -22LC_b & 0 & 4L^2C_b & 0 & 0 & 0 & -13LC_b & 0 & -3L^2C_b & 0 \\
0 & 22LC_b & 0 & 0 & 0 & 4L^2C_b & 0 & 13LC_b & 0 & 0 & 0 & -3L^2C_b \\
C_a & 0 & 0 & 0 & 0 & 0 & 2C_a & 0 & 0 & 0 & 0 & 0 \\
0 & 54C_b & 0 & 0 & 0 & 13LC_b & 0 & 156C_b & 0 & 0 & 0 & -22LC_b \\
0 & 0 & 54C_b & 0 & -13LC_b & 0 & 0 & 0 & 156C_b & 0 & 22LC_b & 0 \\
0 & 0 & 0 & C_r & 0 & 0 & 0 & 0 & 0 & 2C_r & 0 & 0 \\
0 & 0 & 13LC_b & 0 & -3L^2C_b & 0 & 0 & 0 & 22LC_b & 0 & 4L^2C_b & 0 \\
0 & -13LC_b & 0 & 0 & 0 & -3L^2C_b & 0 & -22LC_b & 0 & 0 & 0 & 4L^2C_b
\end{bmatrix} \tag{3.1}$$

with

$$C_b = \frac{\rho AL}{420}, \quad C_a = \frac{\rho AL}{6}, \quad \text{and} \quad C_r = \frac{\rho JL}{6}. \tag{3.2}$$

If the line between the nodes does not pass through the center-of-gravity of the section, then there is coupling between lateral and torsional accelerations. Consider the airfoil section shown in Figure 9. The section coordinate system is defined so that it passes through the pitch axis. This does not necessarily coincide with the elastic, gravity, and shear centers. The offset from the section coordinate system to the bending, gravity, and shear centers is respectively e_b, e_g, and e_s.

For the initial implementation of STAS, the effects of these eccentricities are neglected. As a consequence, the present code should not be used in cases where the bend-twist coupling is expected to be significant, for instance flutter instability during overspeed events.

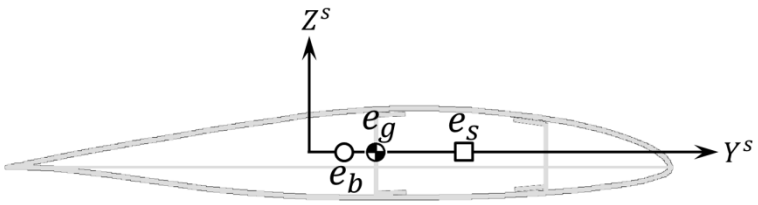

Figure 9: Elastic (bending), gravity, and shear (torsion) centers of an arbitrary airfoil profile.

3.1.2 Element Stiffness Matrix

The element stiffness matrix is

$$\begin{bmatrix}
C_a & 0 & 0 & 0 & 0 & 0 & -C_a & 0 & 0 & 0 & 0 & 0 \\
0 & 12C_{b1} & 0 & 0 & 0 & 6LC_{b1} & 0 & -12C_{b1} & 0 & 0 & 0 & 6LC_{b1} \\
0 & 0 & 12C_{b2} & 0 & -6LC_{b2} & 0 & 0 & 0 & -12C_{b2} & 0 & -6LC_{b2} & 0 \\
0 & 0 & 0 & C_r & 0 & 0 & 0 & 0 & 0 & -C_r & 0 & 0 \\
0 & 0 & -6LC_{b2} & 0 & 4L^2C_{b2} & 0 & 0 & 0 & 6LC_{b2} & 0 & 2L^2C_{b2} & 0 \\
0 & 6LC_{b1} & 0 & 0 & 0 & 4L^2C_{b1} & 0 & -6LC_{b1} & 0 & 0 & 0 & 2L^2C_{b1} \\
-C_a & 0 & 0 & 0 & 0 & 0 & C_a & 0 & 0 & 0 & 0 & 0 \\
0 & -12C_{b1} & 0 & 0 & 0 & -6LC_{b1} & 0 & 12C_{b1} & 0 & 0 & 0 & -6LC_{b1} \\
0 & 0 & -12C_{b2} & 0 & 6LC_{b2} & 0 & 0 & 0 & 12C_{b2} & 0 & 6LC_{b2} & 0 \\
0 & 0 & 0 & -C_r & 0 & 0 & 0 & 0 & 0 & C_r & 0 & 0 \\
0 & 0 & -6LC_{b2} & 0 & 2L^2C_{b2} & 0 & 0 & 0 & 6LC_{b2} & 0 & 4L^2C_{b2} & 0 \\
0 & 6LC_{b1} & 0 & 0 & 0 & 2L^2C_{b1} & 0 & -6LC_{b1} & 0 & 0 & 0 & 4L^2C_{b1}
\end{bmatrix} \tag{3.3}$$

with

$$C_{b1} = \frac{EI_{zz}}{L^3}, \quad C_{b2} = \frac{EI_{yy}}{L^3}, \quad C_a = \frac{EA}{L}, \quad \text{and} \quad C_r = \frac{GJ}{L}. \tag{3.4}$$

The bending and shear offsets shown in Figure 9 are presently ignored.

3.1.3 Element Damping Matrix

Rather than employing a damping matrix along the same lines as the mass and stiffness matrices, a modal approach is adopted. This avoids some of the disadvantages of mass- and stiffness-proportional (Rayleigh) damping, such as a damping ratio that varies widely with frequency.

For a statically-mounted structure, whose response can be decoupled into independent modes of vibration, a damping ratio can be defined for each mode, as

$$\zeta_k = \frac{C_k}{2\sqrt{K_k M_k}}. \tag{3.5}$$

Here M_k, C_k, and K_k are the modal mass, damping, and stiffness, respectively. The extensive survey by Blevins [4] indicates that a reasonable design value for the structural damping ratio is around 0.01, for statically-mounted structures. The damping ratio does not change appreciably with frequency, although it may increase with amplitude.

For a structure such as a wind turbine, with many coupled modes, the damping ratio can be defined according to the real and imaginary parts of the state-space eigenvalues,

$$R := \frac{\Re(\lambda)}{\Im(\lambda)}, \qquad \zeta_k = -\operatorname{sgn}\left(\Re(\lambda)\right)\sqrt{\frac{R^2}{1+R^2}}. \tag{3.6}$$

As discussed in Section 3.7, the wind turbine is represented by several substructures, or bodies: the tower, nacelle, driveshaft, and each blade. In turn, the elastic deformation of each body is represented by several of its natural, uncoupled modes. The modal damping of the body can then be represented by Equation 3.5. A value of $\zeta = 0.008$ is used for all modes. When the full wind turbine structure is assembled, the modes become coupled; but the value of the structural damping ratio for the global modes of the wind turbine, Equation 3.6, is observed to remain in the vicinity of 0.01.

In other words, the damping matrix is defined as a diagonal matrix with zeros associated with the rigid-body motions, and

$$C_k = 2\zeta\sqrt{K_k M_k} \tag{3.7}$$

on the diagonal entry associated with the k^{th} elastic mode of one of the bodies.

Soil damping is modelled by damping elements which act in parallel with the p-y springs representing the soil stiffness. The equivalent soil spring and damping properties are provided as part of the input file.

Aerodynamic damping follows naturally from the methods of Section 2. Hydrodynamic damping is not implemented in the present model, but can be added as part of the applied hydrodynamic loads.

3.1.4 Centrifugal Stiffening

For a wind turbine undergoing small deflections about some mean position, there is for most degrees-of-freedom only a weak relationship between the deflection and the system mass, stiffness, and damping matrices. This is taken advantage of in Section 3.2 to simplify the derivation of the equations of motion. An exception is the centrifugal stiffening of the blades, which must be accounted for in order to obtain the correct natural frequencies of vibration.

Centrifugal stiffening is a function of the instantaneous, deflected position of the blade; this coupling is neglected.

It is most convenient to derive centrifugal stiffening in hub coordinates, with the X^h axis normal to the axis of driveshaft rotation, and pointing along the blade of interest, not including the cone angle. Let the position vector of the degrees-of-freedom associated with node *j* of the blade be $\mathbf{x}_j^h$. Then $r_j = (\mathbf{x}_j^h)_X$.

The rotation of the rotor gives an acceleration in the X^h direction, as

$$\mathbf{a}_j = \begin{bmatrix} r_j\Omega^2 & 0 & 0 & 0 & 0 & 0 \end{bmatrix}^T . \tag{3.8}$$

The force vector seen by a given element, say element k, due to this acceleration is

$$\mathbf{F}_k^h = \sum_{j=k}^{Neb} \mathbf{m}_{e,j}^h \begin{bmatrix} \mathbf{a}_j \\ \mathbf{a}_{j+1} \end{bmatrix} = \sum_{j=k}^{Neb} \mathbf{T}_{s,j}^h \mathbf{m}_{e,j}^s \mathbf{T}_{h,j}^s \begin{bmatrix} \mathbf{a}_j \\ \mathbf{a}_{j+1} \end{bmatrix} . \tag{3.9}$$

If we say that the tension force P within element k is the seventh entry in the vector $\mathbf{F}_k^s := \mathbf{T}_{h,k}^s \mathbf{F}_k^h$, which is the along-blade tension acting on the outer node of the element, then the centrifugal stiffness matrix $\mathbf{k}_\sigma^s$ follows as

$$C_c = \frac{P}{30L}; \tag{3.10}$$

$$\begin{bmatrix}
0 & 0 & 0 & 0 & 0 & 0 & 0 & 0 & 0 & 0 & 0 & 0 \\
0 & 36C_c & 0 & 0 & 0 & 3LC_c & 0 & -36C_c & 0 & 0 & 0 & 3LC_c \\
0 & 0 & 36C_c & 0 & -3LC_c & 0 & 0 & 0 & -36C_c & 0 & -3LC_c & 0 \\
0 & 0 & 0 & 0 & 0 & 0 & 0 & 0 & 0 & 0 & 0 & 0 \\
0 & 0 & -3LC_c & 0 & 4L^2C_c & 0 & 0 & 0 & 3LC_c & 0 & -L^2C_c & 0 \\
0 & 3LC_c & 0 & 0 & 0 & 4L^2C_c & 0 & -3LC_c & 0 & 0 & 0 & -L^2C_c \\
0 & 0 & 0 & 0 & 0 & 0 & 0 & 0 & 0 & 0 & 0 & 0 \\
0 & -36C_c & 0 & 0 & 0 & -3LC_c & 0 & 36C_c & 0 & 0 & 0 & -3LC_c \\
0 & 0 & -36C_c & 0 & 3LC_c & 0 & 0 & 0 & 36C_c & 0 & 3LC_c & 0 \\
0 & 0 & 0 & 0 & 0 & 0 & 0 & 0 & 0 & 0 & 0 & 0 \\
0 & 0 & -3LC_c & 0 & -L^2C_c & 0 & 0 & 0 & 3LC_c & 0 & 4L^2C_c & 0 \\
0 & 3LC_c & 0 & 0 & 0 & -L^2C_c & 0 & -3LC_c & 0 & 0 & 0 & 4L^2C_c
\end{bmatrix} \tag{3.11}$$

In Section 3.2, the derivative with respect to Ω is needed. This is computed using

$$\frac{dC_c}{d\Omega} = \frac{1}{30L}\frac{dP}{d\Omega} = \frac{2}{30L}\Omega\sum_{i=j}^{Neb} m_i r_i , \tag{3.12}$$

from which it is evident that

$$\frac{d\mathbf{k}_\sigma^s}{d\Omega} = \frac{2}{\Omega}\mathbf{k}_\sigma^s . \tag{3.13}$$

3.2 Equations of Motion

The equations of motion are based upon a simplified multi-body formulation. The simplification is related to the way in which large rotations are handled. As the analysis is to be linearized, it was desired to avoid the general nonlinear formulations of large-rotation dynamics as described by, for instance, Shabana [24]. At the same time, it is necessary to accommodate large static rotations of the yaw, driveshaft, and blade pitch joints, and retain important couplings between the joint motions and flexure of the structure.

The Lagrange equations are used to formulate the structural equations of motion. Define the operation

$$\frac{\partial}{\partial \mathbf{x}} := \begin{bmatrix} \partial/\partial x_1 \\ \partial/\partial x_2 \\ \vdots \end{bmatrix} \tag{3.14}$$

The Lagrange equations are

$$\frac{d}{dt}\left(\frac{\partial E_K}{\partial \dot{\mathbf{q}}}\right) - \frac{\partial E_K}{\partial \mathbf{q}} + \frac{1}{2}\frac{\partial \dot{E}_D}{\partial \dot{\mathbf{q}}} + \frac{\partial E_P}{\partial \mathbf{q}} = \mathbf{F}\,, \tag{3.15}$$

where **q** is a vector of the degrees-of-freedom, and **F** is a vector of the (generalized) forces. E_K is the kinetic energy, E_P is the potential energy, and dE_D/dt is the rate of energy dissipation.

Development of the equations of motion proceeds as follows. First the equations are developed, with all degrees-of-freedom expressed in body coordinates. A modal transformation is applied to the elastic degrees-of-freedom, while those representing rigid-body motions are left un-transformed. The bodies are joined at the joints, with constrained degrees-of-freedom eliminated from the equations. This gives terms which depend upon the rotation angles of the joints, and in particular the rotation of the rotor and driveshaft. As the rotor and driveshaft have a steady rotating motion (upon which small fluctuations in speed are imposed), the matrices are functions of the azimuth angle. The rotating degrees-of-freedom in the equations of motion are substituted with multi-blade coordinates, which eliminate dependence of the matrices on the azimuth angle.

3.2.1 Kinetic Energy

In modelling the dynamics of a mechanical system with joints, one has a choice of degrees-of-freedom. They must in the end describe the same motion, but the degree of complexity of the formulation – and where in the equations that complexity appears – depends on the selection of degrees-of-freedom.

At present we use an elastic multi-body representation. Define the position of a node in global coordinates as the sum of the vector to the body origin, which happens, in the present case, to always be the first node on the body; plus the rigid-body offset from the body origin to the undeformed position of each node at its section coordinate system; plus a small elastic deflection relative to the undeformed nodal position:

$$\mathbf{r}^g_{k/g} = \mathbf{O}^g_{1/g} + \mathbf{P}^g_{k/B} + \boldsymbol{\delta}^g_{k/s}\,. \tag{3.16}$$

The position and orientation of the reference node, at the body origin, could be described by

$$\mathbf{P}^g_{1/g} = \left[(\mathbf{O}^g_{1/g})_X \quad (\mathbf{O}^g_{1/g})_Y \quad (\mathbf{O}^g_{1/g})_Z \quad (\boldsymbol{\Theta}^g_{1/g})_X \quad (\boldsymbol{\Theta}^g_{1/g})_Y \quad (\boldsymbol{\Theta}^g_{1/g})_Z\right]^T. \tag{3.17}$$

The vector $\mathbf{O}^g_{1/g}$ is the vector from the global origin to the origin of the body coordinate system. The "angles" $\boldsymbol{\Theta}^g_{1/g}$ are only placeholders; their time derivative is the angular velocity, which is the quantity of interest. In general multi-body formulations, the $\boldsymbol{\Theta}^g_{1/g}$ components are not the time integral of the angular velocity vector, but rather some parameters, like Euler angles, from which the body coordinate transformation matrix $\mathbf{T}^g_B$ and angular velocity matrix $d\mathbf{T}^g_B/dt$ can be reconstructed. This relationship is in the general case nonlinear.

The equations of motion developed at present will subsequently be linearized. This implies that the departure from the selected degrees-of-freedom is small, and hence the motion is constrained. We take advantage of this constraint by selecting the degrees-of-freedom such that the position of the body is defined relative to the undeformed position of the master node on the preceeding body. The nature of the joints as rotations about a single axis (plus small elastic rotations about the other axes) then allow the rotational degrees-of-freedom to be chosen as the time integrals of the relative angular velocity vectors between the two bodies.

The degrees-of-freedom of the body origin are chosen as

$$\mathbf{P}^B_{1/m} = \left[(\mathbf{O}^B_{1/m})_X \quad (\mathbf{O}^B_{1/m})_Y \quad (\mathbf{O}^B_{1/m})_Z \quad (\boldsymbol{\Theta}^B_{1/m})_X \quad (\boldsymbol{\Theta}^B_{1/m})_Y \quad (\boldsymbol{\Theta}^B_{1/m})_Z\right]^T, \tag{3.18}$$

where "*m*" indicates the master body and "*B*" indicates the slave body. One of the rotational components is the joint rotation angle, and the other two are small elastic deformations. The rate of change is

$$\dot{\mathbf{P}}^B_{1/m} = \left[(\mathbf{V}^B_{1/m})_X \quad (\mathbf{V}^B_{1/m})_Y \quad (\mathbf{V}^B_{1/m})_Z \quad (\boldsymbol{\omega}^B_{1/m})_X \quad (\boldsymbol{\omega}^B_{1/m})_Y \quad (\boldsymbol{\omega}^B_{1/m})_Z \right]^T . \tag{3.19}$$

The global position of a point, or node, is recovered by

$$\mathbf{r}^g_{k/g} = \mathbf{P}^g_{m,t/g} + \mathbf{T}^g_y \left(\mathbf{O}^y_{1,n/m} + \mathbf{P}^y_{m,n/y} + \mathbf{T}^y_d \left(\mathbf{O}^d_{1,d/m} + \mathbf{P}^d_{m,d/d} + \mathbf{T}^d_p \left(\mathbf{O}^p_{1,b/m} + \mathbf{P}^p_{k/p} + \boldsymbol{\delta}^p_{k/s} \right) \right) \right), \tag{3.20}$$

using the example of a node on one of the blades, which contains the most terms. As discussed above, the definition of a "global orientation" in terms of time integrals of the angular velocities would not be meaningful. However, angular velocities sum and transform straightforwardly as vectors. Thus while the definition of a "global position and orientation" of a node

$$\mathbf{x}^g_{k/g} := \begin{bmatrix} \mathbf{r}^g_{k/g} \\ \boldsymbol{\theta}^g_{k/g} \end{bmatrix} \tag{3.21}$$

would not be meaningful in the present context, its time derivative

$$\frac{d\mathbf{x}^g_{k/g}}{dt} := \begin{bmatrix} d\mathbf{r}^g_{k/g} / dt \\ \boldsymbol{\omega}^g_{k/g} \end{bmatrix} \tag{3.22}$$

is meaningful.

Defining the total degree-of-freedom vector

$$\mathbf{q}^B = \left[\mathbf{O}^B_{1/m} \quad \boldsymbol{\Theta}^B_{1/m} \quad \mathbf{w}^B_{/s} \quad \cdots \right]^T , \tag{3.23}$$

where the sequence repeats for each body, with

$$\mathbf{w}^B_{/s} = \left[(\boldsymbol{\delta}^B_{k/s})_X \quad (\boldsymbol{\delta}^B_{k/s})_Y \quad (\boldsymbol{\delta}^B_{k/s})_Z \quad (\boldsymbol{\theta}^B_{k/s})_X \quad (\boldsymbol{\theta}^B_{k/s})_Y \quad (\boldsymbol{\theta}^B_{k/s})_Z \cdots \right]^T ; \tag{3.24}$$

and the vector of nodal position offsets

$$\mathbf{P}^B_s := \left[(\mathbf{P}^B_{k/B})_X \quad (\mathbf{P}^B_{k/B})_Y \quad (\mathbf{P}^B_{k/B})_Z \quad 0 \quad 0 \quad 0 \quad \cdots \right]^T , \tag{3.25}$$

where the sequence repeats for each node, the global position of one node, from Equation 3.20 or similar, can be conveniently written in matrix/vector format as

$$\mathbf{r}^g_{k/g} = \mathbf{A}_k \mathbf{T}^g_B \mathbf{q}^B + \mathbf{B}_k \mathbf{T}^g_B \mathbf{P}^B_s . \tag{3.26}$$

Let the coordinates of the two nodes associated with an element *k* connecting nodes *j* and *j*+1 be

$$\mathbf{x}^g_{k/g} = \begin{bmatrix} \mathbf{x}^g_{j/g} \\ \mathbf{x}^g_{j+1/g} \end{bmatrix}, \tag{3.27}$$

that is, twelve degrees-of-freedom. The kinetic energy of the element is

$$E_K = \frac{1}{2} \frac{d(\mathbf{x}^g_{k/g})^T}{dt} (\mathbf{T}^s_{g,k})^T \mathbf{m}^s_{e,k} \mathbf{T}^s_{g,k} \frac{d\mathbf{x}^g_{k/g}}{dt} . \tag{3.28}$$

Note that the operation

$$\mathbf{T}^s_{g,k} \frac{d\mathbf{x}^g_{k/g}}{dt}$$

expresses the linear and rotational velocities, measured relative to the global coordinate system, in coordinates corresponding to the *instantaneous* orientation of the section coordinate system. Also note that with a beam finite element representation, the rigid-body component of the kinetic energy depends only upon the linear velocity of the nodes, and the angular velocity of the element rotation about its axis; the other two rotational degrees-of-freedom, as mentioned, represent small elastic deformations, and are not functions of the bulk motion.

The mass matrix for the element can just as well be written in body coordinates,

$$E_K = \frac{1}{2}\frac{d(\mathbf{x}_{k/g}^g)^T}{dt}\mathbf{T}_B^g\left[\mathbf{T}_{s,k}^B\mathbf{m}_{e,k}^s\mathbf{T}_{B,k}^s\right]\mathbf{T}_g^B\frac{d\mathbf{x}_{k/g}^g}{dt} \tag{3.29}$$

as the quantity in brackets is constant for small elastic deformations. If we say that the k^{th} element mass matrix, nominally 12-by-12 in size, is expanded with zeros to include entries for all the nodal positions, then the expression for kinetic energy can be written as

$$E_K = \frac{1}{2}\frac{d(\mathbf{x}_{/g}^g)^T}{dt}\mathbf{T}_B^g\mathbf{M}^B\mathbf{T}_g^B\frac{d\mathbf{x}_{/g}^g}{dt}, \qquad \mathbf{M}^B := \sum_{k=1}^{Ne}\mathbf{T}_{s,k}^B\mathbf{m}_{e,k}^s\mathbf{T}_{B,k}^s\ . \tag{3.30}$$

The vector $d\mathbf{x}_{/g}^g/dt$ consists of a group of six values for each node in the structure. In each group, the first three values are $d\mathbf{r}_{k/g}^g/dt$, and the latter three values are $\boldsymbol{\omega}_{k/g}^g$. However, $\boldsymbol{\omega}_{k/g}^g$ is *not the total angular velocity of the node*. It is the portion which contributes to the kinetic energy, and this includes all three rotations due to elastic deformation, but, due to the nature of the finite elements, only the X^s component of the rigid-body angular velocity. In general, for a given node, the X^s component of the rigid-body angular velocity can be written

$$\boldsymbol{\omega}_{1/g}^g = \mathbf{T}_{s,k}^g\begin{bmatrix}(\boldsymbol{\omega}_{1/g}^s)_X\\0\\0\end{bmatrix}. \tag{3.31}$$

Taking an example, the axial rotation of a blade element due to rotation of the yaw bearing would be

$$\boldsymbol{\omega}_{1/g}^g = \mathbf{T}_{s,k}^g\begin{bmatrix}(\mathbf{T}_{y,k}^s\boldsymbol{\omega}_{1,n/g}^y)_X\\0\\0\end{bmatrix}. \tag{3.32}$$

That being said, the nature of the wind turbine system leads to considerable simplification. It is noted that the rotation of the pitch bearings is nearly aligned with the section coordinate systems of the blade elements, that the blades are nearly orthogonal to the driveshaft, and that the yaw rotation is expected to be slow. In addition, by far the greatest portion of the inertial resistance to driveshaft and yaw rotation comes from the *positional* offsets of the nodes, not the direct rotational inertia of the elements. (This is analogous to a lumped-mass representation of the structure.) It is concluded that the only rigid-body axial rotations that contribute appreciably to the kinetic energy are the pitching of the blade elements, and the rotation of the driveshaft elements. Thus, for a blade node, we define

$$\boldsymbol{\omega}_{k/g}^g = \mathbf{T}_p^g\left(\begin{bmatrix}(\boldsymbol{\omega}_{1,b/b}^p)_X\\0\\0\end{bmatrix}+\boldsymbol{\omega}_{k/s}^p\right), \tag{3.33}$$

for a driveshaft node, excluding the pitch bearing masters,

$$\boldsymbol{\omega}_{k/g}^g = \mathbf{T}_d^g\left(\begin{bmatrix}0\\0\\(\boldsymbol{\omega}_{1,d/n}^d)_Z\end{bmatrix}+\boldsymbol{\omega}_{k/s}^d\right), \tag{3.34}$$

and for all other nodes,

$$\boldsymbol{\omega}_{k/g}^g = \mathbf{T}_B^g\boldsymbol{\omega}_{k/s}^B, \tag{3.35}$$

as the entries in $d\mathbf{x}^g_{k/g}/dt$, which multiply the mass matrix in the kinetic energy equation. All the $\boldsymbol{\omega}$ variables on the right-hand sides are elements of $\dot{\mathbf{q}}^B$.

The full rigid-body angular velocity of the body is needed in order to compute the kinetic energy associated with the positional displacement of the nodes. Taking the example of a node on one of the blades,

$$\boldsymbol{\omega}^g_{1,b/g} = \mathbf{T}^g_y \left(\boldsymbol{\omega}^y_{1,n/g} + \mathbf{T}^y_d \left(\boldsymbol{\omega}^d_{1,d/y} + \mathbf{T}^d_p \boldsymbol{\omega}^p_{1,b/d} \right) \right). \tag{3.36}$$

The time derivative of Equation 3.26 gives the positional components of $d\mathbf{x}^g_{k/g}/dt$:

$$\frac{d\mathbf{r}^g_{k/g}}{dt} = \mathbf{A}_k \mathbf{T}^g_B \frac{d\mathbf{q}^B}{dt} + \mathbf{A}_k \frac{d\mathbf{T}^g_B}{dt} \mathbf{q}^B + \mathbf{B}_k \frac{d\mathbf{T}^g_B}{dt} \mathbf{P}^B_s . \tag{3.37}$$

It can be shown, for instance Shabana [24], that

$$\frac{d\mathbf{T}^m_B}{dt} = \mathbf{T}^m_B \mathbf{S}^B_{/m} ; \quad \mathbf{S}^B_{/m} = \begin{bmatrix} 0 & -(\boldsymbol{\omega}^B_{1/m})_Z & (\boldsymbol{\omega}^B_{1/m})_Y \\ (\boldsymbol{\omega}^B_{1/m})_Z & 0 & -(\boldsymbol{\omega}^B_{1/m})_X \\ -(\boldsymbol{\omega}^B_{1/m})_Y & (\boldsymbol{\omega}^B_{1/m})_X & 0 \end{bmatrix}, \tag{3.38}$$

where $\mathbf{S}^B_{/m}$ thus consists of elements of $\dot{\mathbf{q}}^B$. Taking the example of a node on one of the blades, we can write

$$\frac{d\mathbf{T}^g_p}{dt} = \mathbf{T}^g_y \mathbf{T}^y_d \frac{d\mathbf{T}^d_p}{dt} + \mathbf{T}^g_y \frac{d\mathbf{T}^y_d}{dt} \mathbf{T}^d_p + \frac{d\mathbf{T}^g_y}{dt} \mathbf{T}^y_d \mathbf{T}^d_p , \tag{3.39}$$

or

$$\frac{d\mathbf{T}^g_p}{dt} = \mathbf{T}^g_y \mathbf{T}^y_d \mathbf{T}^d_p \mathbf{S}^p_{b/d} + \mathbf{T}^g_y \mathbf{T}^y_d \mathbf{S}^d_{d/y} \mathbf{T}^d_p + \mathbf{T}^g_y \mathbf{S}^y_{n/g} \mathbf{T}^y_d \mathbf{T}^d_p , \tag{3.40}$$

where

$$\mathbf{S}^p_{b/d} := \begin{bmatrix} 0 & -(\boldsymbol{\omega}^p_{1,b/d})_Z & (\boldsymbol{\omega}^p_{1,b/d})_Y \\ (\boldsymbol{\omega}^p_{1,b/d})_Z & 0 & -(\boldsymbol{\omega}^p_{1,b/d})_X \\ -(\boldsymbol{\omega}^p_{1,b/d})_Y & (\boldsymbol{\omega}^p_{1,b/d})_X & 0 \end{bmatrix}, \tag{3.41}$$

and so forth. Equation 3.40 can also be written

$$\frac{d\mathbf{T}^g_p}{dt} = \mathbf{T}^g_y \mathbf{T}^y_d \mathbf{T}^d_p \left(\mathbf{S}^p_{b/d} + \mathbf{T}^p_d \mathbf{S}^d_{d/y} \mathbf{T}^d_p + \mathbf{T}^p_d \mathbf{T}^d_y \mathbf{S}^y_{n/g} \mathbf{T}^y_d \mathbf{T}^d_p \right), \tag{3.42}$$

or in general for any of the bodies as

$$\frac{d\mathbf{T}^g_B}{dt} = \mathbf{T}^g_B \mathbf{S}^B , \tag{3.43}$$

with, for the blades,

$$\mathbf{S}^B := \mathbf{S}^p_{b/d} + \mathbf{T}^p_d \mathbf{S}^d_{d/y} \mathbf{T}^d_p + \mathbf{T}^p_d \mathbf{T}^d_y \mathbf{S}^y_{n/g} \mathbf{T}^y_d \mathbf{T}^d_p , \tag{3.44}$$

for the driveshaft,

$$\mathbf{S}^B := \mathbf{S}^d_{d/y} + \mathbf{T}^d_y \mathbf{S}^y_{n/g} \mathbf{T}^y_d , \tag{3.45}$$

and for the nacelle,

$$\mathbf{S}^B := \mathbf{S}^y_{n/g} . \tag{3.46}$$

Equations 3.37 and 3.31 through 3.35 can be combined in the form

$$\frac{d\mathbf{x}_{k/g}^{g}}{dt} = \tilde{\mathbf{A}}_k \mathbf{T}_B^g \frac{d\mathbf{q}^B}{dt} + \mathbf{A}_k \mathbf{T}_B^g \mathbf{S}^B \mathbf{q}^B + \mathbf{B}_k \mathbf{T}_B^g \mathbf{S}^B \mathbf{P}_s^B, \tag{3.47}$$

where $\tilde{\mathbf{A}}_k$ includes the angular velocity terms.

Now define $\mathbf{T}_B^g$ to be a matrix consisting of 3-by-3 blocks of transforms located along the diagonal, that is,

$$\mathbf{T}_B^g = \begin{bmatrix} \mathbf{I} & & & & & & \\ & \mathbf{I} & & & & & \\ & & \ddots & & & & \\ & & & \mathbf{T}_y^g & & & \\ & & & & \ddots & & \\ & & & & & \mathbf{T}_d^g & \\ & & & & & & \ddots \\ & & & & & & & \mathbf{T}_p^g \\ & & & & & & & & \ddots \end{bmatrix}. \tag{3.48}$$

Each block transforms a triplet of the degrees-of-freedom $\mathbf{q}^B$ from body to global coordinates. Then Equation 3.47 can be expanded to the entire structure, as

$$\frac{d\mathbf{x}_{/g}^{g}}{dt} = \tilde{\mathbf{A}}\mathbf{T}_B^g \frac{d\mathbf{q}^B}{dt} + \mathbf{A}\mathbf{T}_B^g \mathbf{\Sigma}^B \mathbf{q}^B + \mathbf{B}\mathbf{T}_B^g \mathbf{\Sigma}^B \mathbf{P}_s^B, \tag{3.49}$$

with

$$\mathbf{\Sigma}^B = \begin{bmatrix} \mathbf{S}^B & \mathbf{0} & \mathbf{0} & \mathbf{0} & \mathbf{0} & \mathbf{0} & \\ \mathbf{0} & \mathbf{0} & \mathbf{0} & \mathbf{0} & \mathbf{0} & \mathbf{0} & \\ \mathbf{0} & \mathbf{0} & \mathbf{S}^B & \mathbf{0} & \mathbf{0} & \mathbf{0} & \cdots \\ \mathbf{0} & \mathbf{0} & \mathbf{0} & \mathbf{0} & \mathbf{0} & \mathbf{0} & \\ \mathbf{0} & \mathbf{0} & \mathbf{0} & \mathbf{0} & \mathbf{S}^B & \mathbf{0} & \\ \mathbf{0} & \mathbf{0} & \mathbf{0} & \mathbf{0} & \mathbf{0} & \mathbf{0} & \\ & & \vdots & & & & \ddots \end{bmatrix}. \tag{3.50}$$

It is noted that Equation 3.43 still holds, in the form

$$\frac{d\mathbf{T}_B^g}{dt} = \mathbf{T}_B^g \mathbf{\Sigma}^B. \tag{3.51}$$

The time derivative of $\mathbf{\Sigma}^B$, as well as the time derivative of $\partial\mathbf{\Sigma}^B/\partial\boldsymbol{\omega}^B$, are required in the equations of motion. These are most conveniently written as

$$\frac{d\mathbf{\Sigma}^B}{dt} = \frac{\partial\mathbf{\Sigma}^B}{\partial\boldsymbol{\omega}^B}\frac{d\boldsymbol{\omega}^B}{dt} + \frac{\partial\mathbf{\Sigma}^B}{\partial\boldsymbol{\theta}^B}\boldsymbol{\omega}^B \tag{3.52}$$

and

$$\frac{d}{dt}\frac{\partial\mathbf{\Sigma}^B}{\partial\boldsymbol{\omega}^B} = \frac{\partial^2\mathbf{\Sigma}^B}{(\partial\boldsymbol{\omega}^B)^2}\frac{d\boldsymbol{\omega}^B}{dt} + \frac{\partial^2\mathbf{\Sigma}^B}{\partial\boldsymbol{\omega}^B\partial\boldsymbol{\theta}^B}\boldsymbol{\omega}^B = \frac{\partial^2\mathbf{\Sigma}^B}{\partial\boldsymbol{\omega}^B\partial\boldsymbol{\theta}^B}\boldsymbol{\omega}^B, \tag{3.53}$$

since $\partial^2\mathbf{\Sigma}^B/(\partial\boldsymbol{\omega}^B)^2 = 0$. Considering the most complicated case of a blade node, the partial derivatives are evaluated with

$$\frac{\partial \mathbf{S}^B}{\partial \boldsymbol{\omega}^B} = \frac{\partial \mathbf{S}^p_{b/d}}{\partial \boldsymbol{\omega}^B} + \mathbf{T}^p_d \frac{\partial \mathbf{S}^d_{d/y}}{\partial \boldsymbol{\omega}^B} \mathbf{T}^d_p + \mathbf{T}^p_d \mathbf{T}^d_y \frac{\partial \mathbf{S}^y_{n/g}}{\partial \boldsymbol{\omega}^B} \mathbf{T}^y_d \mathbf{T}^d_p , \tag{3.54}$$

$$\begin{aligned} \frac{\partial \mathbf{S}^B}{\partial \boldsymbol{\theta}^B} &= \mathbf{T}^p_d \mathbf{S}^d_{d/y} \frac{\partial \mathbf{T}^d_p}{\partial \boldsymbol{\theta}^B} - \left[\mathbf{T}^p_d \mathbf{S}^d_{d/y} \frac{\partial \mathbf{T}^d_p}{\partial \boldsymbol{\theta}^B} \right]^T \\ &+ \mathbf{T}^p_d \mathbf{T}^d_y \mathbf{S}^y_{n/g} \frac{\partial \mathbf{T}^y_d}{\partial \boldsymbol{\theta}^B} \mathbf{T}^d_p - \left[\mathbf{T}^p_d \mathbf{T}^d_y \mathbf{S}^y_{n/g} \frac{\partial \mathbf{T}^y_d}{\partial \boldsymbol{\theta}^B} \mathbf{T}^d_p \right]^T \\ &+ \mathbf{T}^p_d \mathbf{T}^d_y \mathbf{S}^y_{n/g} \mathbf{T}^y_d \frac{\partial \mathbf{T}^d_p}{\partial \boldsymbol{\theta}^B} - \left[\mathbf{T}^p_d \mathbf{T}^d_y \mathbf{S}^y_{n/g} \mathbf{T}^y_d \frac{\partial \mathbf{T}^d_p}{\partial \boldsymbol{\theta}^B} \right]^T , \end{aligned} \tag{3.55}$$

$$\begin{aligned} \frac{\partial^2 \mathbf{S}^B}{\partial \boldsymbol{\omega}^B \partial \boldsymbol{\theta}^B} &= \mathbf{T}^p_d \frac{\partial \mathbf{S}^d_{d/y}}{\partial \boldsymbol{\omega}^B} \frac{\partial \mathbf{T}^d_p}{\partial \boldsymbol{\theta}^B} - \left[\mathbf{T}^p_d \frac{\partial \mathbf{S}^d_{d/y}}{\partial \boldsymbol{\omega}^B} \frac{\partial \mathbf{T}^d_p}{\partial \boldsymbol{\theta}^B} \right]^T \\ &+ \mathbf{T}^p_d \mathbf{T}^d_y \frac{\partial \mathbf{S}^y_{n/g}}{\partial \boldsymbol{\omega}^B} \frac{\partial \mathbf{T}^y_d}{\partial \boldsymbol{\theta}^B} \mathbf{T}^d_p - \left[\mathbf{T}^p_d \mathbf{T}^d_y \frac{\partial \mathbf{S}^y_{n/g}}{\partial \boldsymbol{\omega}^B} \frac{\partial \mathbf{T}^y_d}{\partial \boldsymbol{\theta}^B} \mathbf{T}^d_p \right]^T \\ &+ \mathbf{T}^p_d \mathbf{T}^d_y \frac{\partial \mathbf{S}^y_{n/g}}{\partial \boldsymbol{\omega}^B} \mathbf{T}^y_d \frac{\partial \mathbf{T}^d_p}{\partial \boldsymbol{\theta}^B} - \left[\mathbf{T}^p_d \mathbf{T}^d_y \frac{\partial \mathbf{S}^y_{n/g}}{\partial \boldsymbol{\omega}^B} \mathbf{T}^y_d \frac{\partial \mathbf{T}^d_p}{\partial \boldsymbol{\theta}^B} \right]^T , \end{aligned} \tag{3.56}$$

and

$$\begin{aligned} \frac{\partial^3 \mathbf{S}^B}{\partial \boldsymbol{\omega}^B \partial \psi \partial \boldsymbol{\theta}^B} &= \mathbf{T}^p_d \frac{\partial \mathbf{T}^d_y}{\partial \psi} \frac{\partial \mathbf{S}^y_{n/g}}{\partial \boldsymbol{\omega}^B} \frac{\partial \mathbf{T}^y_d}{\partial \boldsymbol{\theta}^B} \mathbf{T}^d_p - \left[\mathbf{T}^p_d \frac{\partial \mathbf{T}^d_y}{\partial \psi} \frac{\partial \mathbf{S}^y_{n/g}}{\partial \boldsymbol{\omega}^B} \frac{\partial \mathbf{T}^y_d}{\partial \boldsymbol{\theta}^B} \mathbf{T}^d_p \right]^T \\ &+ \mathbf{T}^p_d \mathbf{T}^d_y \frac{\partial \mathbf{S}^y_{n/g}}{\partial \boldsymbol{\omega}^B} \frac{\partial^2 \mathbf{T}^y_d}{\partial \psi \partial \boldsymbol{\theta}^B} \mathbf{T}^d_p - \left[\mathbf{T}^p_d \mathbf{T}^d_y \frac{\partial \mathbf{S}^y_{n/g}}{\partial \boldsymbol{\omega}^B} \frac{\partial^2 \mathbf{T}^y_d}{\partial \psi \partial \boldsymbol{\theta}^B} \mathbf{T}^d_p \right]^T \\ &+ \mathbf{T}^p_d \frac{\partial \mathbf{T}^d_y}{\partial \psi} \frac{\partial \mathbf{S}^y_{n/g}}{\partial \boldsymbol{\omega}^B} \mathbf{T}^y_d \frac{\partial \mathbf{T}^d_p}{\partial \boldsymbol{\theta}^B} - \left[\mathbf{T}^p_d \frac{\partial \mathbf{T}^d_y}{\partial \psi} \frac{\partial \mathbf{S}^y_{n/g}}{\partial \boldsymbol{\omega}^B} \mathbf{T}^y_d \frac{\partial \mathbf{T}^d_p}{\partial \boldsymbol{\theta}^B} \right]^T \\ &+ \mathbf{T}^p_d \mathbf{T}^d_y \frac{\partial \mathbf{S}^y_{n/g}}{\partial \boldsymbol{\omega}^B} \frac{\partial \mathbf{T}^y_d}{\partial \psi} \frac{\partial \mathbf{T}^d_p}{\partial \boldsymbol{\theta}^B} - \left[\mathbf{T}^p_d \mathbf{T}^d_y \frac{\partial \mathbf{S}^y_{n/g}}{\partial \boldsymbol{\omega}^B} \frac{\partial \mathbf{T}^y_d}{\partial \psi} \frac{\partial \mathbf{T}^d_p}{\partial \boldsymbol{\theta}^B} \right]^T . \end{aligned} \tag{3.57}$$

In deriving the above, we have used the fact that $(\mathbf{S}^B_{/m})^T = -\mathbf{S}^B_{/m}$. Equivalent expressions can be derived by using

$$\begin{aligned} &\frac{d\mathbf{T}^p_d}{dt} = (\mathbf{S}^p_{b/d})^T \mathbf{T}^p_d , \quad \frac{d\mathbf{T}^d_p}{dt} = \mathbf{T}^d_p \mathbf{S}^p_{b/d} , \\ &\frac{d\mathbf{T}^d_y}{dt} = (\mathbf{S}^d_{d/y})^T \mathbf{T}^d_y , \quad \text{and} \quad \frac{d\mathbf{T}^y_d}{dt} = \mathbf{T}^y_d \mathbf{S}^d_{d/y} , \end{aligned} \tag{3.58}$$

which leads to

$$\begin{aligned}\frac{d\mathbf{S}^B}{dt} &= \frac{d\mathbf{S}^p_{b/d}}{dt} + \mathbf{T}^p_d \frac{d\mathbf{S}^d_{d/y}}{dt}\mathbf{T}^d_p + \mathbf{T}^p_d\mathbf{T}^d_y \frac{d\mathbf{S}^y_{n/g}}{dt}\mathbf{T}^y_d\mathbf{T}^d_p \\ &+ \mathbf{T}^p_d\mathbf{S}^d_{d/y}\mathbf{T}^d_p\mathbf{S}^p_{b/d} - \left[\mathbf{T}^p_d\mathbf{S}^d_{d/y}\mathbf{T}^d_p\mathbf{S}^p_{b/d}\right]^T \\ &+ \mathbf{T}^p_d\mathbf{T}^d_y\mathbf{S}^y_{n/g}\mathbf{T}^y_d\mathbf{T}^d_p\mathbf{S}^p_{b/d} - \left[\mathbf{T}^p_d\mathbf{T}^d_y\mathbf{S}^y_{n/g}\mathbf{T}^y_d\mathbf{T}^d_p\mathbf{S}^p_{b/d}\right]^T \\ &+ \mathbf{T}^p_d\mathbf{T}^d_y\mathbf{S}^y_{n/g}\mathbf{T}^y_d\mathbf{S}^d_{d/y}\mathbf{T}^d_p - \left[\mathbf{T}^p_d\mathbf{T}^d_y\mathbf{S}^y_{n/g}\mathbf{T}^y_d\mathbf{S}^d_{d/y}\mathbf{T}^d_p\right]^T.\end{aligned} \tag{3.59}$$

and

$$\begin{aligned}\frac{d}{dt}\frac{\partial\mathbf{S}^B}{\partial\boldsymbol{\omega}^B} &= \mathbf{T}^p_d\frac{\partial\mathbf{S}^d_{d/y}}{\partial\boldsymbol{\omega}^B}\mathbf{T}^d_p\mathbf{S}^p_{b/d} - \left[\mathbf{T}^p_d\frac{\partial\mathbf{S}^d_{d/y}}{\partial\boldsymbol{\omega}^B}\mathbf{T}^d_p\mathbf{S}^p_{b/d}\right]^T \\ &+ \mathbf{T}^p_d\mathbf{T}^d_y\frac{\partial\mathbf{S}^y_{n/g}}{\partial\boldsymbol{\omega}^B}\mathbf{T}^y_d\mathbf{T}^d_p\mathbf{S}^p_{b/d} - \left[\mathbf{T}^p_d\mathbf{T}^d_y\frac{\partial\mathbf{S}^y_{n/g}}{\partial\boldsymbol{\omega}^B}\mathbf{T}^y_d\mathbf{T}^d_p\mathbf{S}^p_{b/d}\right]^T \\ &+ \mathbf{T}^p_d\mathbf{T}^d_y\frac{\partial\mathbf{S}^y_{n/g}}{\partial\boldsymbol{\omega}^B}\mathbf{T}^y_d\mathbf{S}^d_{d/y}\mathbf{T}^d_p - \left[\mathbf{T}^p_d\mathbf{T}^d_y\frac{\partial\mathbf{S}^y_{n/g}}{\partial\boldsymbol{\omega}^B}\mathbf{T}^y_d\mathbf{S}^d_{d/y}\mathbf{T}^d_p\right]^T.\end{aligned} \tag{3.60}$$

Note that

$$\frac{d}{dt}\frac{\partial\boldsymbol{\Sigma}^B}{\partial\boldsymbol{\omega}^B} \neq \frac{\partial}{\partial\boldsymbol{\omega}^B}\frac{d\boldsymbol{\Sigma}^B}{dt}; \tag{3.61}$$

the latter contains additional terms.

Using Equation 3.49, the kinetic energy is written as

$$\begin{aligned}E_K = \frac{1}{2}&\left[\frac{d(\mathbf{q}^B)^T}{dt}\mathbf{T}^B_g\tilde{\mathbf{A}}^T + (\mathbf{q}^B)^T(\boldsymbol{\Sigma}^B)^T\mathbf{T}^B_g\mathbf{A}^T + (\mathbf{P}^B_s)^T(\boldsymbol{\Sigma}^B)^T\mathbf{T}^B_g\mathbf{B}^T\right]\mathbf{T}^g_B\mathbf{M}^B\mathbf{T}^B_g \\ &\times\left[\tilde{\mathbf{A}}\mathbf{T}^g_B\frac{d\mathbf{q}^B}{dt} + \mathbf{A}\mathbf{T}^g_B\boldsymbol{\Sigma}^B\mathbf{q}^B + \mathbf{B}\mathbf{T}^g_B\boldsymbol{\Sigma}^B\mathbf{P}^B_s\right].\end{aligned} \tag{3.62}$$

It is convenient to define

$$\mathbf{A}^B := \mathbf{T}^B_g\mathbf{A}\mathbf{T}^g_B; \quad \tilde{\mathbf{A}}^B := \mathbf{T}^B_g\tilde{\mathbf{A}}\mathbf{T}^g_B; \quad \text{and} \quad \mathbf{B}^B := \mathbf{T}^B_g\mathbf{B}\mathbf{T}^g_B, \tag{3.63}$$

noting that these now become functions of the reference node orientations and joint angles. By Equation 3.51, their time derivatives are of the form

$$\frac{d\mathbf{A}^B}{dt} = (\boldsymbol{\Sigma}^B)^T\mathbf{A}^B + \mathbf{A}^B\boldsymbol{\Sigma}^B. \tag{3.64}$$

Then

$$\begin{aligned}E_K = \frac{1}{2}&\left[\frac{d(\mathbf{q}^B)^T}{dt}(\tilde{\mathbf{A}}^B)^T + (\mathbf{q}^B)^T(\boldsymbol{\Sigma}^B)^T(\mathbf{A}^B)^T + (\mathbf{P}^B_s)^T(\boldsymbol{\Sigma}^B)^T(\mathbf{B}^B)^T\right]\mathbf{M}^B \\ &\times\left[\tilde{\mathbf{A}}^B\frac{d\mathbf{q}^B}{dt} + \mathbf{A}^B\boldsymbol{\Sigma}^B\mathbf{q}^B + \mathbf{B}^B\boldsymbol{\Sigma}^B\mathbf{P}^B_s\right].\end{aligned} \tag{3.65}$$

The first term in the Lagrange equations is

$$\frac{d}{dt}\left(\frac{\partial E_K}{\partial \dot{\mathbf{q}}^B}\right) = \frac{d}{dt}\left\{\left[(\tilde{\mathbf{A}}^B)^T + (\mathbf{q}^B)^T \frac{\partial(\boldsymbol{\Sigma}^B)^T}{\partial \dot{\mathbf{q}}^B}(\mathbf{A}^B)^T + (\mathbf{P}_s^B)^T \frac{\partial(\boldsymbol{\Sigma}^B)^T}{\partial \dot{\mathbf{q}}^B}(\mathbf{B}^B)^T\right]\mathbf{M}^B \times \left[\tilde{\mathbf{A}}^B \frac{d\mathbf{q}^B}{dt} + \mathbf{A}^B\boldsymbol{\Sigma}^B\mathbf{q}^B + \mathbf{B}^B\boldsymbol{\Sigma}^B\mathbf{P}_s^B\right]\right\}. \tag{3.66}$$

where we have taken advantage of the symmetry of $\mathbf{M}^B$ to eliminate the 1/2 factor. Performing the time derivative, using Equation 3.64 for the time derivatives of $\mathbf{A}^B$, $\tilde{\mathbf{A}}^B$, and $\mathbf{B}^B$, and multiplying out the terms gives 57 terms. The first term is the mass times the acceleration,

$$(\tilde{\mathbf{A}}^B)^T\mathbf{M}^B\tilde{\mathbf{A}}^B\frac{d^2\mathbf{q}^B}{dt^2}\ldots$$

There are two terms involving angular accelerations and positional offsets,

$$+(\tilde{\mathbf{A}}^B)^T\mathbf{M}^B\mathbf{A}^B\frac{d\boldsymbol{\Sigma}^B}{dt}\mathbf{q}^B + (\tilde{\mathbf{A}}^B)^T\mathbf{M}^B\mathbf{B}^B\frac{d\boldsymbol{\Sigma}^B}{dt}\mathbf{P}_s^B\ldots$$

Five terms contain coriolis forces,

$$+(\tilde{\mathbf{A}}^B)^T\mathbf{M}^B\mathbf{A}^B\boldsymbol{\Sigma}^B\frac{d\mathbf{q}^B}{dt} + (\boldsymbol{\Sigma}^B)^T(\tilde{\mathbf{A}}^B)^T\mathbf{M}^B\tilde{\mathbf{A}}^B\frac{d\mathbf{q}^B}{dt} + (\tilde{\mathbf{A}}^B)^T\boldsymbol{\Sigma}^B\mathbf{M}^B\tilde{\mathbf{A}}^B\frac{d\mathbf{q}^B}{dt}$$
$$+(\tilde{\mathbf{A}}^B)^T\mathbf{M}^B(\boldsymbol{\Sigma}^B)^T\tilde{\mathbf{A}}^B\frac{d\mathbf{q}^B}{dt} + (\tilde{\mathbf{A}}^B)^T\mathbf{M}^B\tilde{\mathbf{A}}^B\boldsymbol{\Sigma}^B\frac{d\mathbf{q}^B}{dt}\ldots$$

and eight contain centrifugal forces, four accounting for the offset due to displacement and four the offset of the nodes in the undisplaced position,

$$+(\boldsymbol{\Sigma}^B)^T(\tilde{\mathbf{A}}^B)^T\mathbf{M}^B\mathbf{A}^B\boldsymbol{\Sigma}^B\mathbf{q}^B + (\tilde{\mathbf{A}}^B)^T\boldsymbol{\Sigma}^B\mathbf{M}^B\mathbf{A}^B\boldsymbol{\Sigma}^B\mathbf{q}^B$$
$$+(\tilde{\mathbf{A}}^B)^T\mathbf{M}^B(\boldsymbol{\Sigma}^B)^T\mathbf{A}^B\boldsymbol{\Sigma}^B\mathbf{q}^B + (\tilde{\mathbf{A}}^B)^T\mathbf{M}^B\mathbf{A}^B\boldsymbol{\Sigma}^B\boldsymbol{\Sigma}^B\mathbf{q}^B$$
$$+(\boldsymbol{\Sigma}^B)^T(\tilde{\mathbf{A}}^B)^T\mathbf{M}^B\mathbf{B}^B\boldsymbol{\Sigma}^B\mathbf{P}_s^B + (\tilde{\mathbf{A}}^B)^T\boldsymbol{\Sigma}^B\mathbf{M}^B\mathbf{B}^B\boldsymbol{\Sigma}^B\mathbf{P}_s^B$$
$$+(\tilde{\mathbf{A}}^B)^T\mathbf{M}^B(\boldsymbol{\Sigma}^B)^T\mathbf{B}^B\boldsymbol{\Sigma}^B\mathbf{P}_s^B + (\tilde{\mathbf{A}}^B)^T\mathbf{M}^B\mathbf{B}^B\boldsymbol{\Sigma}^B\boldsymbol{\Sigma}^B\mathbf{P}_s^B\ldots$$

The above 16 terms appear in all the equations. The remaining 41 terms all contain

$$\frac{\partial(\boldsymbol{\Sigma}^B)^T}{\partial\dot{\mathbf{q}}^B} = \frac{\partial(\boldsymbol{\Sigma}^B)^T}{\partial\boldsymbol{\omega}^B},$$

since $\boldsymbol{\Sigma}^B$ is a function of the angular velocity of the reference node on each body. As a consequence, these terms appear only in the rows of equations associated with rotations of the reference nodes, and are zero for the rows associated with linear displacements of the reference nodes, as well as elastic deformations. The 41 terms can be organized into two which involve accelerations,

$$+(\mathbf{q}^B)^T\frac{\partial(\boldsymbol{\Sigma}^B)^T}{\partial\boldsymbol{\omega}^B}(\mathbf{A}^B)^T\mathbf{M}^B\tilde{\mathbf{A}}^B\frac{d^2\mathbf{q}^B}{dt^2} + (\mathbf{P}_s^B)^T\frac{\partial(\boldsymbol{\Sigma}^B)^T}{\partial\boldsymbol{\omega}^B}(\mathbf{B}^B)^T\mathbf{M}^B\tilde{\mathbf{A}}^B\frac{d^2\mathbf{q}^B}{dt^2}\ldots$$

four which involve angular accelerations,

$$+(\mathbf{q}^B)^T\frac{\partial(\boldsymbol{\Sigma}^B)^T}{\partial\boldsymbol{\omega}^B}(\mathbf{A}^B)^T\mathbf{M}^B\mathbf{A}^B\frac{d\boldsymbol{\Sigma}^B}{dt}\mathbf{q}^B + (\mathbf{q}^B)^T\frac{\partial(\boldsymbol{\Sigma}^B)^T}{\partial\boldsymbol{\omega}^B}(\mathbf{A}^B)^T\mathbf{M}^B\mathbf{B}^B\frac{d\boldsymbol{\Sigma}^B}{dt}\mathbf{P}_s^B$$
$$+(\mathbf{P}_s^B)^T\frac{\partial(\boldsymbol{\Sigma}^B)^T}{\partial\boldsymbol{\omega}^B}(\mathbf{B}^B)^T\mathbf{M}^B\mathbf{A}^B\frac{d\boldsymbol{\Sigma}^B}{dt}\mathbf{q}^B + (\mathbf{P}_s^B)^T\frac{\partial(\boldsymbol{\Sigma}^B)^T}{\partial\boldsymbol{\omega}^B}(\mathbf{B}^B)^T\mathbf{M}^B\mathbf{B}^B\frac{d\boldsymbol{\Sigma}^B}{dt}\mathbf{P}_s^B\ldots$$

one with quadratic terms in the velocities,

$$+\frac{d(\mathbf{q}^B)^T}{dt}\frac{\partial(\boldsymbol{\Sigma}^B)^T}{\partial\boldsymbol{\omega}^B}(\mathbf{A}^B)^T\mathbf{M}^B\tilde{\mathbf{A}}^B\frac{d\mathbf{q}^B}{dt}\ldots$$

seven with coupling between displacements and velocities,

$$+(\mathbf{q}^B)^T \frac{\partial(\mathbf{\Sigma}^B)^T}{\partial \boldsymbol{\omega}^B}(\mathbf{A}^B)^T \mathbf{M}^B \mathbf{A}^B \mathbf{\Sigma}^B \frac{d\mathbf{q}^B}{dt} + \frac{d(\mathbf{q}^B)^T}{dt}\frac{\partial(\mathbf{\Sigma}^B)^T}{\partial \boldsymbol{\omega}^B}(\mathbf{A}^B)^T \mathbf{M}^B \mathbf{A}^B \mathbf{\Sigma}^B \mathbf{q}^B$$

$$+(\mathbf{q}^B)^T \frac{\partial(\mathbf{\Sigma}^B)^T}{\partial \boldsymbol{\omega}^B}(\mathbf{\Sigma}^B)^T(\mathbf{A}^B)^T \mathbf{M}^B \tilde{\mathbf{A}}^B \frac{d\mathbf{q}^B}{dt} + (\mathbf{q}^B)^T \frac{\partial(\mathbf{\Sigma}^B)^T}{\partial \boldsymbol{\omega}^B}(\mathbf{A}^B)^T \mathbf{\Sigma}^B \mathbf{M}^B \tilde{\mathbf{A}}^B \frac{d\mathbf{q}^B}{dt}$$

$$+(\mathbf{q}^B)^T \frac{\partial(\mathbf{\Sigma}^B)^T}{\partial \boldsymbol{\omega}^B}(\mathbf{A}^B)^T \mathbf{M}^B (\mathbf{\Sigma}^B)^T \tilde{\mathbf{A}}^B \frac{d\mathbf{q}^B}{dt} + (\mathbf{q}^B)^T \frac{\partial(\mathbf{\Sigma}^B)^T}{\partial \boldsymbol{\omega}^B}(\mathbf{A}^B)^T \mathbf{M}^B \tilde{\mathbf{A}}^B \mathbf{\Sigma}^B \frac{d\mathbf{q}^B}{dt}$$

$$+(\mathbf{q}^B)^T \left(\frac{d}{dt}\frac{\partial(\mathbf{\Sigma}^B)^T}{\partial \boldsymbol{\omega}^B}\right)(\mathbf{A}^B)^T \mathbf{M}^B \tilde{\mathbf{A}}^B \frac{d\mathbf{q}^B}{dt} \ldots$$

seven with coupling between velocities and positional offsets,

$$+(\mathbf{P}_s^B)^T \frac{\partial(\mathbf{\Sigma}^B)^T}{\partial \boldsymbol{\omega}^B}(\mathbf{\Sigma}^B)^T(\mathbf{B}^B)^T \mathbf{M}^B \tilde{\mathbf{A}}^B \frac{d\mathbf{q}^B}{dt} + (\mathbf{P}_s^B)^T \frac{\partial(\mathbf{\Sigma}^B)^T}{\partial \boldsymbol{\omega}^B}(\mathbf{B}^B)^T \mathbf{\Sigma}^B \mathbf{M}^B \tilde{\mathbf{A}}^B \frac{d\mathbf{q}^B}{dt}$$

$$+\frac{d(\mathbf{q}^B)^T}{dt}\frac{\partial(\mathbf{\Sigma}^B)^T}{\partial \boldsymbol{\omega}^B}(\mathbf{A}^B)^T \mathbf{M}^B \mathbf{B}^B \mathbf{\Sigma}^B \mathbf{P}_s^B + (\mathbf{P}_s^B)^T \frac{\partial(\mathbf{\Sigma}^B)^T}{\partial \boldsymbol{\omega}^B}(\mathbf{B}^B)^T \mathbf{M}^B \mathbf{A}^B \mathbf{\Sigma}^B \frac{d\mathbf{q}^B}{dt}$$

$$+(\mathbf{P}_s^B)^T \frac{\partial(\mathbf{\Sigma}^B)^T}{\partial \boldsymbol{\omega}^B}(\mathbf{B}^B)^T \mathbf{M}^B (\mathbf{\Sigma}^B)^T \tilde{\mathbf{A}}^B \frac{d\mathbf{q}^B}{dt} + (\mathbf{P}_s^B)^T \frac{\partial(\mathbf{\Sigma}^B)^T}{\partial \boldsymbol{\omega}^B}(\mathbf{B}^B)^T \mathbf{M}^B \tilde{\mathbf{A}}^B \mathbf{\Sigma}^B \frac{d\mathbf{q}^B}{dt}$$

$$+(\mathbf{P}_s^B)^T \left(\frac{d}{dt}\frac{\partial(\mathbf{\Sigma}^B)^T}{\partial \boldsymbol{\omega}^B}\right)(\mathbf{B}^B)^T \mathbf{M}^B \tilde{\mathbf{A}}^B \frac{d\mathbf{q}^B}{dt} \ldots$$

five with quadratic terms in displacements,

$$+(\mathbf{q}^B)^T \frac{\partial(\mathbf{\Sigma}^B)^T}{\partial \boldsymbol{\omega}^B}(\mathbf{\Sigma}^B)^T(\mathbf{A}^B)^T \mathbf{M}^B \mathbf{A}^B \mathbf{\Sigma}^B \mathbf{q}^B + (\mathbf{q}^B)^T \frac{\partial(\mathbf{\Sigma}^B)^T}{\partial \boldsymbol{\omega}^B}(\mathbf{A}^B)^T \mathbf{\Sigma}^B \mathbf{M}^B \mathbf{A}^B \mathbf{\Sigma}^B \mathbf{q}^B$$

$$+(\mathbf{q}^B)^T \frac{\partial(\mathbf{\Sigma}^B)^T}{\partial \boldsymbol{\omega}^B}(\mathbf{A}^B)^T \mathbf{M}^B (\mathbf{\Sigma}^B)^T \mathbf{A}^B \mathbf{\Sigma}^B \mathbf{q}^B + (\mathbf{q}^B)^T \frac{\partial(\mathbf{\Sigma}^B)^T}{\partial \boldsymbol{\omega}^B}(\mathbf{A}^B)^T \mathbf{M}^B \mathbf{A}^B \mathbf{\Sigma}^B \mathbf{\Sigma}^B \mathbf{q}^B$$

$$+(\mathbf{q}^B)^T \left(\frac{d}{dt}\frac{\partial(\mathbf{\Sigma}^B)^T}{\partial \boldsymbol{\omega}^B}\right)(\mathbf{A}^B)^T \mathbf{M}^B \mathbf{A}^B \mathbf{\Sigma}^B \mathbf{q}^B \ldots$$

ten with coupling between displacments and positional offsets,

$$+(\mathbf{P}_s^B)^T \frac{\partial(\mathbf{\Sigma}^B)^T}{\partial \boldsymbol{\omega}^B}(\mathbf{\Sigma}^B)^T(\mathbf{B}^B)^T \mathbf{M}^B \mathbf{A}^B \mathbf{\Sigma}^B \mathbf{q}^B + (\mathbf{P}_s^B)^T \frac{\partial(\mathbf{\Sigma}^B)^T}{\partial \boldsymbol{\omega}^B}(\mathbf{B}^B)^T \mathbf{\Sigma}^B \mathbf{M}^B \mathbf{A}^B \mathbf{\Sigma}^B \mathbf{q}^B$$

$$+(\mathbf{q}^B)^T \frac{\partial(\mathbf{\Sigma}^B)^T}{\partial \boldsymbol{\omega}^B}(\mathbf{\Sigma}^B)^T(\mathbf{A}^B)^T \mathbf{M}^B \mathbf{B}^B \mathbf{\Sigma}^B \mathbf{P}_s^B + (\mathbf{q}^B)^T \frac{\partial(\mathbf{\Sigma}^B)^T}{\partial \boldsymbol{\omega}^B}(\mathbf{A}^B)^T \mathbf{\Sigma}^B \mathbf{M}^B \mathbf{B}^B \mathbf{\Sigma}^B \mathbf{P}_s^B$$

$$+(\mathbf{q}^B)^T \frac{\partial(\mathbf{\Sigma}^B)^T}{\partial \boldsymbol{\omega}^B}(\mathbf{A}^B)^T \mathbf{M}^B (\mathbf{\Sigma}^B)^T \mathbf{B}^B \mathbf{\Sigma}^B \mathbf{P}_s^B + (\mathbf{q}^B)^T \frac{\partial(\mathbf{\Sigma}^B)^T}{\partial \boldsymbol{\omega}^B}(\mathbf{A}^B)^T \mathbf{M}^B \mathbf{B}^B \mathbf{\Sigma}^B \mathbf{\Sigma}^B \mathbf{P}_s^B$$

$$+(\mathbf{P}_s^B)^T \frac{\partial(\mathbf{\Sigma}^B)^T}{\partial \boldsymbol{\omega}^B}(\mathbf{B}^B)^T \mathbf{M}^B (\mathbf{\Sigma}^B)^T \mathbf{A}^B \mathbf{\Sigma}^B \mathbf{q}^B + (\mathbf{P}_s^B)^T \frac{\partial(\mathbf{\Sigma}^B)^T}{\partial \boldsymbol{\omega}^B}(\mathbf{B}^B)^T \mathbf{M}^B \mathbf{A}^B \mathbf{\Sigma}^B \mathbf{\Sigma}^B \mathbf{q}^B$$

$$+(\mathbf{q}^B)^T \left(\frac{d}{dt}\frac{\partial(\mathbf{\Sigma}^B)^T}{\partial \boldsymbol{\omega}^B}\right)(\mathbf{A}^B)^T \mathbf{M}^B \mathbf{B}^B \mathbf{\Sigma}^B \mathbf{P}_s^B + (\mathbf{P}_s^B)^T \left(\frac{d}{dt}\frac{\partial(\mathbf{\Sigma}^B)^T}{\partial \boldsymbol{\omega}^B}\right)(\mathbf{B}^B)^T \mathbf{M}^B \mathbf{A}^B \mathbf{\Sigma}^B \mathbf{q}^B \ldots$$

and, finally, five with quadratic terms in the positional offsets,

$$+(\mathbf{P}_s^B)^T \frac{\partial(\mathbf{\Sigma}^B)^T}{\partial \boldsymbol{\omega}^B}(\mathbf{\Sigma}^B)^T(\mathbf{B}^B)^T\mathbf{M}^B\mathbf{B}^B\mathbf{\Sigma}^B\mathbf{P}_s^B + (\mathbf{P}_s^B)^T \frac{\partial(\mathbf{\Sigma}^B)^T}{\partial \boldsymbol{\omega}^B}(\mathbf{B}^B)^T\mathbf{\Sigma}^B\mathbf{M}^B\mathbf{B}^B\mathbf{\Sigma}^B\mathbf{P}_s^B$$
$$+(\mathbf{P}_s^B)^T \frac{\partial(\mathbf{\Sigma}^B)^T}{\partial \boldsymbol{\omega}^B}(\mathbf{B}^B)^T\mathbf{M}^B(\mathbf{\Sigma}^B)^T\mathbf{B}^B\mathbf{\Sigma}^B\mathbf{P}_s^B + (\mathbf{P}_s^B)^T \frac{\partial(\mathbf{\Sigma}^B)^T}{\partial \boldsymbol{\omega}^B}(\mathbf{B}^B)^T\mathbf{M}^B\mathbf{B}^B\mathbf{\Sigma}^B\mathbf{\Sigma}^B\mathbf{P}_s^B$$
$$+(\mathbf{P}_s^B)^T \left(\frac{d}{dt}\frac{\partial(\mathbf{\Sigma}^B)^T}{\partial \boldsymbol{\omega}^B}\right)(\mathbf{B}^B)^T\mathbf{M}^B\mathbf{B}^B\mathbf{\Sigma}^B\mathbf{P}_s^B.$$

The next term in the Lagrange equations is

$$-\frac{\partial E_K}{\partial \mathbf{q}^B}.$$

This evaluates to 18 terms. Three of these appear in every equation, and represent centrifugal and coriolis forces:

$$-(\mathbf{\Sigma}^B)^T(\mathbf{A}^B)^T\mathbf{M}^B\mathbf{A}^B\mathbf{\Sigma}^B\mathbf{q}^B - (\mathbf{\Sigma}^B)^T(\mathbf{A}^B)^T\mathbf{M}^B\mathbf{B}^B\mathbf{\Sigma}^B\mathbf{P}_s^B - (\mathbf{\Sigma}^B)^T(\mathbf{A}^B)^T\mathbf{M}^B\tilde{\mathbf{A}}^B\frac{d\mathbf{q}^B}{dt}...$$

The remaining 15 terms appear in the rows of equations associated with reference node rotations. They include one term which is quadratic in the velocities,

$$-\frac{d(\mathbf{q}^B)^T}{dt}\frac{\partial(\tilde{\mathbf{A}}^B)^T}{\partial \mathbf{q}^B}\mathbf{M}^B\tilde{\mathbf{A}}^B\frac{d\mathbf{q}^B}{dt}...$$

three with coupling between displacements and velocities,

$$-(\mathbf{q}^B)^T\frac{\partial(\mathbf{\Sigma}^B)^T}{\partial \mathbf{q}^B}(\mathbf{A}^B)^T\mathbf{M}^B\tilde{\mathbf{A}}^B\frac{d\mathbf{q}^B}{dt} - (\mathbf{q}^B)^T(\mathbf{\Sigma}^B)^T\frac{\partial(\mathbf{A}^B)^T}{\partial \mathbf{q}^B}\mathbf{M}^B\tilde{\mathbf{A}}^B\frac{d\mathbf{q}^B}{dt}$$
$$-\frac{d(\mathbf{q}^B)^T}{dt}\frac{\partial(\tilde{\mathbf{A}}^B)^T}{\partial \mathbf{q}^B}\mathbf{M}^B\mathbf{A}^B\mathbf{\Sigma}^B\mathbf{q}^B...$$

three with coupling between the positional offsets and velocities,

$$-(\mathbf{P}_s^B)^T\frac{\partial(\mathbf{\Sigma}^B)^T}{\partial \mathbf{q}^B}(\mathbf{B}^B)^T\mathbf{M}^B\tilde{\mathbf{A}}^B\frac{d\mathbf{q}^B}{dt} - (\mathbf{P}_s^B)^T(\mathbf{\Sigma}^B)^T\frac{\partial(\mathbf{B}^B)^T}{\partial \mathbf{q}^B}\mathbf{M}^B\tilde{\mathbf{A}}^B\frac{d\mathbf{q}^B}{dt}$$
$$-\frac{d(\mathbf{q}^B)^T}{dt}\frac{\partial(\tilde{\mathbf{A}}^B)^T}{\partial \mathbf{q}^B}\mathbf{M}^B\mathbf{B}^B\mathbf{\Sigma}^B\mathbf{P}_s^B...$$

two which are quadratic in the displacements,

$$-(\mathbf{q}^B)^T\frac{\partial(\mathbf{\Sigma}^B)^T}{\partial \mathbf{q}^B}(\mathbf{A}^B)^T\mathbf{M}^B\mathbf{A}^B\mathbf{\Sigma}^B\mathbf{q}^B - (\mathbf{q}^B)^T(\mathbf{\Sigma}^B)^T\frac{\partial(\mathbf{A}^B)^T}{\partial \mathbf{q}^B}\mathbf{M}^B\mathbf{A}^B\mathbf{\Sigma}^B\mathbf{q}^B...$$

four which couple displacements and positional offsets,

$$-(\mathbf{P}_s^B)^T\frac{\partial(\mathbf{\Sigma}^B)^T}{\partial \mathbf{q}^B}(\mathbf{B}^B)^T\mathbf{M}^B\mathbf{A}^B\mathbf{\Sigma}^B\mathbf{q}^B - (\mathbf{P}_s^B)^T(\mathbf{\Sigma}^B)^T\frac{\partial(\mathbf{B}^B)^T}{\partial \mathbf{q}^B}\mathbf{M}^B\mathbf{A}^B\mathbf{\Sigma}^B\mathbf{q}^B$$
$$-(\mathbf{q}^B)^T\frac{\partial(\mathbf{\Sigma}^B)^T}{\partial \mathbf{q}^B}(\mathbf{A}^B)^T\mathbf{M}^B\mathbf{B}^B\mathbf{\Sigma}^B\mathbf{P}_s^B - (\mathbf{q}^B)^T(\mathbf{\Sigma}^B)^T\frac{\partial(\mathbf{A}^B)^T}{\partial \mathbf{q}^B}\mathbf{M}^B\mathbf{B}^B\mathbf{\Sigma}^B\mathbf{P}_s^B...$$

and finally, two which are quadratic in the positional offsets,

$$-(\mathbf{P}_s^B)^T\frac{\partial(\mathbf{\Sigma}^B)^T}{\partial \mathbf{q}^B}(\mathbf{B}^B)^T\mathbf{M}^B\mathbf{B}^B\mathbf{\Sigma}^B\mathbf{P}_s^B - (\mathbf{P}_s^B)^T(\mathbf{\Sigma}^B)^T\frac{\partial(\mathbf{B}^B)^T}{\partial \mathbf{q}^B}\mathbf{M}^B\mathbf{B}^B\mathbf{\Sigma}^B\mathbf{P}_s^B.$$

3.2.2 Damping (Dissipated) Energy

The rate of energy dissipated due to the equivalent viscous damping, resulting from elastic deformation of an element, can be written

$$\frac{1}{2}\dot{E}_D = \frac{1}{2}\frac{d(\mathbf{w}^B)^T}{dt}\left[\sum_{k=1}^{Ne}\mathbf{T}_{s,k}^B\mathbf{c}_{e,k}^s\mathbf{T}_{B,k}^s\right]\frac{d\mathbf{w}^B}{dt} = \frac{1}{2}\frac{d(\mathbf{w}^B)^T}{dt}\mathbf{C}^B\frac{d\mathbf{w}^B}{dt}. \tag{3.67}$$

For the elastic degrees-of-freedom, the term in the Lagrange equations is simply

$$\frac{1}{2}\frac{\partial\dot{E}_D}{\partial\dot{\mathbf{w}}^B} = \mathbf{C}^B\frac{d\mathbf{w}^B}{dt}. \tag{3.68}$$

3.2.3 Potential Energy

The potential energy stored in the elastic deformation of the structure is

$$E_P = \frac{1}{2}(\mathbf{w}^B)^T\left[\sum_{k=1}^{Ne}\mathbf{T}_{s,k}^B\left(\mathbf{k}_{e,k}^s + \mathbf{k}_{c,k}^s\right)\mathbf{T}_{B,k}^s\right]\mathbf{w}^B = \frac{1}{2}(\mathbf{w}^B)^T\mathbf{K}^B\mathbf{w}^B. \tag{3.69}$$

The term in the Lagrange equations, for elastic degrees-of-freedom, is

$$\frac{\partial E_P}{\partial\mathbf{w}^B} = \mathbf{K}^B\mathbf{w}^B, \tag{3.70}$$

and there is no dependence on rigid-body motion. (Here gravity is considered to be an applied force.)

3.2.4 Work by External Forces

The work done by the external forces acting on a body, due to the (small, or virtual) displacement of the elastic degrees-of-freedom of the body, is

$$\delta W = (\delta\mathbf{x}_{/g}^g)^T\mathbf{F}^g, \tag{3.71}$$

where, as in Equation 3.21, $\delta\mathbf{x}_{/g}^g$ contains both displacements and rotations, and $\mathbf{F}^g$ the corresponding forces and moments. This can be expressed in terms of the degrees-of-freedom,

$$\delta\mathbf{x}_{/g}^g = \frac{\partial\mathbf{x}_{/g}^g}{\partial\mathbf{q}^B}\delta\mathbf{q}^B. \tag{3.72}$$

The term in the Lagrange equations is

$$\frac{\partial W}{\partial\mathbf{q}^B} = \frac{\partial(\mathbf{x}_{/g}^g)^T}{\partial\mathbf{q}^B}\mathbf{T}_B^g\mathbf{F}^B.$$

Equation 3.26 is relevant for the displacements, such that

$$\frac{\partial\mathbf{r}_{k/g}^g}{\partial\mathbf{q}^B} = \mathbf{A}_k\mathbf{T}_B^g + \mathbf{A}_k\frac{\partial\mathbf{T}_B^g}{\partial\boldsymbol{\theta}^B}\mathbf{q}^B + \mathbf{B}_k\frac{\partial\mathbf{T}_B^g}{\partial\boldsymbol{\theta}^B}\mathbf{P}_s^B. \tag{3.73}$$

It is also valid to compute the partial derivative of an equation for rotations similar to Equation 3.36 for the angular velocity, giving, in the manner of Equation 3.49,

$$\frac{\partial\mathbf{x}_{/g}^g}{\partial\mathbf{q}^B} = \tilde{\mathbf{A}}\mathbf{T}_B^g + \mathbf{A}\frac{\partial\mathbf{T}_B^g}{\partial\boldsymbol{\theta}^B}\mathbf{q}^B + \mathbf{B}\frac{\partial\mathbf{T}_B^g}{\partial\boldsymbol{\theta}^B}\mathbf{P}_s^B. \tag{3.74}$$

Thus

$$\tilde{\mathbf{F}}^B := \frac{\partial W}{\partial\mathbf{q}^B} = \left(\mathbf{T}_g^B\tilde{\mathbf{A}}^T\mathbf{T}_B^g + (\mathbf{q}^B)^T\frac{\partial\mathbf{T}_g^B}{\partial\boldsymbol{\theta}^B}\mathbf{A}^T\mathbf{T}_B^g + (\mathbf{P}_s^B)^T\frac{\partial\mathbf{T}_g^B}{\partial\boldsymbol{\theta}^B}\mathbf{B}^T\mathbf{T}_B^g\right)\mathbf{F}^B. \tag{3.75}$$

It is evident, from the structure of the $\tilde{\mathbf{A}}$, **A**, and **B** matrices, that *sums* of components of the nodal forces $\mathbf{F}^B$ act at the reference nodes. For linear analysis (Section 3.4.2), this expression can be evaluated at the steady-state condition,

$$\tilde{\mathbf{F}}^B = \left(\mathbf{T}^B_{g0} \tilde{\mathbf{A}}^T \mathbf{T}^g_{B0} + (\mathbf{q}^B_0)^T \left. \frac{\partial \mathbf{T}^B_g}{\partial \boldsymbol{\theta}^B} \right|_0 \mathbf{A}^T \mathbf{T}^g_{B0} + (\mathbf{P}^B_s)^T \left. \frac{\partial \mathbf{T}^B_g}{\partial \boldsymbol{\theta}^B} \right|_0 \mathbf{B}^T \mathbf{T}^g_{B0} \right) \mathbf{F}^B . \tag{3.76}$$

3.3 Linking Bodies with Constraints

The equations for the structure are obtained by stacking the equations for individual bodies; the bodies are as yet not connected at the joints.

A body is linked to the previous body by equating degrees-of-freedom at the reference node (and in the case of the drivetrain also the node at the front bearing) with degrees-of-freedom of the master node on the previous body. The basic consideration is that the location of both nodes, relative to the reference coordinate system on the master body, must be the same; and the deflected orientation differs only by the joint rotation angle.

There are two ways in which the constraints could be implemented. One is to consider the degrees-of-freedom of the reference node to represent displacements from the undeformed position of the structure. That is,

$$\mathbf{P}^B_{1/m} := \mathbf{w}^B_{1/m} , \tag{3.77}$$

with the exception of the joint rotation degree-of-freedom. The coordinate transformations are functions only of the joint rotation angles, not of the displacements. The constraint equations are

$$\boldsymbol{\delta}^m_{1/m} - \boldsymbol{\delta}^m_{m/m} = 0 \quad \text{and} \quad \boldsymbol{\theta}^m_{1/m} - \boldsymbol{\theta}^m_{m/m} = 0 , \tag{3.78}$$

again with the exception of the joint rotation degree-of-freedom. This is the preferred approach for the case in which the joints are locked; the problem with this approach comes when the joints are rotating, and the mean displacements are not negligible. Then, for instance, the position and orientation of the rotating shaft could depart from the undeformed axis about which it is assumed to be rotating, leading to anomalous centrifugal forces.

The other way in which the constraints could be implemented is to consider the displaced position of $\mathbf{P}^B_{1/m}$ to define the reference coordinate system on the slave body, with respect to which body displacements are zero. The displaced position is given in reference to the undeformed coordinate system of the master body. The elastic degrees-of-freedom on the slave body are defined relative to the undeformed position on the slave body, rather than the undeformed position of the global structure.

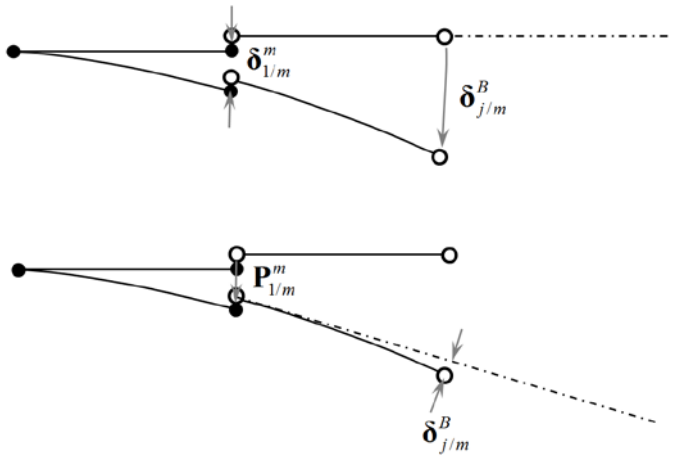

Figure 10: Two ways of implementing constraints between bodies.

Figure 10 compares the two approaches. It is seen that the position and rotational constraints in the latter case are, in essence, the same as the former:

$$\mathbf{O}^m_{1/m} - \boldsymbol{\delta}^m_{m/s} = 0\,, \quad (\boldsymbol{\Theta}^m_{1/m})_i - (\boldsymbol{\theta}^m_{m/s})_i = 0\,, \tag{3.79}$$

where *i* represents the two components which are not the joint rotation angle. However, the damping and stiffness matrices are modified, such that the rows and columns associated with the degrees-of-freedom at the reference node are zero. The elastic displacements must then be interpreted differently, as they are measured relative to the offset and rotated reference node. In addition, as evident in the derivation of the equations of motion in Section 3.2, displacement of the reference node must account for the inertia of the entire body.

Here the latter approach is adopted, since it is desired to account for deflection of the reference axis about which the rotor rotates.

3.3.1 Constraint Equations

We first consider the yaw bearing. The joint rotation of the nacelle is about the Z^y axis, which in the undeflected state is aligned with the Z^g axis of the tower. The positional constraints are

$$\mathbf{T}^g_y \mathbf{O}^y_{1,n/m} - \boldsymbol{\delta}^g_{m,t/s} = \mathbf{0} \tag{3.80}$$

The transformation matrix is

$$\mathbf{T}^g_y = \begin{bmatrix} \cos\chi & -\sin\chi & (\boldsymbol{\theta}^g_{m,t/s})_Y \\ \sin\chi & \cos\chi & -(\boldsymbol{\theta}^g_{m,t/s})_X \\ -(\boldsymbol{\theta}^g_{m,t/s})_Y & (\boldsymbol{\theta}^g_{m,t/s})_X & 1 \end{bmatrix}, \tag{3.81}$$

where the axial rotation of the reference node

$$\chi := (\boldsymbol{\Theta}^y_{1,n/m})_Z \tag{3.82}$$

is measured relative to the undeflected master body coordinate system (for the yaw bearing, the global coordinate system), not the torsionally-deflected master node on the tower. For a linear elastic calculation of mean displacements, the elastic rotations in the transformation matrix are set to zero.

The rotational constraints are

$$(\mathbf{T}^g_y \boldsymbol{\Theta}^y_{1,n/m})_{X,Y} - (\boldsymbol{\theta}^g_{m,t/s})_{X,Y} = 0\,. \tag{3.83}$$

At the rear bearing of the driveshaft, it is assumed that all three positions and two rotations are constrained. Rotation is about the nacelle Z^n axis. This gives the position constraint equations

$$\mathbf{T}^n_d \mathbf{O}^d_{1,d/m} - \mathbf{T}^n_y \boldsymbol{\delta}^y_{m,n/s} = \mathbf{0}\,, \tag{3.84}$$

where

$$\mathbf{T}^y_n = \begin{bmatrix} 0 & \sin\delta & \cos\delta \\ 1 & 0 & 0 \\ 0 & \cos\delta & -\sin\delta \end{bmatrix}; \quad \mathbf{T}^n_y = (\mathbf{T}^y_n)^T; \tag{3.85}$$

accounts for driveshaft tilt angle δ (not to be confused with displacement $\boldsymbol{\delta}$) and conversion to a coordinate system whose *Z* axis is aligned with the nacelle nose, and

$$\mathbf{T}^n_d = \begin{bmatrix} \cos\psi & -\sin\psi & (\mathbf{T}^n_y \boldsymbol{\theta}^y_{m,n/s})_Y \\ \sin\psi & \cos\psi & -(\mathbf{T}^n_y \boldsymbol{\theta}^y_{m,n/s})_X \\ -(\mathbf{T}^n_y \boldsymbol{\theta}^y_{m,n/s})_Y & (\mathbf{T}^n_y \boldsymbol{\theta}^y_{m,n/s})_X & 1 \end{bmatrix} \tag{3.86}$$

accounts for the driveshaft rotation

$$\psi := (\boldsymbol{\Theta}^d_{1,d/m})_Z \,, \tag{3.87}$$

as well as the elastic deformation of the nacelle structure. The rotational constraints are

$$(\mathbf{T}^n_d \boldsymbol{\Theta}^d_{1,d/m})_{X,Y} - (\mathbf{T}^n_y \boldsymbol{\theta}^y_{m,n/s})_{X,Y} = 0 \,. \tag{3.88}$$

At the front bearing, there are two positional constraints,

$$(\mathbf{T}^n_d \boldsymbol{\delta}^d_{s,d/m})_X + (\mathbf{T}^n_d \boldsymbol{\Theta}^d_{1,d/m})_Y (\mathbf{P}^d_{s,d/d})_Z - (\mathbf{T}^n_y \boldsymbol{\delta}^y_{m,n/s})_X = 0 \tag{3.89}$$

and

$$(\mathbf{T}^n_d \boldsymbol{\delta}^d_{s,d/m})_Y - (\mathbf{T}^n_d \boldsymbol{\Theta}^d_{1,d/m})_X (\mathbf{P}^d_{s,d/d})_Z - (\mathbf{T}^n_y \boldsymbol{\delta}^y_{m,n/s})_Y = 0 \,. \tag{3.90}$$

At the pitch bearing, the rotation is about the X^b axis. This gives positional constraints

$$\mathbf{T}^b_p \mathbf{O}^p_{1,b/m} - \mathbf{T}^b_h \mathbf{T}^h_d \boldsymbol{\delta}^d_{m,d/s} = \mathbf{0} \,, \tag{3.91}$$

with

$$\mathbf{T}^d_h = \begin{bmatrix} \cos(b-1)2\pi/3 & -\sin(b-1)2\pi/3 & 0 \\ \sin(b-1)2\pi/3 & \cos(b-1)2\pi/3 & 0 \\ 0 & 0 & 1 \end{bmatrix}; \quad \mathbf{T}^h_d = (\mathbf{T}^d_h)^T \,; \tag{3.92}$$

$$\mathbf{T}^h_b = \begin{bmatrix} \cos\phi & 0 & \sin\phi \\ 0 & 1 & 0 \\ -\sin\phi & 0 & \cos\phi \end{bmatrix}; \quad \mathbf{T}^b_h = (\mathbf{T}^h_b)^T \,; \tag{3.93}$$

and

$$\mathbf{T}^b_p = \begin{bmatrix} 1 & -(\mathbf{T}^b_h \mathbf{T}^h_d \boldsymbol{\theta}^d_{m,d/s})_Z & (\mathbf{T}^b_h \mathbf{T}^h_d \boldsymbol{\theta}^d_{m,d/s})_Y \\ (\mathbf{T}^b_h \mathbf{T}^h_d \boldsymbol{\theta}^d_{m,d/s})_Z & \cos\beta & \sin\beta \\ -(\mathbf{T}^b_h \mathbf{T}^h_d \boldsymbol{\theta}^d_{m,d/s})_Y & -\sin\beta & \cos\beta \end{bmatrix}, \tag{3.94}$$

where

$$\beta := -(\boldsymbol{\Theta}^p_{1,b/m})_X \,. \tag{3.95}$$

The rotational constraints are

$$(\mathbf{T}^b_p \boldsymbol{\Theta}^p_{1,b/m})_{Y,Z} - (\mathbf{T}^b_h \mathbf{T}^h_d \boldsymbol{\theta}^d_{m,h/s})_{Y,Z} = 0 \,. \tag{3.96}$$

Together, all the positional and rotational constraint equations can be written in the form

$$\left(\mathbf{T}^I_B \mathbf{B}_s - \mathbf{T}^I_m \mathbf{B}_m\right) \mathbf{q}^B = \mathbf{0} \,. \tag{3.97}$$

The "I" index stands for some intermediate coordinate system. $\mathbf{T}^I_B$ is a function of some of the rotational degrees-of-freedom, while $\mathbf{T}^I_m$ is constant. The Jacobian (partial derivatives with respect to the degrees-of-freedom) of these constraint equations is needed for implementation in the equations of motion. The Jacobian is

$$\mathbf{L}^B = \mathbf{T}^I_B \mathbf{B}_s - \mathbf{T}^I_m \mathbf{B}_m + \frac{\partial \mathbf{T}^I_B}{\partial \mathbf{q}^B} \mathbf{B}_s \mathbf{q}^B \,. \tag{3.98}$$

3.3.2 Example of Implementation in the Equations of Motion

Following Shabana [24], the uncoupled equations of motion can be written in the form

$$\mathbf{M}\frac{d^2\mathbf{q}}{dt^2} = \mathbf{R}, \tag{3.99}$$

where **R** represents some likely nonlinear right-hand side terms. In developing this equation using variational methods, the details of which we skip (as we proceeded directly from the related Lagrange equations), the dependent degrees-of-freedom in the virtual displacements $\delta\mathbf{q}$ are eliminated using the constraint equations. This is a linear operation. First the constraint functions and equations of motion are partitioned such that the independent degrees-of-freedom come first, and the dependent degrees-of-freedom are grouped at the end. Then the variation of the constraint functions, applied to the virtual displacements, can be written

$$\hat{\mathbf{L}}\,\delta\hat{\mathbf{q}} + \mathbf{L}_s\,\delta\mathbf{q}_s = 0, \tag{3.100}$$

such that

$$\delta\mathbf{q}_s = -\mathbf{L}_s^{-1}\hat{\mathbf{L}}\,\delta\hat{\mathbf{q}}. \tag{3.101}$$

Here $\hat{\mathbf{q}}$ represents the independent degrees-of-freedom, and $\mathbf{q}_s$ the dependent (slave) degrees-of-freedom. Defining

$$\mathbf{\Lambda} := \begin{bmatrix} \mathbf{I} \\ -(\mathbf{L}_s)^{-1}\hat{\mathbf{L}} \end{bmatrix}, \tag{3.102}$$

where $\mathbf{I}$ is the identity matrix of dimension equal to the number of independent degrees-of-freedom, the equations of motion are

$$\mathbf{\Lambda}^T\mathbf{M}\mathbf{\Lambda}\frac{d^2\hat{\mathbf{q}}}{dt^2} = \mathbf{\Lambda}^T\mathbf{R} \tag{3.103}$$

in terms of the purely independent degrees-of-freedom.

If the equations of motion are linear, then Equation 3.101 applies directly as a transformation of the degrees-of-freedom:

$$\mathbf{q}_s = -\mathbf{L}_{s0}^{-1}\hat{\mathbf{L}}_0\,\hat{\mathbf{q}}; \qquad \mathbf{q} = \mathbf{\Lambda}_0\hat{\mathbf{q}}. \tag{3.104}$$

The implementation of constraints is further discussed in Sections 3.6.1 and 3.7.2.

3.4 Linearized Equations

The majority of the terms in the equations of motion are nonlinear, each containing products of $\mathbf{q}^B$, $d\mathbf{q}^B/dt$, and $d^2\mathbf{q}^B/dt^2$. In general, a function of a vector **x** and its first two time derivatives can be linearized as

$$\begin{aligned}\mathbf{g}(\mathbf{x},\dot{\mathbf{x}},\ddot{\mathbf{x}}) \approx \mathbf{g}(\mathbf{x}_0,\dot{\mathbf{x}}_0,\ddot{\mathbf{x}}_0) + \left(\Delta\mathbf{x}^T\left.\frac{\partial}{\partial\mathbf{x}}\right|_0 + \Delta\dot{\mathbf{x}}^T\left.\frac{\partial}{\partial\dot{\mathbf{x}}}\right|_0 + \Delta\ddot{\mathbf{x}}^T\left.\frac{\partial}{\partial\ddot{\mathbf{x}}}\right|_0\right)\mathbf{g} \\ + O\left(\Delta\mathbf{x}^2,\Delta\dot{\mathbf{x}}^2,\Delta\ddot{\mathbf{x}}^2\right),\end{aligned} \tag{3.105}$$

where the operator $\partial/\partial s\big|_0$ is understood to mean "first take the derivative with respect to *s*, then evaluate this at the steady-state condition."

It is evident from Equation 3.105 that the linearized equations of motion will involve products of one or more of the steady-state terms

$$\mathbf{q}_0^B,\ \left.\frac{d\mathbf{q}^B}{dt}\right|_0,\ \left.\frac{d^2\mathbf{q}^B}{dt^2}\right|_0,\ \mathbf{\Sigma}_0^B,\ \left.\frac{\partial\mathbf{\Sigma}^B}{\partial\boldsymbol{\theta}_m}\right|_0,\ \left.\frac{\partial\mathbf{\Sigma}^B}{\partial\boldsymbol{\alpha}}\right|_0, \text{ and } \left.\frac{\partial\mathbf{\Sigma}^B}{\partial\boldsymbol{\omega}}\right|_0$$

with small dynamic fluctuations

$$\Delta\mathbf{q}^B,\ \frac{d\Delta\mathbf{q}^B}{dt},\ \text{and}\ \frac{d^2\Delta\mathbf{q}^B}{dt^2}.$$

Here $\boldsymbol{\theta}_m$ and $\boldsymbol{\alpha}$ are subsets of $\mathbf{q}^B$, and represent the elastic master node rotations and joint rotations, respectively. The body angular velocity $\boldsymbol{\omega}$ is a subset of $\dot{\mathbf{q}}^B$. The equations are greatly simplified by making intelligent assumptions about which of the steady-state components can be considered small, on the same order as $\Delta\mathbf{q}^B$, and neglecting orders higher than one.

3.4.1 Small-Displacement Assumptions

On the tower, all steady-state displacements $\mathbf{q}_0^B$ are small. The steady-state velocity and acceleration, $\dot{\mathbf{q}}_0^B$, and $\ddot{\mathbf{q}}_0^B$, are zero.

On the nacelle, the steady-state yaw angle $\chi_0 := (\boldsymbol{\Theta}^y_{1,n/m})_Z\big|_0$ is not necessarily small. Otherwise, all displacements are small, and all steady-state time derivatives are zero.

On the driveshaft, the azimuth angle $\psi_0 := (\boldsymbol{\Theta}^d_{1,d/m})_Z\big|_0$ is prescribed, for reasons discussed in Section 3.8. The steady-state rotational speed $\Omega_0 := \dot{\psi}_0 = (\dot{\boldsymbol{\Theta}}^d_{1,d/m})_Z\big|_0$ is not small. All other displacements, in the rotating driveshaft coordinate system, are small, and all other steady-state time derivatives are zero.

On the blades, the steady-state pitch angle $\beta_0 := (\boldsymbol{\Theta}^p_{1,b/m})_X\big|_0$ may not be small. It is questionable whether the mean blade deflection $\mathbf{w}^p_{0,b/s}$ can be considered small, especially near the tips; this depends upon the desired accuracy of the analysis. The equations are presently formulated assuming that $\mathbf{w}^p_{0,b/s}$ is small. The steady-state values of the displacements $\mathbf{O}^p_{1,b/m}\big|_0$ and rotations $(\boldsymbol{\Theta}^p_{1,b/m})_{Y,Z}\big|_0$ of the reference node at the pitch bearing are small.

As a consequence of the above assumptions, the steady-state values of Equations 3.44 through 3.46 are, for the blades,

$$\mathbf{S}_0^B = \mathbf{T}^p_{d0}\mathbf{S}_{\Omega 0}\mathbf{T}^d_{p0}, \tag{3.106}$$

with

$$\mathbf{S}_{\Omega 0} = \begin{bmatrix} 0 & -\Omega_0 & 0 \\ \Omega_0 & 0 & 0 \\ 0 & 0 & 0 \end{bmatrix}, \tag{3.107}$$

for the driveshaft,

$$\mathbf{S}_0^B = \mathbf{S}_{\Omega 0}, \tag{3.108}$$

and for the tower and nacelle,

$$\mathbf{S}_0^B = 0. \tag{3.109}$$

Thus, the steady-state $\boldsymbol{\Sigma}_0^B$ is only a function of the mean rotational speed Ω_0 and, for the blades, the steady-state transform from driveshaft to pitch coordinates. Also,

$$\left.\frac{d\mathbf{S}^B}{dt}\right|_0 = 0, \quad \text{for all nodes, so} \quad \left.\frac{d\boldsymbol{\Sigma}^B}{dt}\right|_0 = 0. \tag{3.110}$$

The mean acceleration of all degrees-of-freedom is zero:

$$\left.\frac{d^2\mathbf{q}^B}{dt^2}\right|_0 = 0\,; \tag{3.111}$$

that being said, nonzero accelerations in global coordinates may result from products of the rotational speed Ω_0 and other terms.

The only terms in $\mathbf{q}_0^B$ which are of order zero are the joint angles χ_0 and ψ_0, and, for each blade, β_0. The only nonzero mean velocity, with degrees-of-freedom in body coordinates, is the rotational speed Ω_0. Thus

$$\left.\frac{d\mathbf{q}^B}{dt}\right|_0 = \boldsymbol{\Omega}_0 := \begin{bmatrix} 0 & 0 & \cdots & \Omega_0 & \cdots & 0 \end{bmatrix}^T. \tag{3.112}$$

Again, nonzero velocities in global coordinates result from products of Ω_0 with other terms.

Examine the term

$$\frac{d\boldsymbol{\Sigma}^B}{dt}\mathbf{q}^B$$

which appears in the equations of motion. This is linearized as

$$\frac{d\boldsymbol{\Sigma}^B}{dt}\mathbf{q}^B \approx \left.\frac{d\boldsymbol{\Sigma}^B}{dt}\right|_0 \mathbf{q}_0^B + \left.\frac{d\boldsymbol{\Sigma}^B}{dt}\right|_0 \Delta\mathbf{q}^B + \left.\left(\frac{\partial}{\partial\boldsymbol{\omega}^B}\frac{d\boldsymbol{\Sigma}^B}{dt}\right)\right|_0 \mathbf{q}_0^B\Delta\boldsymbol{\omega}^B + \left.\left(\frac{\partial}{\partial\mathbf{q}^B}\frac{d\boldsymbol{\Sigma}^B}{dt}\right)\right|_0 \mathbf{q}_0^B\Delta\mathbf{q}^B. \tag{3.113}$$

The first two terms on the right-hand side are zero, by Equation 3.110. The vector $\mathbf{q}_0^B$ contains only joint angles as zero-order terms. Yet the matrix $\boldsymbol{\Sigma}^B$ contains all zeros in the columns associated with the joint angles. Therefore the latter two terms are also zero, to first order, and

$$\frac{d\boldsymbol{\Sigma}^B}{dt}\mathbf{q}^B \approx \mathbf{0}\,. \tag{3.114}$$

wherever it appears in the equations. By the same argument, any expressions involving $\boldsymbol{\Sigma}^B$ or its derivatives times $\mathbf{q}_0^B$, will be linearized as

$$\boldsymbol{\Sigma}^B\mathbf{q}^B \approx \boldsymbol{\Sigma}_0^B\mathbf{q}_0^B + \boldsymbol{\Sigma}_0^B\Delta\mathbf{q}^B, \tag{3.115}$$

and any products like

$$\boldsymbol{\Sigma}_0^B\mathbf{q}_0^B\Delta\mathbf{q}^B$$

are zero to first order. The above statements also apply to the rate of change of $\mathbf{q}^B$, that is,

$$\frac{d\boldsymbol{\Sigma}^B}{dt}\frac{d\mathbf{q}^B}{dt} \approx \mathbf{0} \quad \text{and e.g.} \quad \boldsymbol{\Sigma}^B\left.\frac{d\mathbf{q}^B}{dt}\right|_0 = \boldsymbol{\Sigma}^B\boldsymbol{\Omega}_0 = \mathbf{0}\,. \tag{3.116}$$

From Equation 3.110, it can be seen that

$$\left.\left(\frac{\partial}{\partial\boldsymbol{\theta}^B}\frac{d\boldsymbol{\Sigma}^B}{dt}\right)\right|_0 = \mathbf{0}\,. \tag{3.117}$$

3.4.2 Terms in the Linearized Equations of Motion

We proceed term-by-term, beginning with the Jacobian of the constraint equation. This already represents the constraint equations to first order, and so the steady-state value is used:

$$\mathbf{L}_0^B = \mathbf{T}_{B0}^I \mathbf{B}_s - \mathbf{T}_{m0}^I \mathbf{B}_m + \left.\frac{\partial \mathbf{T}_B^I}{\partial \mathbf{q}^B}\right|_0 \mathbf{B}_s \mathbf{q}_0^B \tag{3.118}$$

Moving on to the equations of motion, the first term is

$$(\tilde{\mathbf{A}}^B)^T \mathbf{M}^B \tilde{\mathbf{A}}^B \frac{d^2\mathbf{q}^B}{dt^2} \approx (\tilde{\mathbf{A}}_0^B)^T \mathbf{M}^B \tilde{\mathbf{A}}_0^B \frac{d^2\Delta\mathbf{q}^B}{dt^2}. \tag{3.119}$$

The two terms involving angular accelerations are

$$(\tilde{\mathbf{A}}^B)^T \mathbf{M}^B \mathbf{A}^B \frac{d\boldsymbol{\Sigma}^B}{dt}\mathbf{q}^B \approx \mathbf{0} \tag{3.120}$$

by Equation 3.114, and

$$\begin{aligned}(\tilde{\mathbf{A}}^B)^T \mathbf{M}^B \mathbf{B}^B \frac{d\boldsymbol{\Sigma}^B}{dt}\mathbf{P}_s^B \approx{}& (\tilde{\mathbf{A}}_0^B)^T \mathbf{M}^B \mathbf{B}_0^B \left.\frac{\partial \boldsymbol{\Sigma}^B}{\partial \boldsymbol{\omega}^B}\right|_0 \mathbf{P}_s^B \frac{d\Delta\boldsymbol{\omega}^B}{dt} \\ &+ (\tilde{\mathbf{A}}_0^B)^T \mathbf{M}^B \mathbf{B}_0^B \left.\frac{\partial \boldsymbol{\Sigma}^B}{\partial \boldsymbol{\theta}^B}\right|_0 \mathbf{P}_s^B \Delta\boldsymbol{\omega}^B.\end{aligned} \tag{3.121}$$

Here $\boldsymbol{\theta}^B$ indicates the entries in $\mathbf{q}^B$ associated with master node and joint rotations.

For the coriolis force terms,

$$\begin{aligned}(\tilde{\mathbf{A}}^B)^T \mathbf{M}^B \mathbf{A}^B \boldsymbol{\Sigma}^B \frac{d\mathbf{q}^B}{dt} &\approx (\tilde{\mathbf{A}}_0^B)^T \mathbf{M}^B \mathbf{A}_0^B \boldsymbol{\Sigma}_0^B \frac{d\Delta\mathbf{q}^B}{dt}; \\ (\tilde{\mathbf{A}}^B)^T \mathbf{M}^B \tilde{\mathbf{A}}^B \boldsymbol{\Sigma}^B \frac{d\mathbf{q}^B}{dt} &\approx (\tilde{\mathbf{A}}_0^B)^T \mathbf{M}^B \tilde{\mathbf{A}}_0^B \boldsymbol{\Sigma}_0^B \frac{d\Delta\mathbf{q}^B}{dt};\end{aligned} \tag{3.122}$$

$$\begin{aligned}(\boldsymbol{\Sigma}^B)^T (\tilde{\mathbf{A}}^B)^T \mathbf{M}^B \tilde{\mathbf{A}}^B \frac{d\mathbf{q}^B}{dt} \approx{}& (\boldsymbol{\Sigma}_0^B)^T (\tilde{\mathbf{A}}_0^B)^T \mathbf{M}^B \tilde{\mathbf{A}}_0^B \boldsymbol{\Omega}_0 \\ &+ (\boldsymbol{\Sigma}_0^B)^T (\tilde{\mathbf{A}}_0^B)^T \mathbf{M}^B \tilde{\mathbf{A}}_0^B \frac{d\Delta\mathbf{q}^B}{dt} + \left.\frac{\partial (\boldsymbol{\Sigma}^B)^T}{\partial \boldsymbol{\omega}^B}\right|_0 (\tilde{\mathbf{A}}_0^B)^T \mathbf{M}^B \tilde{\mathbf{A}}_0^B \boldsymbol{\Omega}_0 \Delta\boldsymbol{\omega}^B \\ &+ \left[\left.\frac{\partial (\boldsymbol{\Sigma}^B)^T}{\partial \boldsymbol{\theta}^B}\right|_0 (\tilde{\mathbf{A}}_0^B)^T \mathbf{M}^B \tilde{\mathbf{A}}_0^B \boldsymbol{\Omega}_0 + (\boldsymbol{\Sigma}_0^B)^T \left.\frac{\partial (\tilde{\mathbf{A}}^B)^T}{\partial \boldsymbol{\theta}^B}\right|_0 \mathbf{M}^B \tilde{\mathbf{A}}_0^B \boldsymbol{\Omega}_0 \right. \\ &+ \left. (\boldsymbol{\Sigma}_0^B)^T (\tilde{\mathbf{A}}_0^B)^T \mathbf{M}^B \left.\frac{\partial \tilde{\mathbf{A}}^B}{\partial \boldsymbol{\theta}^B}\right|_0 \boldsymbol{\Omega}_0 \right] \Delta\boldsymbol{\theta}^B;\end{aligned} \tag{3.123}$$

and similarly in an obvious manner for the terms

$$(\tilde{\mathbf{A}}^B)^T \boldsymbol{\Sigma}^B \mathbf{M}^B \tilde{\mathbf{A}}^B \frac{d\mathbf{q}^B}{dt} \quad \text{and} \quad (\tilde{\mathbf{A}}^B)^T \mathbf{M}^B (\boldsymbol{\Sigma}^B)^T \tilde{\mathbf{A}}^B \frac{d\mathbf{q}^B}{dt}.$$

For the centrifugal force terms, centrifugal stiffening is represented by

$$\begin{aligned}(\boldsymbol{\Sigma}^B)^T (\tilde{\mathbf{A}}^B)^T \mathbf{M}^B \mathbf{A}^B \boldsymbol{\Sigma}^B \mathbf{q}^B &\approx (\boldsymbol{\Sigma}_0^B)^T (\tilde{\mathbf{A}}_0^B)^T \mathbf{M}^B \mathbf{A}_0^B \boldsymbol{\Sigma}_0^B \left(\mathbf{q}_0^B + \Delta\mathbf{q}^B\right), \\ (\tilde{\mathbf{A}}^B)^T \boldsymbol{\Sigma}^B \mathbf{M}^B \mathbf{A}^B \boldsymbol{\Sigma}^B \mathbf{q}^B &\approx (\tilde{\mathbf{A}}_0^B)^T \boldsymbol{\Sigma}_0^B \mathbf{M}^B \mathbf{A}_0^B \boldsymbol{\Sigma}_0^B \left(\mathbf{q}_0^B + \Delta\mathbf{q}^B\right), \\ (\tilde{\mathbf{A}}^B)^T \mathbf{M}^B (\boldsymbol{\Sigma}^B)^T \mathbf{A}^B \boldsymbol{\Sigma}^B \mathbf{q}^B &\approx (\tilde{\mathbf{A}}_0^B)^T \mathbf{M}^B (\boldsymbol{\Sigma}_0^B)^T \mathbf{A}_0^B \boldsymbol{\Sigma}_0^B \left(\mathbf{q}_0^B + \Delta\mathbf{q}^B\right), \\ (\tilde{\mathbf{A}}^B)^T \mathbf{M}^B \mathbf{A}^B \boldsymbol{\Sigma}^B \boldsymbol{\Sigma}^B \mathbf{q}^B &\approx (\tilde{\mathbf{A}}_0^B)^T \mathbf{M}^B \mathbf{A}_0^B \boldsymbol{\Sigma}_0^B \boldsymbol{\Sigma}_0^B \left(\mathbf{q}_0^B + \Delta\mathbf{q}^B\right),\end{aligned} \tag{3.124}$$

and other centrifugal forces by

$$
\begin{aligned}
(\boldsymbol{\Sigma}^B)^T(\tilde{\mathbf{A}}^B)^T\mathbf{M}^B\mathbf{B}^B\boldsymbol{\Sigma}^B\mathbf{P}_s^B \approx\ & (\boldsymbol{\Sigma}_0^B)^T(\tilde{\mathbf{A}}_0^B)^T\mathbf{M}^B\mathbf{B}_0^B\boldsymbol{\Sigma}_0^B\mathbf{P}_s^B \\
&+\left[\left.\frac{\partial(\boldsymbol{\Sigma}^B)^T}{\partial\boldsymbol{\omega}^B}\right|_0(\tilde{\mathbf{A}}_0^B)^T\mathbf{M}^B\mathbf{B}_0^B\boldsymbol{\Sigma}_0^B\mathbf{P}_s^B+(\boldsymbol{\Sigma}_0^B)^T(\tilde{\mathbf{A}}_0^B)^T\mathbf{M}^B\mathbf{B}_0^B\left.\frac{\partial\boldsymbol{\Sigma}^B}{\partial\boldsymbol{\omega}^B}\right|_0\mathbf{P}_s^B\right]\Delta\boldsymbol{\omega}^B \\
&+\left[\left.\frac{\partial(\boldsymbol{\Sigma}^B)^T}{\partial\boldsymbol{\theta}^B}\right|_0(\tilde{\mathbf{A}}_0^B)^T\mathbf{M}^B\mathbf{B}_0^B\boldsymbol{\Sigma}_0^B\mathbf{P}_s^B+(\boldsymbol{\Sigma}_0^B)^T(\tilde{\mathbf{A}}_0^B)^T\mathbf{M}^B\mathbf{B}_0^B\left.\frac{\partial\boldsymbol{\Sigma}^B}{\partial\boldsymbol{\theta}^B}\right|_0\mathbf{P}_s^B\right. \\
&+\left.(\boldsymbol{\Sigma}_0^B)^T\left.\frac{\partial(\tilde{\mathbf{A}}^B)^T}{\partial\boldsymbol{\theta}^B}\right|_0\mathbf{M}^B\mathbf{B}_0^B\boldsymbol{\Sigma}_0^B\mathbf{P}_s^B+(\boldsymbol{\Sigma}_0^B)^T(\tilde{\mathbf{A}}_0^B)^T\mathbf{M}^B\left.\frac{\partial\mathbf{B}^B}{\partial\boldsymbol{\theta}^B}\right|_0\boldsymbol{\Sigma}_0^B\mathbf{P}_s^B\right]\Delta\boldsymbol{\theta}^B,
\end{aligned}
\tag{3.125}
$$

with similar expressions for

$$(\tilde{\mathbf{A}}^B)^T\boldsymbol{\Sigma}^B\mathbf{M}^B\mathbf{B}^B\boldsymbol{\Sigma}^B\mathbf{P}_s^B,\ (\tilde{\mathbf{A}}^B)^T\mathbf{M}^B(\boldsymbol{\Sigma}^B)^T\mathbf{B}^B\boldsymbol{\Sigma}^B\mathbf{P}_s^B, \text{ and } (\tilde{\mathbf{A}}^B)^T\mathbf{M}^B\mathbf{B}^B\boldsymbol{\Sigma}^B\boldsymbol{\Sigma}^B\mathbf{P}_s^B.$$

The first equation involving coupling between displacement and acceleration is zero:

$$(\mathbf{q}^B)^T\frac{\partial(\boldsymbol{\Sigma}^B)^T}{\partial\boldsymbol{\omega}^B}(\mathbf{A}^B)^T\mathbf{M}^B\tilde{\mathbf{A}}^B\frac{d^2\mathbf{q}^B}{dt^2}\approx\mathbf{0}. \tag{3.126}$$

The second is

$$(\mathbf{P}_s^B)^T\frac{\partial(\boldsymbol{\Sigma}^B)^T}{\partial\boldsymbol{\omega}^B}(\mathbf{B}^B)^T\mathbf{M}^B\tilde{\mathbf{A}}^B\frac{d^2\mathbf{q}^B}{dt^2}\approx(\mathbf{P}_s^B)^T\left.\frac{\partial(\boldsymbol{\Sigma}^B)^T}{\partial\boldsymbol{\omega}^B}\right|_0(\mathbf{B}_0^B)^T\mathbf{M}^B\tilde{\mathbf{A}}_0^B\frac{d^2\Delta\mathbf{q}^B}{dt^2}. \tag{3.127}$$

By Equations 3.113 and 3.114,

$$
\begin{aligned}
&(\mathbf{q}^B)^T\frac{\partial(\boldsymbol{\Sigma}^B)^T}{\partial\boldsymbol{\omega}^B}(\mathbf{A}^B)^T\mathbf{M}^B\mathbf{A}^B\frac{d\boldsymbol{\Sigma}^B}{dt}\mathbf{q}^B\approx\mathbf{0};\\
&(\mathbf{q}^B)^T\frac{\partial(\boldsymbol{\Sigma}^B)^T}{\partial\boldsymbol{\omega}^B}(\mathbf{A}^B)^T\mathbf{M}^B\mathbf{B}^B\frac{d\boldsymbol{\Sigma}^B}{dt}\mathbf{P}_s^B\approx\mathbf{0};\\
&(\mathbf{P}_s^B)^T\frac{\partial(\boldsymbol{\Sigma}^B)^T}{\partial\boldsymbol{\omega}^B}(\mathbf{B}^B)^T\mathbf{M}^B\mathbf{A}^B\frac{d\boldsymbol{\Sigma}^B}{dt}\mathbf{q}^B\approx\mathbf{0}.
\end{aligned}
\tag{3.128}
$$

The only nonzero angular acceleration term is

$$
\begin{aligned}
(\mathbf{P}_s^B)^T\frac{\partial(\boldsymbol{\Sigma}^B)^T}{\partial\boldsymbol{\omega}^B}(\mathbf{B}^B)^T\mathbf{M}^B\mathbf{B}^B\frac{d\boldsymbol{\Sigma}^B}{dt}\mathbf{P}_s^B\approx\ & \\
&(\mathbf{P}_s^B)^T\left.\frac{\partial(\boldsymbol{\Sigma}^B)^T}{\partial\boldsymbol{\omega}^B}\right|_0(\mathbf{B}_0^B)^T\mathbf{M}^B\mathbf{B}_0^B\left.\frac{\partial\boldsymbol{\Sigma}^B}{\partial\boldsymbol{\omega}^B}\right|_0\mathbf{P}_s^B\frac{d\Delta\boldsymbol{\omega}^B}{dt} \\
&+\quad(\mathbf{P}_s^B)^T\left.\frac{\partial(\boldsymbol{\Sigma}^B)^T}{\partial\boldsymbol{\omega}^B}\right|_0(\mathbf{B}_0^B)^T\mathbf{M}^B\mathbf{B}_0^B\left.\frac{\partial\boldsymbol{\Sigma}^B}{\partial\boldsymbol{\theta}^B}\right|_0\mathbf{P}_s^B\Delta\boldsymbol{\omega}^B.
\end{aligned}
\tag{3.129}
$$

The quadratic velocity term is

$$\frac{d(\mathbf{q}^B)^T}{dt}\frac{\partial(\boldsymbol{\Sigma}^B)^T}{\partial\boldsymbol{\omega}^B}(\mathbf{A}^B)^T\mathbf{M}^B\tilde{\mathbf{A}}^B\frac{d\mathbf{q}^B}{dt}\approx\boldsymbol{\Omega}_0^T(\tilde{\mathbf{A}}_0^B)^T\mathbf{M}^B\mathbf{A}_0^B\left.\frac{\partial\boldsymbol{\Sigma}^B}{\partial\boldsymbol{\omega}^B}\right|_0\frac{d\Delta\mathbf{q}^B}{dt}, \tag{3.130}$$

with other terms zero by Equation 3.115.

For the seven terms with coupling between displacements and velocities,

$$(\mathbf{q}^B)^T\frac{\partial(\boldsymbol{\Sigma}^B)^T}{\partial\boldsymbol{\omega}^B}(\mathbf{A}^B)^T\mathbf{M}^B\mathbf{A}^B\boldsymbol{\Sigma}^B\frac{d\mathbf{q}^B}{dt}\approx\mathbf{0}; \tag{3.131}$$

$$\frac{d(\mathbf{q}^B)^T}{dt}\frac{\partial(\boldsymbol{\Sigma}^B)^T}{\partial\boldsymbol{\omega}^B}(\mathbf{A}^B)^T\mathbf{M}^B\mathbf{A}^B\boldsymbol{\Sigma}^B\mathbf{q}^B \approx \mathbf{0};$$
$$(\mathbf{q}^B)^T\frac{\partial(\boldsymbol{\Sigma}^B)^T}{\partial\boldsymbol{\omega}^B}(\mathbf{A}^B)^T\mathbf{M}^B\tilde{\mathbf{A}}^B\boldsymbol{\Sigma}^B\frac{d\mathbf{q}^B}{dt} \approx \mathbf{0}.$$

Then,

$$\begin{aligned}
&(\mathbf{q}^B)^T\frac{\partial(\boldsymbol{\Sigma}^B)^T}{\partial\boldsymbol{\omega}^B}(\boldsymbol{\Sigma}^B)^T(\mathbf{A}^B)^T\mathbf{M}^B\tilde{\mathbf{A}}^B\frac{d\mathbf{q}^B}{dt} \approx \boldsymbol{\Omega}_0^T(\tilde{\mathbf{A}}_0^B)^T\mathbf{M}^B\mathbf{A}_0^B\boldsymbol{\Sigma}_0^B\left.\frac{\partial\boldsymbol{\Sigma}^B}{\partial\boldsymbol{\omega}^B}\right|_0(\mathbf{q}_0^B+\Delta\mathbf{q}^B);\\
&(\mathbf{q}^B)^T\frac{\partial(\boldsymbol{\Sigma}^B)^T}{\partial\boldsymbol{\omega}^B}(\mathbf{A}^B)^T\boldsymbol{\Sigma}^B\mathbf{M}^B\tilde{\mathbf{A}}^B\frac{d\mathbf{q}^B}{dt} \approx \boldsymbol{\Omega}_0^T(\tilde{\mathbf{A}}_0^B)^T\mathbf{M}^B(\boldsymbol{\Sigma}_0^B)^T\mathbf{A}_0^B\left.\frac{\partial\boldsymbol{\Sigma}^B}{\partial\boldsymbol{\omega}^B}\right|_0(\mathbf{q}_0^B+\Delta\mathbf{q}^B);\\
&(\mathbf{q}^B)^T\frac{\partial(\boldsymbol{\Sigma}^B)^T}{\partial\boldsymbol{\omega}^B}(\mathbf{A}^B)^T\mathbf{M}^B(\boldsymbol{\Sigma}^B)^T\tilde{\mathbf{A}}^B\frac{d\mathbf{q}^B}{dt} \approx \boldsymbol{\Omega}_0^T(\tilde{\mathbf{A}}_0^B)^T(\boldsymbol{\Sigma}_0^B)^T\mathbf{M}^B\mathbf{A}_0^B\left.\frac{\partial\boldsymbol{\Sigma}^B}{\partial\boldsymbol{\omega}^B}\right|_0(\mathbf{q}_0^B+\Delta\mathbf{q}^B);\\
&(\mathbf{q}^B)^T\left(\frac{d}{dt}\frac{\partial(\boldsymbol{\Sigma}^B)^T}{\partial\boldsymbol{\omega}^B}\right)(\mathbf{A}^B)^T\mathbf{M}^B\tilde{\mathbf{A}}^B\frac{d\mathbf{q}^B}{dt} \approx \Omega_0\boldsymbol{\Omega}_0^T(\tilde{\mathbf{A}}^B)^T\mathbf{M}^B\mathbf{A}^B\left.\frac{\partial^2\boldsymbol{\Sigma}^B}{\partial\boldsymbol{\omega}^B\partial\psi}\right|_0(\mathbf{q}_0^B+\Delta\mathbf{q}^B)\cdot
\end{aligned} \tag{3.132}$$

The seven terms coupling velocities and positional offsets linearize as

$$\begin{aligned}
(\mathbf{P}_s^B)^T\frac{\partial(\boldsymbol{\Sigma}^B)^T}{\partial\boldsymbol{\omega}^B}(\boldsymbol{\Sigma}^B)^T(\mathbf{B}^B)^T\mathbf{M}^B\tilde{\mathbf{A}}^B\frac{d\mathbf{q}^B}{dt} &\approx (\mathbf{P}_s^B)^T\left.\frac{\partial(\boldsymbol{\Sigma}^B)^T}{\partial\boldsymbol{\omega}^B}\right|_0(\boldsymbol{\Sigma}_0^B)^T(\mathbf{B}_0^B)^T\mathbf{M}^B\tilde{\mathbf{A}}_0^B\boldsymbol{\Omega}_0\\
&+(\mathbf{P}_s^B)^T\left.\frac{\partial(\boldsymbol{\Sigma}^B)^T}{\partial\boldsymbol{\omega}^B}\right|_0(\boldsymbol{\Sigma}_0^B)^T(\mathbf{B}_0^B)^T\mathbf{M}^B\tilde{\mathbf{A}}_0^B\frac{d\Delta\mathbf{q}^B}{dt}\\
&+(\mathbf{P}_s^B)^T\left.\frac{\partial(\boldsymbol{\Sigma}^B)^T}{\partial\boldsymbol{\omega}^B}\right|_0\left.\frac{\partial(\boldsymbol{\Sigma}^B)^T}{\partial\boldsymbol{\omega}^B}\right|_0(\mathbf{B}_0^B)^T\mathbf{M}^B\tilde{\mathbf{A}}_0^B\boldsymbol{\Omega}_0\Delta\boldsymbol{\omega}^B\\
&+\Bigg[(\mathbf{P}_s^B)^T\left.\frac{\partial^2(\boldsymbol{\Sigma}^B)^T}{\partial\boldsymbol{\omega}^B\partial\boldsymbol{\theta}^B}\right|_0(\boldsymbol{\Sigma}_0^B)^T(\mathbf{B}_0^B)^T\mathbf{M}^B\tilde{\mathbf{A}}_0^B\boldsymbol{\Omega}_0\\
&\quad+(\mathbf{P}_s^B)^T\left.\frac{\partial(\boldsymbol{\Sigma}^B)^T}{\partial\boldsymbol{\omega}^B}\right|_0\left.\frac{\partial(\boldsymbol{\Sigma}^B)^T}{\partial\boldsymbol{\theta}^B}\right|_0(\mathbf{B}_0^B)^T\mathbf{M}^B\tilde{\mathbf{A}}_0^B\boldsymbol{\Omega}_0\\
&\quad+(\mathbf{P}_s^B)^T\left.\frac{\partial(\boldsymbol{\Sigma}^B)^T}{\partial\boldsymbol{\omega}^B}\right|_0(\boldsymbol{\Sigma}_0^B)^T\left.\frac{\partial(\mathbf{B}^B)^T}{\partial\boldsymbol{\theta}^B}\right|_0\mathbf{M}^B\tilde{\mathbf{A}}_0^B\boldsymbol{\Omega}_0\\
&\quad+(\mathbf{P}_s^B)^T\left.\frac{\partial(\boldsymbol{\Sigma}^B)^T}{\partial\boldsymbol{\omega}^B}\right|_0(\boldsymbol{\Sigma}_0^B)^T(\mathbf{B}_0^B)^T\mathbf{M}^B\left.\frac{\partial\tilde{\mathbf{A}}^B}{\partial\boldsymbol{\theta}^B}\right|_0\boldsymbol{\Omega}_0\Bigg]\Delta\boldsymbol{\theta}^B,
\end{aligned} \tag{3.133}$$

with the terms

$$(\mathbf{P}_s^B)^T\frac{\partial(\boldsymbol{\Sigma}^B)^T}{\partial\boldsymbol{\omega}^B}(\mathbf{B}^B)^T\boldsymbol{\Sigma}^B\mathbf{M}^B\tilde{\mathbf{A}}^B\frac{d\mathbf{q}^B}{dt} \text{ and } (\mathbf{P}_s^B)^T\frac{\partial(\boldsymbol{\Sigma}^B)^T}{\partial\boldsymbol{\omega}^B}(\mathbf{B}^B)^T\mathbf{M}^B(\boldsymbol{\Sigma}^B)^T\tilde{\mathbf{A}}^B\frac{d\mathbf{q}^B}{dt}$$

having similar expressions. Next,

$$\begin{aligned}
(\mathbf{P}_s^B)^T\frac{\partial(\boldsymbol{\Sigma}^B)^T}{\partial\boldsymbol{\omega}^B}(\mathbf{B}^B)^T\mathbf{M}^B\mathbf{A}^B\boldsymbol{\Sigma}^B\frac{d\mathbf{q}^B}{dt} &\approx (\mathbf{P}_s^B)^T\left.\frac{\partial(\boldsymbol{\Sigma}^B)^T}{\partial\boldsymbol{\omega}^B}\right|_0(\mathbf{B}_0^B)^T\mathbf{M}^B\mathbf{A}_0^B\boldsymbol{\Sigma}_0^B\frac{d\Delta\mathbf{q}^B}{dt};\\
(\mathbf{P}_s^B)^T\frac{\partial(\boldsymbol{\Sigma}^B)^T}{\partial\boldsymbol{\omega}^B}(\mathbf{B}^B)^T\mathbf{M}^B\tilde{\mathbf{A}}^B\boldsymbol{\Sigma}^B\frac{d\mathbf{q}^B}{dt} &\approx (\mathbf{P}_s^B)^T\left.\frac{\partial(\boldsymbol{\Sigma}^B)^T}{\partial\boldsymbol{\omega}^B}\right|_0(\mathbf{B}_0^B)^T\mathbf{M}^B\tilde{\mathbf{A}}_0^B\boldsymbol{\Sigma}_0^B\frac{d\Delta\mathbf{q}^B}{dt}.
\end{aligned} \tag{3.134}$$

The two remaining terms are

$$\frac{d(\mathbf{q}^B)^T}{dt}\frac{\partial(\boldsymbol{\Sigma}^B)^T}{\partial\boldsymbol{\omega}^B}(\mathbf{A}^B)^T\mathbf{M}^B\mathbf{B}^B\boldsymbol{\Sigma}^B\mathbf{P}_s^B \approx (\mathbf{P}_s^B)^T(\boldsymbol{\Sigma}_0^B)^T(\mathbf{B}_0^B)^T\mathbf{M}^B\mathbf{A}_0^B\left.\frac{\partial\boldsymbol{\Sigma}^B}{\partial\boldsymbol{\omega}^B}\right|_0\frac{d\Delta\mathbf{q}^B}{dt} \tag{3.135}$$

and

$$
\begin{aligned}
&(\mathbf{P}_s^B)^T\left(\frac{d}{dt}\frac{\partial(\boldsymbol{\Sigma}^B)^T}{\partial\boldsymbol{\omega}^B}\right)(\mathbf{B}^B)^T\mathbf{M}^B\tilde{\mathbf{A}}^B\frac{d\mathbf{q}^B}{dt}\approx\Omega_0(\mathbf{P}_s^B)^T\left.\frac{\partial^2(\boldsymbol{\Sigma}^B)^T}{\partial\boldsymbol{\omega}^B\partial\psi}\right|_0(\mathbf{B}_0^B)^T\mathbf{M}^B\tilde{\mathbf{A}}_0^B\boldsymbol{\Omega}_0\\
&\quad+\Omega_0(\mathbf{P}_s^B)^T\left.\frac{\partial^2(\boldsymbol{\Sigma}^B)^T}{\partial\boldsymbol{\omega}^B\partial\psi}\right|_0(\mathbf{B}_0^B)^T\mathbf{M}^B\tilde{\mathbf{A}}_0^B\frac{d\Delta\mathbf{q}^B}{dt}+(\mathbf{P}_s^B)^T\left.\frac{\partial^2(\boldsymbol{\Sigma}^B)^T}{\partial\boldsymbol{\omega}^B\partial\boldsymbol{\theta}^B}\right|_0(\mathbf{B}_0^B)^T\mathbf{M}^B\tilde{\mathbf{A}}_0^B\boldsymbol{\Omega}_0\Delta\boldsymbol{\omega}^B\\
&\quad+\left(\Omega_0(\mathbf{P}_s^B)^T\left.\frac{\partial^3(\boldsymbol{\Sigma}^B)^T}{\partial\boldsymbol{\omega}^B\partial\psi\partial\boldsymbol{\theta}^B}\right|_0(\mathbf{B}_0^B)^T\mathbf{M}^B\tilde{\mathbf{A}}_0^B\boldsymbol{\Omega}_0+\Omega_0(\mathbf{P}_s^B)^T\left.\frac{\partial^2(\boldsymbol{\Sigma}^B)^T}{\partial\boldsymbol{\omega}^B\partial\psi}\right|_0\left.\frac{\partial(\mathbf{B}^B)^T}{\partial\boldsymbol{\theta}^B}\right|_0\mathbf{M}^B\tilde{\mathbf{A}}_0^B\boldsymbol{\Omega}_0\right.\\
&\quad+\left.\Omega_0(\mathbf{P}_s^B)^T\left.\frac{\partial^2(\boldsymbol{\Sigma}^B)^T}{\partial\boldsymbol{\omega}^B\partial\psi}\right|_0(\mathbf{B}_0^B)^T\mathbf{M}^B\frac{\partial\tilde{\mathbf{A}}^B}{\partial\boldsymbol{\theta}^B}\boldsymbol{\Omega}_0\right)\Delta\boldsymbol{\theta}^B.
\end{aligned}
\tag{3.136}
$$

The five terms which are quadratic in displacements are all zero.

The ten terms with coupling between displacements and positional offsets all contain products of $\mathbf{q}^B$ and $\boldsymbol{\Sigma}^B$ or its derivatives, so to first order,

$$
\begin{aligned}
&(\mathbf{P}_s^B)^T\frac{\partial(\boldsymbol{\Sigma}^B)^T}{\partial\boldsymbol{\omega}^B}(\boldsymbol{\Sigma}^B)^T(\mathbf{B}^B)^T\mathbf{M}^B\mathbf{A}^B\boldsymbol{\Sigma}^B\mathbf{q}^B\approx\\
&\quad(\mathbf{P}_s^B)^T\left.\frac{\partial(\boldsymbol{\Sigma}^B)^T}{\partial\boldsymbol{\omega}^B}\right|_0(\boldsymbol{\Sigma}_0^B)^T(\mathbf{B}_0^B)^T\mathbf{M}^B\mathbf{A}_0^B\boldsymbol{\Sigma}_0^B\left(\mathbf{q}_0^B+\Delta\mathbf{q}^B\right),
\end{aligned}
\tag{3.137}
$$

and similarly for

$$
\begin{aligned}
&(\mathbf{P}_s^B)^T\frac{\partial(\boldsymbol{\Sigma}^B)^T}{\partial\boldsymbol{\omega}^B}(\mathbf{B}^B)^T\boldsymbol{\Sigma}^B\mathbf{M}^B\mathbf{A}^B\boldsymbol{\Sigma}^B\mathbf{q}^B,\\
&(\mathbf{P}_s^B)^T\frac{\partial(\boldsymbol{\Sigma}^B)^T}{\partial\boldsymbol{\omega}^B}(\mathbf{B}^B)^T\mathbf{M}^B(\boldsymbol{\Sigma}^B)^T\mathbf{A}^B\boldsymbol{\Sigma}^B\mathbf{q}^B,\text{ and}\\
&(\mathbf{P}_s^B)^T\frac{\partial(\boldsymbol{\Sigma}^B)^T}{\partial\boldsymbol{\omega}^B}(\mathbf{B}^B)^T\mathbf{M}^B\mathbf{A}^B\boldsymbol{\Sigma}^B\boldsymbol{\Sigma}^B\mathbf{q}^B.
\end{aligned}
$$

Then,

$$
\begin{aligned}
&(\mathbf{q}^B)^T\frac{\partial(\boldsymbol{\Sigma}^B)^T}{\partial\boldsymbol{\omega}^B}(\boldsymbol{\Sigma}^B)^T(\mathbf{A}^B)^T\mathbf{M}^B\mathbf{B}^B\boldsymbol{\Sigma}^B\mathbf{P}_s^B\approx\\
&\quad(\mathbf{P}_s^B)^T(\boldsymbol{\Sigma}_0^B)^T(\mathbf{B}_0^B)^T\mathbf{M}^B\mathbf{A}_0^B\boldsymbol{\Sigma}_0^B\left.\frac{\partial\boldsymbol{\Sigma}^B}{\partial\boldsymbol{\omega}^B}\right|_0\left(\mathbf{q}_0^B+\Delta\mathbf{q}^B\right),
\end{aligned}
\tag{3.138}
$$

and similarly for

$$
\begin{aligned}
&(\mathbf{q}^B)^T\frac{\partial(\boldsymbol{\Sigma}^B)^T}{\partial\boldsymbol{\omega}^B}(\mathbf{A}^B)^T\boldsymbol{\Sigma}^B\mathbf{M}^B\mathbf{B}^B\boldsymbol{\Sigma}^B\mathbf{P}_s^B,\\
&(\mathbf{q}^B)^T\frac{\partial(\boldsymbol{\Sigma}^B)^T}{\partial\boldsymbol{\omega}^B}(\mathbf{A}^B)^T\mathbf{M}^B(\boldsymbol{\Sigma}^B)^T\mathbf{B}^B\boldsymbol{\Sigma}^B\mathbf{P}_s^B,\text{ and}\\
&(\mathbf{q}^B)^T\frac{\partial(\boldsymbol{\Sigma}^B)^T}{\partial\boldsymbol{\omega}^B}(\mathbf{A}^B)^T\mathbf{M}^B\mathbf{B}^B\boldsymbol{\Sigma}^B\boldsymbol{\Sigma}^B\mathbf{P}_s^B.
\end{aligned}
$$

Finally,

$$
\begin{aligned}
&(\mathbf{q}^B)^T\left(\frac{d}{dt}\frac{\partial(\boldsymbol{\Sigma}^B)^T}{\partial\boldsymbol{\omega}^B}\right)(\mathbf{A}^B)^T\mathbf{M}^B\mathbf{B}^B\boldsymbol{\Sigma}^B\mathbf{P}_s^B\approx\Omega_0(\mathbf{P}_s^B)^T(\boldsymbol{\Sigma}_0^B)^T(\mathbf{B}_0^B)^T\mathbf{M}^B\mathbf{A}_0^B\left.\frac{\partial^2\boldsymbol{\Sigma}^B}{\partial\boldsymbol{\omega}^B\partial\psi}\right|_0(\mathbf{q}_0^B+\Delta\mathbf{q}^B)\\
&(\mathbf{P}_s^B)^T\left(\frac{d}{dt}\frac{\partial(\boldsymbol{\Sigma}^B)^T}{\partial\boldsymbol{\omega}^B}\right)(\mathbf{B}^B)^T\mathbf{M}^B\mathbf{A}^B\boldsymbol{\Sigma}^B\mathbf{q}^B\approx\Omega_0(\mathbf{P}_s^B)^T\left.\frac{\partial^2(\boldsymbol{\Sigma}^B)^T}{\partial\boldsymbol{\omega}^B\partial\psi}\right|_0(\mathbf{B}_0^B)^T\mathbf{M}^B\mathbf{A}_0^B\boldsymbol{\Sigma}_0^B(\mathbf{q}_0^B+\Delta\mathbf{q}^B)
\end{aligned}
\tag{3.139}
$$

The five terms which are quadratic in the positional offsets are linearized as

$$
\begin{aligned}
(\mathbf{P}_s^B)^T \frac{\partial(\boldsymbol{\Sigma}^B)^T}{\partial \boldsymbol{\omega}^B}(\boldsymbol{\Sigma}^B)^T(\mathbf{B}^B)^T\mathbf{M}^B\mathbf{B}^B\boldsymbol{\Sigma}^B\mathbf{P}_s^B &\approx (\mathbf{P}_s^B)^T \frac{\partial(\boldsymbol{\Sigma}^B)^T}{\partial \boldsymbol{\omega}^B}\bigg|_0 (\boldsymbol{\Sigma}_0^B)^T(\mathbf{B}_0^B)^T\mathbf{M}^B\mathbf{B}_0^B\boldsymbol{\Sigma}_0^B\mathbf{P}_s^B \\
&+\Bigg[(\mathbf{P}_s^B)^T \frac{\partial^2(\boldsymbol{\Sigma}^B)^T}{(\partial \boldsymbol{\omega}^B)^2}\bigg|_0 (\boldsymbol{\Sigma}_0^B)^T(\mathbf{B}_0^B)^T\mathbf{M}^B\mathbf{B}_0^B\boldsymbol{\Sigma}_0^B\mathbf{P}_s^B \\
&+ (\mathbf{P}_s^B)^T \frac{\partial(\boldsymbol{\Sigma}^B)^T}{\partial \boldsymbol{\omega}^B}\bigg|_0 \frac{\partial(\boldsymbol{\Sigma}^B)^T}{\partial \boldsymbol{\omega}^B}\bigg|_0 (\mathbf{B}_0^B)^T\mathbf{M}^B\mathbf{B}_0^B\boldsymbol{\Sigma}_0^B\mathbf{P}_s^B \\
&+ (\mathbf{P}_s^B)^T \frac{\partial(\boldsymbol{\Sigma}^B)^T}{\partial \boldsymbol{\omega}^B}\bigg|_0 (\boldsymbol{\Sigma}_0^B)^T(\mathbf{B}_0^B)^T\mathbf{M}^B\mathbf{B}_0^B\frac{\partial\boldsymbol{\Sigma}^B}{\partial \boldsymbol{\omega}^B}\bigg|_0 \mathbf{P}_s^B\Bigg]\Delta\boldsymbol{\omega}^B \\
&+\Bigg[(\mathbf{P}_s^B)^T \frac{\partial(\boldsymbol{\Sigma}^B)^T}{\partial \boldsymbol{\omega}^B}\bigg|_0 (\boldsymbol{\Sigma}_0^B)^T\frac{\partial(\mathbf{B}^B)^T}{\partial \boldsymbol{\theta}^B}\bigg|_0 \mathbf{M}^B\mathbf{B}_0^B\boldsymbol{\Sigma}_0^B\mathbf{P}_s^B \\
&+ (\mathbf{P}_s^B)^T \frac{\partial(\boldsymbol{\Sigma}^B)^T}{\partial \boldsymbol{\omega}^B}\bigg|_0 (\boldsymbol{\Sigma}_0^B)^T(\mathbf{B}_0^B)^T\mathbf{M}^B\frac{\partial\mathbf{B}^B}{\partial \boldsymbol{\theta}^B}\bigg|_0 \boldsymbol{\Sigma}_0^B\mathbf{P}_s^B \\
&+ (\mathbf{P}_s^B)^T \frac{\partial^2(\boldsymbol{\Sigma}^B)^T}{\partial \boldsymbol{\omega}^B\partial \boldsymbol{\theta}^B}\bigg|_0 (\boldsymbol{\Sigma}_0^B)^T(\mathbf{B}_0^B)^T\mathbf{M}^B\mathbf{B}_0^B\boldsymbol{\Sigma}_0^B\mathbf{P}_s^B \\
&+ (\mathbf{P}_s^B)^T \frac{\partial(\boldsymbol{\Sigma}^B)^T}{\partial \boldsymbol{\omega}^B}\bigg|_0 \frac{\partial(\boldsymbol{\Sigma}^B)^T}{\partial \boldsymbol{\theta}^B}\bigg|_0 (\mathbf{B}_0^B)^T\mathbf{M}^B\mathbf{B}_0^B\boldsymbol{\Sigma}_0^B\mathbf{P}_s^B \\
&+ (\mathbf{P}_s^B)^T \frac{\partial(\boldsymbol{\Sigma}^B)^T}{\partial \boldsymbol{\omega}^B}\bigg|_0 (\boldsymbol{\Sigma}_0^B)^T(\mathbf{B}_0^B)^T\mathbf{M}^B\mathbf{B}_0^B\frac{\partial\boldsymbol{\Sigma}^B}{\partial \boldsymbol{\theta}^B}\bigg|_0 \mathbf{P}_s^B\Bigg]\Delta\boldsymbol{\theta}^B
\end{aligned}
\tag{3.140}
$$

and similarly for

$$(\mathbf{P}_s^B)^T \frac{\partial(\boldsymbol{\Sigma}^B)^T}{\partial \boldsymbol{\omega}^B}(\mathbf{B}^B)^T\boldsymbol{\Sigma}^B\mathbf{M}^B\mathbf{B}^B\boldsymbol{\Sigma}^B\mathbf{P}_s^B,$$

$$(\mathbf{P}_s^B)^T \frac{\partial(\boldsymbol{\Sigma}^B)^T}{\partial \boldsymbol{\omega}^B}(\mathbf{B}^B)^T\mathbf{M}^B(\boldsymbol{\Sigma}^B)^T\mathbf{B}^B\boldsymbol{\Sigma}^B\mathbf{P}_s^B, \text{ and}$$

$$(\mathbf{P}_s^B)^T \frac{\partial(\boldsymbol{\Sigma}^B)^T}{\partial \boldsymbol{\omega}^B}(\mathbf{B}^B)^T\mathbf{M}^B\mathbf{B}^B\boldsymbol{\Sigma}^B\boldsymbol{\Sigma}^B\mathbf{P}_s^B.$$

The fifth term is

$$
\begin{aligned}
(\mathbf{P}_s^B)^T\left(\frac{d}{dt}\frac{\partial(\boldsymbol{\Sigma}^B)^T}{\partial \boldsymbol{\omega}^B}\right)(\mathbf{B}^B)^T\mathbf{M}^B\mathbf{B}^B\boldsymbol{\Sigma}^B\mathbf{P}_s^B &\approx \Omega_0(\mathbf{P}_s^B)^T\frac{\partial^2(\boldsymbol{\Sigma}^B)^T}{\partial \boldsymbol{\omega}^B\partial\psi}\bigg|_0 (\mathbf{B}_0^B)^T\mathbf{M}^B\mathbf{B}_0^B\boldsymbol{\Sigma}_0^B\mathbf{P}_s^B \\
&+\left((\mathbf{P}_s^B)^T\frac{\partial^2(\boldsymbol{\Sigma}^B)^T}{\partial \boldsymbol{\omega}^B\partial \boldsymbol{\theta}^B}\bigg|_0 (\mathbf{B}_0^B)^T\mathbf{M}^B\mathbf{B}_0^B\boldsymbol{\Sigma}_0^B\mathbf{P}_s^B+\Omega_0(\mathbf{P}_s^B)^T\frac{\partial^2(\boldsymbol{\Sigma}^B)^T}{\partial \boldsymbol{\omega}^B\partial\psi}\bigg|_0 (\mathbf{B}_0^B)^T\mathbf{M}^B\mathbf{B}_0^B\frac{\partial\boldsymbol{\Sigma}^B}{\partial \boldsymbol{\omega}^B}\mathbf{P}_s^B\right)\Delta\boldsymbol{\omega}^B \\
&+\left(\Omega_0(\mathbf{P}_s^B)^T\frac{\partial^3(\boldsymbol{\Sigma}^B)^T}{\partial \boldsymbol{\omega}^B\partial\psi\partial \boldsymbol{\theta}^B}\bigg|_0 (\mathbf{B}_0^B)^T\mathbf{M}^B\mathbf{B}_0^B\boldsymbol{\Sigma}_0^B\mathbf{P}_s^B+\Omega_0(\mathbf{P}_s^B)^T\frac{\partial^2(\boldsymbol{\Sigma}^B)^T}{\partial \boldsymbol{\omega}^B\partial\psi}\bigg|_0 (\mathbf{B}_0^B)^T\mathbf{M}^B\mathbf{B}_0^B\frac{\partial\boldsymbol{\Sigma}^B}{\partial \boldsymbol{\theta}^B}\mathbf{P}_s^B\right. \\
&\left.+\Omega_0(\mathbf{P}_s^B)^T\frac{\partial^2(\boldsymbol{\Sigma}^B)^T}{\partial \boldsymbol{\omega}^B\partial\psi}\bigg|_0 \frac{\partial(\mathbf{B}^B)^T}{\partial \boldsymbol{\theta}^B}\mathbf{M}^B\mathbf{B}_0^B\boldsymbol{\Sigma}_0^B\mathbf{P}_s^B+\Omega_0(\mathbf{P}_s^B)^T\frac{\partial^2(\boldsymbol{\Sigma}^B)^T}{\partial \boldsymbol{\omega}^B\partial\psi}\bigg|_0 (\mathbf{B}_0^B)^T\mathbf{M}^B\frac{\partial\mathbf{B}^B}{\partial \boldsymbol{\theta}^B}\boldsymbol{\Sigma}_0^B\mathbf{P}_s^B\right)\Delta\boldsymbol{\theta}^B.
\end{aligned}
\tag{3.141}
$$

The next group of centrifugal and coriolis terms are linearized as

$$-(\boldsymbol{\Sigma}^B)^T(\mathbf{A}^B)^T\mathbf{M}^B\mathbf{A}^B\boldsymbol{\Sigma}^B\mathbf{q}^B \approx -(\boldsymbol{\Sigma}_0^B)^T(\mathbf{A}_0^B)^T\mathbf{M}^B\mathbf{A}_0^B\boldsymbol{\Sigma}_0^B\left(\mathbf{q}_0^B+\Delta\mathbf{q}^B\right), \tag{3.142}$$

$$
\begin{aligned}
-(\boldsymbol{\Sigma}^B)^T(\mathbf{A}^B)^T\mathbf{M}^B\mathbf{B}^B\boldsymbol{\Sigma}^B\mathbf{P}_s^B \approx\ & -(\boldsymbol{\Sigma}_0^B)^T(\mathbf{A}_0^B)^T\mathbf{M}^B\mathbf{B}_0^B\boldsymbol{\Sigma}_0^B\mathbf{P}_s^B \\
& -\left[\left.\frac{\partial(\boldsymbol{\Sigma}^B)^T}{\partial\boldsymbol{\omega}^B}\right|_0(\mathbf{A}_0^B)^T\mathbf{M}^B\mathbf{B}_0^B\boldsymbol{\Sigma}_0^B\mathbf{P}_s^B+(\boldsymbol{\Sigma}_0^B)^T(\mathbf{A}_0^B)^T\mathbf{M}^B\mathbf{B}_0^B\left.\frac{\partial\boldsymbol{\Sigma}^B}{\partial\boldsymbol{\omega}^B}\right|_0\mathbf{P}_s^B\right]\Delta\boldsymbol{\omega}^B \\
& -\left[\left.\frac{\partial(\boldsymbol{\Sigma}^B)^T}{\partial\boldsymbol{\theta}^B}\right|_0(\mathbf{A}_0^B)^T\mathbf{M}^B\mathbf{B}_0^B\boldsymbol{\Sigma}_0^B\mathbf{P}_s^B+(\boldsymbol{\Sigma}_0^B)^T(\mathbf{A}_0^B)^T\mathbf{M}^B\mathbf{B}_0^B\left.\frac{\partial\boldsymbol{\Sigma}^B}{\partial\boldsymbol{\theta}^B}\right|_0\mathbf{P}_s^B\right. \\
& \left.+\ (\boldsymbol{\Sigma}_0^B)^T\left.\frac{\partial(\mathbf{A}^B)^T}{\partial\boldsymbol{\theta}^B}\right|_0\mathbf{M}^B\mathbf{B}_0^B\boldsymbol{\Sigma}_0^B\mathbf{P}_s^B+(\boldsymbol{\Sigma}_0^B)^T(\mathbf{A}_0^B)^T\mathbf{M}^B\left.\frac{\partial\mathbf{B}^B}{\partial\boldsymbol{\theta}^B}\right|_0\boldsymbol{\Sigma}_0^B\mathbf{P}_s^B\right]\Delta\boldsymbol{\theta}^B,
\end{aligned}
\tag{3.143}
$$

and

$$
\begin{aligned}
-(\boldsymbol{\Sigma}^B)^T(\mathbf{A}^B)^T\mathbf{M}^B\tilde{\mathbf{A}}^B\frac{d\mathbf{q}^B}{dt} \approx\ & -(\boldsymbol{\Sigma}_0^B)^T(\mathbf{A}_0^B)^T\mathbf{M}^B\tilde{\mathbf{A}}_0^B\boldsymbol{\Omega}_0 \\
& -(\boldsymbol{\Sigma}_0^B)^T(\mathbf{A}_0^B)^T\mathbf{M}^B\tilde{\mathbf{A}}_0^B\frac{d\Delta\mathbf{q}^B}{dt}-\left.\frac{\partial(\boldsymbol{\Sigma}^B)^T}{\partial\boldsymbol{\omega}^B}\right|_0(\mathbf{A}_0^B)^T\mathbf{M}^B\tilde{\mathbf{A}}_0^B\boldsymbol{\Omega}_0\Delta\boldsymbol{\omega}^B \\
& -\left[\left.\frac{\partial(\boldsymbol{\Sigma}^B)^T}{\partial\boldsymbol{\theta}^B}\right|_0(\mathbf{A}_0^B)^T\mathbf{M}^B\tilde{\mathbf{A}}_0^B\boldsymbol{\Omega}_0+(\boldsymbol{\Sigma}_0^B)^T\left.\frac{\partial(\mathbf{A}^B)^T}{\partial\boldsymbol{\theta}^B}\right|_0\mathbf{M}^B\tilde{\mathbf{A}}_0^B\boldsymbol{\Omega}_0\right. \\
& \left.+\ (\boldsymbol{\Sigma}_0^B)^T(\mathbf{A}_0^B)^T\mathbf{M}^B\frac{\partial\tilde{\mathbf{A}}^B}{\partial\boldsymbol{\theta}^B}\boldsymbol{\Omega}_0\right]\Delta\boldsymbol{\theta}^B.
\end{aligned}
\tag{3.144}
$$

The term which is quadratic in the velocities is

$$
\begin{aligned}
-\frac{d(\mathbf{q}^B)^T}{dt}\frac{\partial(\tilde{\mathbf{A}}^B)^T}{\partial\mathbf{q}^B}\mathbf{M}^B\tilde{\mathbf{A}}^B\frac{d\mathbf{q}^B}{dt} \approx\ & -\boldsymbol{\Omega}_0^T\left.\frac{\partial(\tilde{\mathbf{A}}^B)^T}{\partial\boldsymbol{\theta}^B}\right|_0\mathbf{M}^B\tilde{\mathbf{A}}_0^B\boldsymbol{\Omega}_0 \\
& -\left[\boldsymbol{\Omega}_0^T\left.\frac{\partial(\tilde{\mathbf{A}}^B)^T}{\partial\boldsymbol{\theta}^B}\right|_0\mathbf{M}^B\tilde{\mathbf{A}}_0^B+\boldsymbol{\Omega}_0^T(\tilde{\mathbf{A}}_0^B)^T\mathbf{M}^B\left.\frac{\partial\tilde{\mathbf{A}}^B}{\partial\boldsymbol{\theta}^B}\right|_0\right]\frac{d\Delta\mathbf{q}^B}{dt} \\
& -\left[\boldsymbol{\Omega}_0^T\frac{\partial^2(\tilde{\mathbf{A}}^B)^T}{(\partial\boldsymbol{\theta}^B)^2}\mathbf{M}^B\tilde{\mathbf{A}}_0^B\boldsymbol{\Omega}_0+\boldsymbol{\Omega}_0^T\left.\frac{\partial(\tilde{\mathbf{A}}^B)^T}{\partial\boldsymbol{\theta}^B}\right|_0\mathbf{M}^B\left.\frac{\partial\tilde{\mathbf{A}}^B}{\partial\boldsymbol{\theta}^B}\right|_0\boldsymbol{\Omega}_0\right]\Delta\boldsymbol{\theta}^B.
\end{aligned}
\tag{3.145}
$$

The three terms coupling displacements and velocities are

$$
-(\mathbf{q}^B)^T\frac{\partial(\boldsymbol{\Sigma}^B)^T}{\partial\mathbf{q}^B}(\mathbf{A}^B)^T\mathbf{M}^B\tilde{\mathbf{A}}^B\frac{d\mathbf{q}^B}{dt} \approx -\boldsymbol{\Omega}_0^T(\tilde{\mathbf{A}}_0^B)^T\mathbf{M}^B\mathbf{A}_0^B\left.\frac{\partial\boldsymbol{\Sigma}^B}{\partial\boldsymbol{\theta}^B}\right|_0\left(\mathbf{q}_0^B+\Delta\mathbf{q}^B\right),
\tag{3.146}
$$

$$
-(\mathbf{q}^B)^T(\boldsymbol{\Sigma}^B)^T\frac{\partial(\mathbf{A}^B)^T}{\partial\mathbf{q}^B}\mathbf{M}^B\tilde{\mathbf{A}}^B\frac{d\mathbf{q}^B}{dt} \approx -\boldsymbol{\Omega}_0^T(\tilde{\mathbf{A}}_0^B)^T\mathbf{M}^B\left.\frac{\partial\mathbf{A}^B}{\partial\boldsymbol{\theta}^B}\right|_0\boldsymbol{\Sigma}_0^B\left(\mathbf{q}_0^B+\Delta\mathbf{q}^B\right),
\tag{3.147}
$$

and

$$
-\frac{d(\mathbf{q}^B)^T}{dt}\frac{\partial(\tilde{\mathbf{A}}^B)^T}{\partial\mathbf{q}^B}\mathbf{M}^B\mathbf{A}^B\boldsymbol{\Sigma}^B\mathbf{q}^B \approx -\boldsymbol{\Omega}_0^T\left.\frac{\partial(\tilde{\mathbf{A}}^B)^T}{\partial\boldsymbol{\theta}^B}\right|_0\mathbf{M}^B\mathbf{A}_0^B\boldsymbol{\Sigma}_0^B\left(\mathbf{q}_0^B+\Delta\mathbf{q}^B\right).
\tag{3.148}
$$

The three terms coupling positional offsets and velocities are

$$
\begin{aligned}
-(\mathbf{P}_s^B)^T \frac{\partial(\boldsymbol{\Sigma}^B)^T}{\partial \mathbf{q}^B}(\mathbf{B}^B)^T \mathbf{M}^B \tilde{\mathbf{A}}^B \frac{d\mathbf{q}^B}{dt} &\approx -(\mathbf{P}_s^B)^T \left.\frac{\partial(\boldsymbol{\Sigma}^B)^T}{\partial \boldsymbol{\theta}^B}\right|_0 (\mathbf{B}_0^B)^T \mathbf{M}^B \tilde{\mathbf{A}}_0^B \boldsymbol{\Omega}_0 \\
&- (\mathbf{P}_s^B)^T \left.\frac{\partial(\boldsymbol{\Sigma}^B)^T}{\partial \boldsymbol{\theta}^B}\right|_0 (\mathbf{B}_0^B)^T \mathbf{M}^B \tilde{\mathbf{A}}_0^B \frac{d\Delta\mathbf{q}^B}{dt} - (\mathbf{P}_s^B)^T \left.\frac{\partial^2(\boldsymbol{\Sigma}^B)^T}{\partial \boldsymbol{\omega}^B \partial \boldsymbol{\theta}^B}\right|_0 (\mathbf{B}_0^B)^T \mathbf{M}^B \tilde{\mathbf{A}}_0^B \boldsymbol{\Omega}_0 \Delta\boldsymbol{\omega}^B \\
&- \left[(\mathbf{P}_s^B)^T \left.\frac{\partial^2(\boldsymbol{\Sigma}^B)^T}{(\partial \boldsymbol{\theta}^B)^2}\right|_0 (\mathbf{B}_0^B)^T \mathbf{M}^B \tilde{\mathbf{A}}_0^B \boldsymbol{\Omega}_0 + (\mathbf{P}_s^B)^T \left.\frac{\partial(\boldsymbol{\Sigma}^B)^T}{\partial \boldsymbol{\theta}^B}\right|_0 \left.\frac{\partial(\mathbf{B}^B)^T}{\partial \boldsymbol{\theta}^B}\right|_0 \mathbf{M}^B \tilde{\mathbf{A}}_0^B \boldsymbol{\Omega}_0 \right. \\
&+ \left. (\mathbf{P}_s^B)^T \left.\frac{\partial(\boldsymbol{\Sigma}^B)^T}{\partial \boldsymbol{\theta}^B}\right|_0 (\mathbf{B}_0^B)^T \mathbf{M}^B \left.\frac{\partial \tilde{\mathbf{A}}^B}{\partial \boldsymbol{\theta}^B}\right|_0 \boldsymbol{\Omega}_0 \right] \Delta\boldsymbol{\theta}^B,
\end{aligned}
\tag{3.149}
$$

$$
\begin{aligned}
-(\mathbf{P}_s^B)^T (\boldsymbol{\Sigma}^B)^T \frac{\partial(\mathbf{B}^B)^T}{\partial \mathbf{q}^B}\mathbf{M}^B \tilde{\mathbf{A}}^B \frac{d\mathbf{q}^B}{dt} &\approx -(\mathbf{P}_s^B)^T (\boldsymbol{\Sigma}_0^B)^T \left.\frac{\partial(\mathbf{B}^B)^T}{\partial \boldsymbol{\theta}^B}\right|_0 \mathbf{M}^B \tilde{\mathbf{A}}_0^B \boldsymbol{\Omega}_0 \\
&- (\mathbf{P}_s^B)^T (\boldsymbol{\Sigma}_0^B)^T \left.\frac{\partial(\mathbf{B}^B)^T}{\partial \boldsymbol{\theta}^B}\right|_0 \mathbf{M}^B \tilde{\mathbf{A}}_0^B \frac{d\Delta\mathbf{q}^B}{dt} - (\mathbf{P}_s^B)^T \left.\frac{\partial(\boldsymbol{\Sigma}^B)^T}{\partial \boldsymbol{\omega}^B}\right|_0 \left.\frac{\partial(\mathbf{B}^B)^T}{\partial \boldsymbol{\theta}^B}\right|_0 \mathbf{M}^B \tilde{\mathbf{A}}_0^B \boldsymbol{\Omega}_0 \Delta\boldsymbol{\omega}^B \\
&- \left[(\mathbf{P}_s^B)^T \left.\frac{\partial(\boldsymbol{\Sigma}^B)^T}{\partial \boldsymbol{\theta}^B}\right|_0 \left.\frac{\partial(\mathbf{B}^B)^T}{\partial \boldsymbol{\theta}^B}\right|_0 \mathbf{M}^B \tilde{\mathbf{A}}_0^B \boldsymbol{\Omega}_0 + (\mathbf{P}_s^B)^T (\boldsymbol{\Sigma}_0^B)^T \left.\frac{\partial^2(\mathbf{B}^B)^T}{(\partial \boldsymbol{\theta}^B)^2}\right|_0 \mathbf{M}^B \tilde{\mathbf{A}}_0^B \boldsymbol{\Omega}_0 \right. \\
&+ \left. (\mathbf{P}_s^B)^T (\boldsymbol{\Sigma}_0^B)^T \left.\frac{\partial(\mathbf{B}^B)^T}{\partial \boldsymbol{\theta}^B}\right|_0 \mathbf{M}^B \left.\frac{\partial \tilde{\mathbf{A}}^B}{\partial \boldsymbol{\theta}^B}\right|_0 \boldsymbol{\Omega}_0 \right] \Delta\boldsymbol{\theta}^B,
\end{aligned}
\tag{3.150}
$$

and

$$
\begin{aligned}
-\frac{d(\mathbf{q}^B)^T}{dt}\frac{\partial(\tilde{\mathbf{A}}^B)^T}{\partial \mathbf{q}^B}\mathbf{M}^B \mathbf{B}^B \boldsymbol{\Sigma}^B \mathbf{P}_s^B &\approx -(\mathbf{P}_s^B)^T (\boldsymbol{\Sigma}_0^B)^T (\mathbf{B}^B)^T \mathbf{M}^B \left.\frac{\partial \tilde{\mathbf{A}}^B}{\partial \boldsymbol{\theta}^B}\right|_0 \boldsymbol{\Omega}_0 \\
&- (\mathbf{P}_s^B)^T (\boldsymbol{\Sigma}_0^B)^T (\mathbf{B}_0^B)^T \mathbf{M}^B \left.\frac{\partial \tilde{\mathbf{A}}^B}{\partial \boldsymbol{\theta}^B}\right|_0 \frac{d\Delta\mathbf{q}^B}{dt} - (\mathbf{P}_s^B)^T \left.\frac{\partial(\boldsymbol{\Sigma}^B)^T}{\partial \boldsymbol{\omega}^B}\right|_0 (\mathbf{B}_0^B)^T \mathbf{M}^B \left.\frac{\partial \tilde{\mathbf{A}}^B}{\partial \boldsymbol{\theta}^B}\right|_0 \boldsymbol{\Omega}_0 \Delta\boldsymbol{\omega}^B \\
&- \left[(\mathbf{P}_s^B)^T \left.\frac{\partial(\boldsymbol{\Sigma}^B)^T}{\partial \boldsymbol{\theta}^B}\right|_0 (\mathbf{B}_0^B)^T \mathbf{M}^B \left.\frac{\partial \tilde{\mathbf{A}}^B}{\partial \boldsymbol{\theta}^B}\right|_0 \boldsymbol{\Omega}_0 + (\mathbf{P}_s^B)^T (\boldsymbol{\Sigma}_0^B)^T \left.\frac{\partial(\mathbf{B}^B)^T}{\partial \boldsymbol{\theta}^B}\right|_0 \mathbf{M}^B \left.\frac{\partial \tilde{\mathbf{A}}^B}{\partial \boldsymbol{\theta}^B}\right|_0 \boldsymbol{\Omega}_0 \right. \\
&+ \left. (\mathbf{P}_s^B)^T (\boldsymbol{\Sigma}_0^B)^T (\mathbf{B}_0^B)^T \mathbf{M}^B \left.\frac{\partial^2 \tilde{\mathbf{A}}^B}{(\partial \boldsymbol{\theta}^B)^2}\right|_0 \boldsymbol{\Omega}_0 \right] \Delta\boldsymbol{\theta}^B.
\end{aligned}
\tag{3.151}
$$

(On implementation, caution is needed on the above and following equations, as to which partial derivative determines the column in the matrix and which determines the row.)

The two terms which are quadratic in displacements are both zero to first order. The four terms coupling displacements and positional offsets are linearized as

$$
-(\mathbf{P}_s^B)^T \frac{\partial(\boldsymbol{\Sigma}^B)^T}{\partial \mathbf{q}^B}(\mathbf{B}^B)^T \mathbf{M}^B \mathbf{A}^B \boldsymbol{\Sigma}^B \mathbf{q}^B \approx -(\mathbf{P}_s^B)^T \left.\frac{\partial(\boldsymbol{\Sigma}^B)^T}{\partial \boldsymbol{\theta}^B}\right|_0 (\mathbf{B}_0^B)^T \mathbf{M}^B \mathbf{A}_0^B \boldsymbol{\Sigma}_0^B \left(\mathbf{q}_0^B + \Delta\mathbf{q}^B\right),
\tag{3.152}
$$

and similarly for

$$
-(\mathbf{P}_s^B)^T (\boldsymbol{\Sigma}^B)^T \frac{\partial(\mathbf{B}^B)^T}{\partial \mathbf{q}^B}\mathbf{M}^B \mathbf{A}^B \boldsymbol{\Sigma}^B \mathbf{q}^B,
$$

$$
-(\mathbf{q}^B)^T \frac{\partial(\boldsymbol{\Sigma}^B)^T}{\partial \mathbf{q}^B}(\mathbf{A}^B)^T \mathbf{M}^B \mathbf{B}^B \boldsymbol{\Sigma}^B \mathbf{P}_s^B, \text{ and}
$$

$$
-(\mathbf{q}^B)^T (\boldsymbol{\Sigma}^B)^T \frac{\partial(\mathbf{A}^B)^T}{\partial \mathbf{q}^B}\mathbf{M}^B \mathbf{B}^B \boldsymbol{\Sigma}^B \mathbf{P}_s^B.
$$

The two terms which are quadratic in positional offsets are linearized as

$$
\begin{aligned}
-(\mathbf{P}_s^B)^T \frac{\partial(\boldsymbol{\Sigma}^B)^T}{\partial \mathbf{q}^B}(\mathbf{B}^B)^T \mathbf{M}^B \mathbf{B}^B \boldsymbol{\Sigma}^B \mathbf{P}_s^B \approx & -(\mathbf{P}_s^B)^T \left.\frac{\partial(\boldsymbol{\Sigma}^B)^T}{\partial \boldsymbol{\theta}^B}\right|_0 (\mathbf{B}_0^B)^T \mathbf{M}^B \mathbf{B}_0^B \boldsymbol{\Sigma}_0^B \mathbf{P}_s^B \\
& - \left[(\mathbf{P}_s^B)^T \left.\frac{\partial(\boldsymbol{\Sigma}^B)^T}{\partial \boldsymbol{\omega}^B \partial \boldsymbol{\theta}^B}\right|_0 (\mathbf{B}_0^B)^T \mathbf{M}^B \mathbf{B}_0^B \boldsymbol{\Sigma}_0^B \mathbf{P}_s^B \right. \\
& + \left. (\mathbf{P}_s^B)^T \left.\frac{\partial(\boldsymbol{\Sigma}^B)^T}{\partial \boldsymbol{\theta}^B}\right|_0 (\mathbf{B}_0^B)^T \mathbf{M}^B \mathbf{B}_0^B \left.\frac{\partial \boldsymbol{\Sigma}^B}{\partial \boldsymbol{\omega}^B}\right|_0 \mathbf{P}_s^B \right] \Delta\boldsymbol{\omega}^B \\
& - \left[(\mathbf{P}_s^B)^T \left.\frac{\partial^2(\boldsymbol{\Sigma}^B)^T}{(\partial \boldsymbol{\theta}^B)^2}\right|_0 (\mathbf{B}_0^B)^T \mathbf{M}^B \mathbf{B}_0^B \boldsymbol{\Sigma}_0^B \mathbf{P}_s^B \right. \\
& + (\mathbf{P}_s^B)^T \left.\frac{\partial(\boldsymbol{\Sigma}^B)^T}{\partial \boldsymbol{\theta}^B}\right|_0 (\mathbf{B}_0^B)^T \mathbf{M}^B \mathbf{B}_0^B \left.\frac{\partial \boldsymbol{\Sigma}^B}{\partial \boldsymbol{\theta}^B}\right|_0 \mathbf{P}_s^B \\
& + (\mathbf{P}_s^B)^T \left.\frac{\partial(\boldsymbol{\Sigma}^B)^T}{\partial \boldsymbol{\theta}^B}\right|_0 \left.\frac{\partial(\mathbf{B}^B)^T}{\partial \boldsymbol{\theta}^B}\right|_0 \mathbf{M}^B \mathbf{B}_0^B \boldsymbol{\Sigma}_0^B \mathbf{P}_s^B \\
& + \left. (\mathbf{P}_s^B)^T \left.\frac{\partial(\boldsymbol{\Sigma}^B)^T}{\partial \boldsymbol{\theta}^B}\right|_0 (\mathbf{B}_0^B)^T \mathbf{M}^B \left.\frac{\partial \mathbf{B}^B}{\partial \boldsymbol{\theta}^B}\right|_0 \boldsymbol{\Sigma}_0^B \mathbf{P}_s^B \right] \Delta\boldsymbol{\theta}^B ,
\end{aligned}
\tag{3.153}
$$

and similarly for

$$
-(\mathbf{P}_s^B)^T (\boldsymbol{\Sigma}^B)^T \frac{\partial(\mathbf{B}^B)^T}{\partial \mathbf{q}^B}\mathbf{M}^B \mathbf{B}^B \boldsymbol{\Sigma}^B \mathbf{P}_s^B .
$$

The two remaining terms are

$$
\tilde{\mathbf{C}}^B \frac{d\mathbf{q}^B}{dt} \approx \tilde{\mathbf{C}}_0^B \frac{d\Delta\mathbf{q}^B}{dt} \tag{3.154}
$$

and

$$
\tilde{\mathbf{K}}^B \mathbf{q}^B \approx \tilde{\mathbf{K}}_0^B \mathbf{q}_0^B + \tilde{\mathbf{K}}_0^B \Delta\mathbf{q}^B + \left.\frac{\partial \tilde{\mathbf{K}}^B}{\partial \Omega}\right|_0 \mathbf{q}_0^B \Delta\Omega , \tag{3.155}
$$

where the latter term appears due to the centrifugal stiffening effect described in Section 3.1.4; this term may be neglected for cases in which the mean elastic blade displacements are considered to be small. The six rows and columns of $\tilde{\mathbf{C}}^B$ and $\tilde{\mathbf{K}}^B$ associated with the reference node on each body are set to zero, as the stiffness and damping do not act on the degrees-of-freedom associated with rigid-body motions.

The linearized equations can be written in the form

$$
\begin{aligned}
(\mathbf{G}_M^B + \tilde{\mathbf{M}}_0^B)\frac{d^2\Delta\mathbf{q}^B}{dt^2} = & \tilde{\mathbf{F}}_0^B - \mathbf{G}_{\Omega 0}^B - (\mathbf{G}_{K0}^B + \tilde{\mathbf{K}}^B)\mathbf{q}_0^B \\
& + \Delta\tilde{\mathbf{F}}^B - (\mathbf{G}_C^B + \tilde{\mathbf{C}}^B)\frac{d\Delta\mathbf{q}^B}{dt} - (\mathbf{G}_K^B + \tilde{\mathbf{K}}^B)\Delta\mathbf{q}^B .
\end{aligned}
\tag{3.156}
$$

Here $\mathbf{G}_{K0}^B$ represents steady-state terms which are dependent on $\boldsymbol{\Omega}_0$ and multiply $\mathbf{q}_0^B$, and $\mathbf{G}_{\Omega 0}^B$ represents the remainder of the steady-state terms which are dependent upon $\boldsymbol{\Omega}_0$. $\mathbf{G}_C^B$ and $\mathbf{G}_K^B$ are terms which are dependent upon $\boldsymbol{\Omega}_0$ and which multiply fluctuations in velocity and position, respectively. $\mathbf{G}_M^B$ accounts for the rotational acceleration terms. Also,

$$\tilde{\mathbf{M}}_0^B \coloneqq (\tilde{\mathbf{A}}_0^B)^T \mathbf{M}^B \tilde{\mathbf{A}}_0^B \tag{3.157}$$

3.4.3 Comments on the Equations of Motion

If all the matrix multiplications in the terms of $\mathbf{G}_C^B$ and $\mathbf{G}_K^B$ were written out, it would be seen that many of the terms cancel, and others are insignificantly small. This has not been pursued further, in the initial implementation of the STAS program. It has been observed that $\mathbf{G}_C^B$ and $\mathbf{G}_K^B$ have only a minor influence on the rotor dynamics of utility-scale wind turbines. With the exception of centrifugal stiffening (Section 3.1.4), centrifugal and gyroscopic effects can be neglected, to within the level of uncertainty expected for other aspects of the linearized analysis. Further discussion of this point is provided in Section 5.2.2.

3.5 Static and Dynamic Analysis in the Parked State

When the turbine is parked, $\Omega = 0$, and the linearized equations of motion are

$$\begin{aligned}
&\left((\tilde{\mathbf{A}}_0^B)^T \mathbf{M}^B \tilde{\mathbf{A}}_0^B + (\mathbf{P}_s^B)^T \left. \frac{\partial (\boldsymbol{\Sigma}^B)^T}{\partial \boldsymbol{\omega}^B} \right|_0 (\mathbf{B}_0^B)^T \mathbf{M}^B \tilde{\mathbf{A}}_0^B \right) \frac{d^2 \Delta \mathbf{q}^B}{dt^2} \\
&+ \left((\tilde{\mathbf{A}}_0^B)^T \mathbf{M}^B \mathbf{B}_0^B \left. \frac{\partial \dot{\boldsymbol{\Sigma}}^B}{\partial \dot{\boldsymbol{\omega}}^B} \right|_0 \mathbf{P}_s^B + (\mathbf{P}_s^B)^T \left. \frac{\partial (\boldsymbol{\Sigma}^B)^T}{\partial \boldsymbol{\omega}^B} \right|_0 (\mathbf{B}_0^B)^T \mathbf{M}^B \mathbf{B}_0^B \left. \frac{\partial \dot{\boldsymbol{\Sigma}}^B}{\partial \dot{\boldsymbol{\omega}}^B} \right|_0 \mathbf{P}_s^B \right) \frac{d \Delta \boldsymbol{\omega}^B}{dt} = \\
&\tilde{\mathbf{F}}_0^B - \tilde{\mathbf{K}}^B \mathbf{q}_0^B + \Delta \tilde{\mathbf{F}}^B - \tilde{\mathbf{C}}^B \frac{d \Delta \mathbf{q}^B}{dt} - \tilde{\mathbf{K}}^B \Delta \mathbf{q}^B .
\end{aligned} \tag{3.158}$$

The first term accounts for the inertia of elastic deformation, direct displacement of the reference nodes, and joint rotation. The next two terms account for the inertia of reference node rotation.

3.5.1 Constraints

In addition to the constraints given in Section 3.3, the joint rotations are locked by providing five additional constraint equations. The constraints are then implemented by the linear transformation of Equation 3.104. Applying this transformation to Equation 3.158, after partitioning the dependent and independent degrees-of-freedom, gives

$$\begin{aligned}
\boldsymbol{\Lambda}_0^T \left(\mathbf{G}_M^B + \tilde{\mathbf{M}}_0^B \right) \boldsymbol{\Lambda}_0 \frac{d^2 \Delta \hat{\mathbf{q}}^B}{dt^2} &= \boldsymbol{\Lambda}_0^T \mathbf{F}_0^B - \boldsymbol{\Lambda}_0^T \tilde{\mathbf{K}}^B \boldsymbol{\Lambda}_0 \hat{\mathbf{q}}_0^B \\
&+ \boldsymbol{\Lambda}_0^T \Delta \mathbf{F}^B - \boldsymbol{\Lambda}_0^T \tilde{\mathbf{C}}^B \boldsymbol{\Lambda}_0 \frac{d \Delta \hat{\mathbf{q}}^B}{dt} - \boldsymbol{\Lambda}_0^T \tilde{\mathbf{K}}^B \boldsymbol{\Lambda}_0 \Delta \hat{\mathbf{q}}^B .
\end{aligned} \tag{3.159}$$

3.5.2 Static Analysis

Considering only the static terms in Equation 3.159, the mean displacements of the independent degrees-of-freedom are computed by

$$\hat{\mathbf{q}}_0^B = \left(\boldsymbol{\Lambda}_0^T \tilde{\mathbf{K}}^B \boldsymbol{\Lambda}_0 \right)^{-1} \boldsymbol{\Lambda}_0^T \mathbf{F}_0^B . \tag{3.160}$$

The full set of displacements, including the slave degrees-of-freedom, is recovered by computing $\mathbf{q}_{s0}^B = -\mathbf{L}_{s0}^{-1} \hat{\mathbf{L}}_0 \, \hat{\mathbf{q}}_0^B$, and reordering so as to form $\mathbf{q}_0^B$.

3.5.3 Dynamic Analysis

The equations of motion are

$$\boldsymbol{\Lambda}_0^T\left(\mathbf{G}_M^B+\tilde{\mathbf{M}}_0^B\right)\boldsymbol{\Lambda}_0\frac{d^2\Delta\hat{\mathbf{q}}^B}{dt^2}=\boldsymbol{\Lambda}_0^T\Delta\mathbf{F}^B-\boldsymbol{\Lambda}_0^T\tilde{\mathbf{C}}^B\boldsymbol{\Lambda}_0\frac{d\Delta\hat{\mathbf{q}}^B}{dt}-\boldsymbol{\Lambda}_0^T\tilde{\mathbf{K}}^B\boldsymbol{\Lambda}_0\Delta\hat{\mathbf{q}}^B, \tag{3.161}$$

whose solution can be found by standard techniques of structural dynamics. The undamped eigenvalues and mode shapes are also of interest, and are to be found by the nontrivial solutions of

$$\boldsymbol{\Lambda}_0^T\tilde{\mathbf{K}}^B\boldsymbol{\Lambda}_0\Delta\hat{\mathbf{q}}^B-\omega^2\boldsymbol{\Lambda}_0^T\left(\mathbf{G}_M^B+\tilde{\mathbf{M}}_0^B\right)\boldsymbol{\Lambda}_0\Delta\hat{\mathbf{q}}^B=0. \tag{3.162}$$

Alternatively, Equation 3.162 can be represented in state space, as described in the next section.

3.6 Equations of Motion in State Space

We now consider the general case, where the rotor may be either fixed or spinning. In the case of a spinning rotor, a physically meaningful solution does not follow directly from these equations, as the degree-of-freedom ψ associated with the driveshaft and rotor azimuth undergoes a large steady rotation. Rather, the multi-blade coordinate transform of Section 3.8 is used afterwards to eliminate the dependence of the system matrices upon ψ.

3.6.1 Constraints

First the bodies are linked by constraints, as described in Section 3.3.1. The constraints are implemented by the linear transformation of Equation 3.104, after partitioning the degrees-of-freedom. Yaw and pitch rotations may be locked or free as appropriate, but driveshaft rotation is free. The equations of motion become

$$\begin{aligned}\boldsymbol{\Lambda}_0^T(\mathbf{G}_M^B+\tilde{\mathbf{M}}_0^B)\boldsymbol{\Lambda}_0\frac{d^2\Delta\hat{\mathbf{q}}^B}{dt^2}&=\boldsymbol{\Lambda}_0^T\mathbf{F}^B-\boldsymbol{\Lambda}_0^T\mathbf{G}_{\Omega 0}^B-\boldsymbol{\Lambda}_0^T(\mathbf{G}_{K0}^B+\tilde{\mathbf{K}}^B)\boldsymbol{\Lambda}_0\hat{\mathbf{q}}_0^B\\&\quad-\boldsymbol{\Lambda}_0^T(\mathbf{G}_C^B+\tilde{\mathbf{C}}^B)\boldsymbol{\Lambda}_0\frac{d\Delta\hat{\mathbf{q}}^B}{dt}-\boldsymbol{\Lambda}_0^T(\mathbf{G}_K^B+\tilde{\mathbf{K}}^B)\boldsymbol{\Lambda}_0\Delta\hat{\mathbf{q}}^B.\end{aligned} \tag{3.163}$$

For simplicity of notation, rewrite these equations as

$$\mathbf{M}\frac{d^2\Delta\mathbf{q}}{dt^2}=\mathbf{F}_0-\mathbf{G}_{\Omega 0}-\mathbf{K}_0\mathbf{q}_0+\Delta\mathbf{F}-\mathbf{C}\frac{d\Delta\mathbf{q}}{dt}-\mathbf{K}\Delta\mathbf{q}, \tag{3.164}$$

or

$$\mathbf{M}\frac{d^2\Delta\mathbf{q}}{dt^2}=\Delta\mathbf{F}-\mathbf{C}\frac{d\Delta\mathbf{q}}{dt}-\mathbf{K}\Delta\mathbf{q} \tag{3.165}$$

and

$$\mathbf{F}_0-\mathbf{G}_{\Omega 0}-\mathbf{K}_0\mathbf{q}_0=\mathbf{0}. \tag{3.166}$$

The terms in Equation 3.166 are not necessarily constant; they may have a fluctuating component that is a function of ψ_0.

3.6.2 State Equations in Physical Coordinates

There is more than one way to write Equation 3.164 in state-space form. The most direct way is to define

$$\mathbf{q}_1:=\mathbf{q}\quad\text{and}\quad\mathbf{q}_2:=\frac{d\mathbf{q}}{dt}, \tag{3.167}$$

such that

$$\begin{bmatrix}\mathbf{I}&\mathbf{0}\\\mathbf{0}&\mathbf{M}\end{bmatrix}\frac{d}{dt}\begin{bmatrix}\mathbf{q}_1\\\mathbf{q}_2\end{bmatrix}=\begin{bmatrix}\mathbf{0}&\mathbf{I}\\-\mathbf{K}&-\mathbf{C}\end{bmatrix}\begin{bmatrix}\mathbf{q}_1\\\mathbf{q}_2\end{bmatrix}+\begin{bmatrix}\mathbf{0}\\\Delta\mathbf{F}\end{bmatrix}. \tag{3.168}$$

An alternate form is obtained by switching the order of the states and balancing the **L** matrix using the mass matrix, for instance . The result is

$$\begin{bmatrix} \mathbf{0} & \mathbf{M} \\ \mathbf{M} & \mathbf{C} \end{bmatrix} \frac{d}{dt} \begin{bmatrix} \mathbf{q}_2 \\ \mathbf{q}_1 \end{bmatrix} = \begin{bmatrix} \mathbf{M} & \mathbf{0} \\ \mathbf{0} & -\mathbf{K} \end{bmatrix} \begin{bmatrix} \mathbf{q}_2 \\ \mathbf{q}_1 \end{bmatrix} + \begin{bmatrix} \mathbf{0} \\ \Delta\mathbf{F} \end{bmatrix}. \tag{3.169}$$

Here the former version, Equation 3.168, is adopted, as it is more intuitive. The potential advantage of Equation 3.169, that the matrices may be symmetric, is not realized in the present case, due to gyroscopic terms. In addition, the structural equations are but a part of a larger state-space.

3.7 Modal Reduction

It is desirable to reduce the number of degrees-of-freedom in the model. One reason is to increase the computational speed. Even more importantly, limiting the model to the lowest modes improves the numerical conditioning of the global eigenvalue calculation [11].

Begin with the unconstrained equations of motion, Equation 3.156. These represent a series of bodies, each of whose position and orientation is determined by a reference node. The elastic deformation of the body is then measured with respect to the reference node. This arrangement is ideally suited to independent modal decomposition of each body, using the Craig-Bampton method ([8],[31]).

3.7.1 Mode Shapes for Each Body

For each body, the mass and stiffness sub-matrices, associated with the elastic degrees-of-freedom, are extracted from the full-body matrices $\mathbf{G}_M^B + \tilde{\mathbf{M}}_0^B$ and $\tilde{\mathbf{K}}^B$ of Equation 3.156. The reference node degrees-of-freedom are not included in the sub-matrices; in effect, this fixes the reference node for purposes of calculating the modes.

On the tower, there is no reference node, and the modes are calculated including the soil stiffness terms. The tower modes are calculated using an augmented mass matrix, where the 6-by-6 block associated with the node at the yaw bearing is assigned the inertia matrix of the rotor-nacelle assembly. This gives tower modes which closely approximate the deformed shapes expected from the full structural model. Without the augmented inertia, the natural bending modes do not curve enough near the free end; in comparison with the full model, a modal model employing the first few bending modes cannot represent the internal loads on the tower side of the yaw bearing. With the augmented inertia, the internal loads are well approximated.

If the input file indicates the appropriate number of modes for the nacelle and driveshaft (8 and 18, respectively), Ritz vectors are used to represent the mode shapes, as described below. If the input file indicates some other number of modes for the nacelle and driveshaft, then these are computed using an augmented mass matrix for the master nodes, as in the case of the tower.

In either case, the Ritz or natural modes are computed with fixed X^d and Y^d degrees-of-freedom at the front bearing. To represent deformation of these two degrees-of-freedom, which are slaved to the nacelle, the driveshaft contains two additional modes. These are Ritz vectors computed as in Equation 3.170, with unit forces in the slave degrees-of-freedom.

The blades are represented by natural modes, computed with a fixed pitch bearing.

The above combination of body modes was found to reproduce the natural frequencies, through at least the first 20 modes of the assembled wind turbine, obtained from the full mass and stiffness matrices. Also, this combination of body modes reproduced the internal loads of the full model under various combinations of static loading.

Ritz vectors are obtained by applying unit loads to each of the master degrees-of-freedom, and solving for the static deformation, following Cook *et al.* [7], as

$$\mathbf{k}_j \boldsymbol{\varphi}_{jk} = \mathbf{f}_k , \tag{3.170}$$

where $\mathbf{f}_k$ contains a unit value in the appropriate degree-of-freedom and $\mathbf{k}_j$ is the stiffness sub-matrix associated with the body (nacelle or driveshaft). In the case of the nacelle, there are six master degrees-of-freedom at the rear bearing node, and two at the front bearing node. The driveshaft has 18 master degrees-of-freedom, 6 at each pitch bearing.

Otherwise, the mode shapes for body *j* are obtained by the eigenvectors of

$$\left(\mathbf{k}_j - \omega^2 \mathbf{m}_j\right)\boldsymbol{\varphi}_j = 0, \tag{3.171}$$

where $\mathbf{k}_j$ and $\mathbf{m}_j$ are the sub-matrices for the body's elastic degrees-of-freedom, and $\boldsymbol{\varphi}_j$ are the mode shapes. The mode shape vectors are normalized such that the maximum value in each vector is 1, and expanded with zeros so as to include entries for all the structural degrees-of-freedom, giving a matrix $\boldsymbol{\Phi}$.

A reduced list of degrees-of-freedom is defined for each body as

$$\bar{\mathbf{q}}^B = \begin{bmatrix} \mathbf{O}^B_{1/m} & \boldsymbol{\Theta}^B_{1/m} & \mathbf{d}^B & \dots \end{bmatrix}^T, \tag{3.172}$$

where **d** represents the modal amplitudes. In the case of the driveshaft, the sequence is modified to

$$\bar{\mathbf{q}}^B = \begin{bmatrix} \dots & \mathbf{O}^d_{1,d/n} & \boldsymbol{\Theta}^d_{1,d/n} & (\mathbf{w}^d_{f/s})_X & (\mathbf{w}^d_{f/s})_Y & \mathbf{d}^d & \dots \end{bmatrix}^T, \tag{3.173}$$

so as to include the two slave nodes at the front bearing.

The transform between physical and modal degrees-of-freedom is

$$\mathbf{q}^B = \boldsymbol{\Phi}\bar{\mathbf{q}}^B. \tag{3.174}$$

3.7.2 Constraint Equations

By Equation 3.174, the variation of the constraint functions, applied to the virtual displacements, becomes

$$\mathbf{L}^B\boldsymbol{\Phi}\delta\bar{\mathbf{q}}^B = \mathbf{0}. \tag{3.175}$$

Thus the matrix $\bar{\mathbf{L}}^B := \mathbf{L}^B\boldsymbol{\Phi}$ can be manipulated in the same manner as $\mathbf{L}^B$. The slave degrees-of-freedom are all separate, not included in the modes, thus it is straightforward to partition Equation 3.175 in the manner of Equation 3.104,

$$\delta\bar{\mathbf{q}}_s = -\bar{\mathbf{L}}_s^{-1}\hat{\mathbf{L}}\,\delta\hat{\mathbf{q}}, \tag{3.176}$$

where $\hat{\mathbf{q}}$ now includes only the joint rotations and modal amplitudes. The end result is the set of relations

$$\bar{\mathbf{q}}_s = -\bar{\mathbf{L}}_{s0}^{-1}\hat{\mathbf{L}}_0\,\hat{\mathbf{q}}; \quad \bar{\mathbf{q}} = \bar{\boldsymbol{\Lambda}}_0\hat{\mathbf{q}}; \quad \bar{\boldsymbol{\Lambda}}_0 := \begin{bmatrix} \mathbf{I} \\ -(\bar{\mathbf{L}}_{s0})^{-1}\hat{\mathbf{L}}_0 \end{bmatrix}. \tag{3.177}$$

3.7.3 Equations of Motion

Beginning with Equation 3.156, modal reduction is employed, giving

$$\begin{aligned} &\boldsymbol{\Phi}^T(\mathbf{G}^B_M + \tilde{\mathbf{M}}^B_0)\boldsymbol{\Phi}\frac{d^2\Delta\bar{\mathbf{q}}^B}{dt^2} = \\ &\qquad \boldsymbol{\Phi}^T\Delta\tilde{\mathbf{F}}^B - \boldsymbol{\Phi}^T(\mathbf{G}^B_C + \tilde{\mathbf{C}}^B)\boldsymbol{\Phi}\frac{d\Delta\bar{\mathbf{q}}^B}{dt} - \boldsymbol{\Phi}^T(\mathbf{G}^B_K + \tilde{\mathbf{K}}^B)\boldsymbol{\Phi}\Delta\bar{\mathbf{q}}^B. \end{aligned} \tag{3.178}$$

Then, the constraint relations, Equation 3.177, give the constrained equations of motion,

$$\begin{aligned} &\bar{\boldsymbol{\Lambda}}_0^T\boldsymbol{\Phi}^T(\mathbf{G}^B_M + \tilde{\mathbf{M}}^B_0)\boldsymbol{\Phi}\bar{\boldsymbol{\Lambda}}_0\frac{d^2\Delta\hat{\mathbf{q}}^B}{dt^2} = \\ &\qquad \bar{\boldsymbol{\Lambda}}_0^T\boldsymbol{\Phi}^T\Delta\tilde{\mathbf{F}}^B - \bar{\boldsymbol{\Lambda}}_0^T\boldsymbol{\Phi}^T(\mathbf{G}^B_C + \tilde{\mathbf{C}}^B)\boldsymbol{\Phi}\bar{\boldsymbol{\Lambda}}_0\frac{d\Delta\hat{\mathbf{q}}^B}{dt} - \bar{\boldsymbol{\Lambda}}_0^T\boldsymbol{\Phi}^T(\mathbf{G}^B_K + \tilde{\mathbf{K}}^B)\boldsymbol{\Phi}\bar{\boldsymbol{\Lambda}}_0\Delta\hat{\mathbf{q}}^B. \end{aligned} \tag{3.179}$$

The obvious definitions of **M**, **C**, **K**, and **F** lead to Equation 3.168 in state space form.

3.8 Multi-Blade Coordinates

The multi-blade coordinate transform is employed in the analysis of rotating systems like helicopters [15] and wind turbines ([3],[11],[25]). It is also known as the Coleman transform, after Coleman and Feingold [6].

Let some portion of the **x**, **y**, and **u** variables in Equation 1.3 be associated with the three blades of the wind turbine. That is, such variables appear in triplets (not necessarily consecutively in the vectors), as $[x_1^B \quad x_2^B \quad x_3^B]^T$, where the subscript here refers to the blade number. We define corresponding multi-blade coordinates $[x_0^\psi \quad x_c^\psi \quad x_s^\psi]^T$, where x_0^ψ represents collective motion, x_c^ψ represents motion when the blade is oriented along the cosine of the azimuth (the X^r axis), and x_s^ψ represents motion when the blade is oriented along the sine of the azimuth (the Y^r axis). The transforms between the triplets of variables are

$$\begin{bmatrix} x_1^B \\ x_2^B \\ x_3^B \end{bmatrix} = \mathbf{T}_\psi^B \begin{bmatrix} x_0^\psi \\ x_c^\psi \\ x_s^\psi \end{bmatrix}, \tag{3.180}$$

where

$$\mathbf{T}_\psi^B = \begin{bmatrix} 1 & \cos\psi & \sin\psi \\ 1 & \cos(\psi + 2\pi/3) & \sin(\psi + 2\pi/3) \\ 1 & \cos(\psi + 4\pi/3) & \sin(\psi + 4\pi/3) \end{bmatrix}, \tag{3.181}$$

ψ being the azimuth angle of blade 1, and

$$\mathbf{T}_B^\psi = (\mathbf{T}_\psi^B)^{-1} = \begin{bmatrix} \frac{1}{3} & \frac{1}{3} & \frac{1}{3} \\ \frac{2}{3}\cos\psi & \frac{2}{3}\cos(\psi + 2\pi/3) & \frac{2}{3}\cos(\psi + 4\pi/3) \\ \frac{2}{3}\sin\psi & \frac{2}{3}\sin(\psi + 2\pi/3) & \frac{2}{3}\sin(\psi + 4\pi/3) \end{bmatrix}. \tag{3.182}$$

The relevant derivatives are

$$\frac{d\mathbf{T}_\psi^B}{d\psi} = \begin{bmatrix} 0 & -\sin\psi & \cos\psi \\ 0 & -\sin(\psi + 2\pi/3) & \cos(\psi + 2\pi/3) \\ 0 & -\sin(\psi + 4\pi/3) & \cos(\psi + 4\pi/3) \end{bmatrix} \tag{3.183}$$

and

$$\frac{d^2\mathbf{T}_\psi^B}{d\psi^2} = \begin{bmatrix} 0 & -\cos\psi & -\sin\psi \\ 0 & -\cos(\psi + 2\pi/3) & -\sin(\psi + 2\pi/3) \\ 0 & -\cos(\psi + 4\pi/3) & -\sin(\psi + 4\pi/3) \end{bmatrix}. \tag{3.184}$$

The transformation of blade variables to multi-blade coordinates has the effect that the state equations can be written in a form that is only a weak function of ψ. The equations are evaluated at a number of values of ψ, and, subsequent to transformation, the matrices averaged. Stol *et al.* [25] have shown that this gives modal dynamics which are close approximations to that obtained by a more advanced Floquet (periodic-coefficient [15]) analysis.

The multi-blade transform is akin to the transformation of structural degrees-of-freedom into mode shapes, in the sense that physical quantities like an [*x y z*] vector are mapped to a set of generalized coordinates. Things which are expressed in physical coordinates, like mass, will appear in the transformed equations in the form

$$\mathbf{T}_B^{\psi}\left(\text{physical quantity or operation}\right)\mathbf{T}_{\psi}^{B}\mathbf{x}^{\psi}.$$

This can be interpreted as that the degrees-of-freedom in multi-blade coordinates are transformed to physical coordinates, fed into the operation conducted in physical coordinates, and then the result is transformed back to multi-blade coordinates.

The multi-blade transform converts between physical and multi-blade coordinates, which are in essence aligned with the rotorplane coordinate system. This in turn is aligned with the nacelle coordinate system, at an offset along the Z^n axis of $-L_d$.[2] The transform forms a "barrier" between the physical coordinates on each side. Thus quantities like airfoil forces on the blade (rotating) side are expressed first in pitch or hub coordinates, by the standard physical coordinate transformations, and then transformed to multi-blade coordinates for incorporation in the equations of motion. Any quantity that its associated with each blade has an analogue in multi-blade coordinates. This includes aerodynamic variables such as the angle-of-attack, lift and drag forces, and so forth.

Only some of the equations of motion – those associated with the blade degrees-of-freedom – are expressed in multi-blade coordinates. The remaining equations – those associated with the nonrotating degrees-of-freedom, plus the axisymmetric driveshaft – are expressed in physical coordinates.

The state equations transform as

$$\mathbf{T}_{Bx}^{\psi}\mathbf{L}\mathbf{T}_{\psi x}^{B}\frac{d\mathbf{x}^{\psi}}{dt}=\left(\mathbf{T}_{Bx}^{\psi}\mathbf{A}\mathbf{T}_{\psi x}^{B}-\Omega\mathbf{T}_{Bx}^{\psi}\mathbf{L}\frac{\partial\mathbf{T}_{\psi x}^{B}}{\partial\psi}\right)\mathbf{x}^{\psi}+\mathbf{T}_{Bx}^{\psi}\mathbf{B}\mathbf{T}_{\psi u}^{B}\mathbf{u}^{\psi}, \tag{3.185}$$

and the output equations

$$\mathbf{y}^{\psi}=\mathbf{T}_{By}^{\psi}\mathbf{C}\mathbf{T}_{\psi x}^{B}\mathbf{x}^{\psi}+\mathbf{T}_{By}^{\psi}\mathbf{D}\mathbf{T}_{\psi u}^{B}\mathbf{u}^{\psi}. \tag{3.186}$$

Here a distinction is made between the multi-blade transforms associated with the state (*x*), input (*u*), and output (*y*) vectors.

Equations 3.185 and 3.186 are not identical to the multi-blade transform of state-space described by Bir [3], also Johnson [15], who prefer to decompose the states as

$$\mathbf{x}=\begin{bmatrix}\mathbf{q}\\ \dot{\mathbf{q}}\end{bmatrix} \tag{3.187}$$

and then make the substitutions

$$\mathbf{q}=\mathbf{T}_{\psi q}^{B}\mathbf{q}^{\psi},$$

$$\frac{d\mathbf{q}}{dt}=\frac{d}{dt}\left(\mathbf{T}_{\psi q}^{B}\mathbf{q}^{\psi}\right)=\mathbf{T}_{\psi q}^{B}\frac{d\mathbf{q}^{\psi}}{dt}+\Omega\frac{d\mathbf{T}_{\psi q}^{B}}{d\psi}\mathbf{q}^{\psi},\quad\text{and} \tag{3.188}$$

$$\frac{d^2\mathbf{q}}{dt^2}=\mathbf{T}_{\psi q}^{B}\frac{d^2\mathbf{q}^{\psi}}{dt^2}+2\Omega\frac{\partial\mathbf{T}_{\psi q}^{B}}{\partial\psi}\frac{d\mathbf{q}^{\psi}}{dt}+\Omega^2\frac{\partial^2\mathbf{T}_{\psi q}^{B}}{\partial\psi^2}\mathbf{q}^{\psi}+\frac{d\Omega}{dt}\frac{\partial\mathbf{T}_{\psi q}^{B}}{\partial\psi}\mathbf{q}^{\psi},$$

giving for the state-space

[2] The rotorplane and nacelle coordinate systems are not exactly aligned due to elastic displacements and rotations of the driveshaft.

$$\begin{bmatrix} \mathbf{T}_{Bq}^{\psi} & \mathbf{0} \\ \mathbf{0} & \mathbf{T}_{Bq}^{\psi} \end{bmatrix} \mathbf{L} \begin{bmatrix} \mathbf{T}_{\psi q}^{B} & \mathbf{0} \\ \mathbf{0} & \mathbf{T}_{\psi q}^{B} \end{bmatrix} \frac{d}{dt} \begin{bmatrix} \mathbf{q}^{\psi} \\ \dot{\mathbf{q}}^{\psi} \end{bmatrix} =$$

$$\begin{bmatrix} \mathbf{T}_{Bq}^{\psi} & \mathbf{0} \\ \mathbf{0} & \mathbf{T}_{Bq}^{\psi} \end{bmatrix} \left\{ \mathbf{A} \begin{bmatrix} \mathbf{T}_{\psi q}^{B} & \mathbf{0} \\ \Omega \dfrac{\partial \mathbf{T}_{\psi q}^{B}}{\partial \psi} & \mathbf{T}_{\psi q}^{B} \end{bmatrix} - \mathbf{L} \begin{bmatrix} \Omega \dfrac{\partial \mathbf{T}_{\psi q}^{B}}{\partial \psi} & \mathbf{0} \\ \Omega^2 \dfrac{\partial^2 \mathbf{T}_{\psi q}^{B}}{\partial \psi^2} + \dfrac{d\Omega}{dt} \dfrac{\partial \mathbf{T}_{\psi q}^{B}}{\partial \psi} & 2\Omega \dfrac{\partial \mathbf{T}_{\psi q}^{B}}{\partial \psi} \end{bmatrix} \right\} \begin{bmatrix} \mathbf{q}^{\psi} \\ \dot{\mathbf{q}}^{\psi} \end{bmatrix} \qquad (3.189)$$

$$+ \begin{bmatrix} \mathbf{T}_{Bq}^{\psi} & \mathbf{0} \\ \mathbf{0} & \mathbf{T}_{Bq}^{\psi} \end{bmatrix} \mathbf{B} \mathbf{T}_{\psi u}^{B} \mathbf{u}^{\psi}.$$

Here the relationship

$$\frac{d}{dt} \mathbf{q}^{\psi} = \dot{\mathbf{q}}^{\psi}$$

is preserved.

Consider again the transformation of Equation 3.185. For the present illustration, which is not representative of the entire STAS state space, let the state vector be decomposed in the manner proposed by Bir,

$$\mathbf{x} = \begin{bmatrix} \mathbf{q} \\ \dot{\mathbf{q}} \end{bmatrix}.$$

However, the velocity variables are defined so that they transform as

$$\mathbf{v}^{\psi} = \mathbf{T}_{Bq}^{\psi} \frac{d\mathbf{q}}{dt}; \qquad \frac{d\mathbf{q}}{dt} = \mathbf{T}_{\psi q}^{B} \mathbf{v}^{\psi}, \qquad (3.190)$$

where $\mathbf{v}^{\psi}$ is used to emphasize that this is not the rate of change of $\mathbf{q}^{\psi}$; rather, it represents the velocities of the blade degrees-of-freedom, expressed in multi-blade coordinates. Equation 3.185, if the state vector is decomposed in this manner, gives

$$\begin{bmatrix} \mathbf{T}_{Bq}^{\psi} & \mathbf{0} \\ \mathbf{0} & \mathbf{T}_{Bq}^{\psi} \end{bmatrix} \mathbf{L} \begin{bmatrix} \mathbf{T}_{\psi q}^{B} & \mathbf{0} \\ \mathbf{0} & \mathbf{T}_{\psi q}^{B} \end{bmatrix} \frac{d}{dt} \begin{bmatrix} \mathbf{q}^{\psi} \\ \mathbf{v}^{\psi} \end{bmatrix} =$$

$$\begin{bmatrix} \mathbf{T}_{Bq}^{\psi} & \mathbf{0} \\ \mathbf{0} & \mathbf{T}_{Bq}^{\psi} \end{bmatrix} \left\{ \mathbf{A} \begin{bmatrix} \mathbf{T}_{\psi q}^{B} & \mathbf{0} \\ \mathbf{0} & \mathbf{T}_{\psi q}^{B} \end{bmatrix} - \Omega \mathbf{L} \begin{bmatrix} \dfrac{d\mathbf{T}_{\psi q}^{B}}{d\psi} & \mathbf{0} \\ \mathbf{0} & \dfrac{d\mathbf{T}_{\psi q}^{B}}{d\psi} \end{bmatrix} \right\} \begin{bmatrix} \mathbf{q}^{\psi} \\ \mathbf{v}^{\psi} \end{bmatrix} \qquad (3.191)$$

$$+ \begin{bmatrix} \mathbf{T}_{Bq}^{\psi} & \mathbf{0} \\ \mathbf{0} & \mathbf{T}_{Bq}^{\psi} \end{bmatrix} \mathbf{B} \mathbf{T}_{\psi u}^{B} \mathbf{u}^{\psi}.$$

Either Equation 3.189 or Equation 3.191 is a valid transformation of the state space. STAS implements Equation 3.191: it makes the transformations to and from multi-blade coordinates simpler. The full state-space of a wind turbine contains a variety of states, inputs, and outputs associated with the blades: forces, turbulence, induced velocities, pitch actuator commands, and so on. It is desireable from a practical standpoint to be able to transform these in one consistent operation, on the global state-space.

The distinction between Equations 3.189 and 3.191 may be illustrated with a trivial example. Let the deflection of a particular triplet of blade degrees-of-freedom vary about the azimuth as

$$\begin{bmatrix} q_1 \\ q_2 \\ q_3 \end{bmatrix} = \begin{bmatrix} \cos\psi \\ \cos(\psi + 2\pi/3) \\ \cos(\psi + 4\pi/3) \end{bmatrix}, \tag{3.192}$$

such that the velocities are

$$\frac{d}{dt}\begin{bmatrix} q_1 \\ q_2 \\ q_3 \end{bmatrix} = \Omega \begin{bmatrix} -\sin\psi \\ -\sin(\psi + 2\pi/3) \\ -\sin(\psi + 4\pi/3) \end{bmatrix}. \tag{3.193}$$

Transforming the deflections gives, for either method,

$$\begin{bmatrix} q_0 \\ q_c \\ q_s \end{bmatrix} = \begin{bmatrix} \frac{1}{3} & \frac{1}{3} & \frac{1}{3} \\ \frac{2}{3}\cos\psi & \frac{2}{3}\cos(\psi + 2\pi/3) & \frac{2}{3}\cos(\psi + 4\pi/3) \\ \frac{2}{3}\sin\psi & \frac{2}{3}\sin(\psi + 2\pi/3) & \frac{2}{3}\sin(\psi + 4\pi/3) \end{bmatrix} \begin{bmatrix} \cos\psi \\ \cos(\psi + 2\pi/3) \\ \cos(\psi + 4\pi/3) \end{bmatrix} = \begin{bmatrix} 0 \\ 1 \\ 0 \end{bmatrix}. \tag{3.194}$$

It is clear that the time derivative of the multi-blade coordinate transformed deflections is zero; and indeed, Bir and Johnson's definition of the transformed velocity gives

$$\begin{aligned} \frac{d}{dt}\begin{bmatrix} q_0 \\ q_c \\ q_s \end{bmatrix} &= \Omega \begin{bmatrix} 0 & 0 & 0 \\ -\frac{2}{3}\sin\psi & -\frac{2}{3}\sin(\psi + 2\pi/3) & -\frac{2}{3}\sin(\psi + 4\pi/3) \\ \frac{2}{3}\cos\psi & \frac{2}{3}\cos(\psi + 2\pi/3) & \frac{2}{3}\cos(\psi + 4\pi/3) \end{bmatrix} \begin{bmatrix} \cos\psi \\ \cos(\psi + 2\pi/3) \\ \cos(\psi + 4\pi/3) \end{bmatrix} \\ &+ \Omega \begin{bmatrix} \frac{1}{3} & \frac{1}{3} & \frac{1}{3} \\ \frac{2}{3}\cos\psi & \frac{2}{3}\cos(\psi + 2\pi/3) & \frac{2}{3}\cos(\psi + 4\pi/3) \\ \frac{2}{3}\sin\psi & \frac{2}{3}\sin(\psi + 2\pi/3) & \frac{2}{3}\sin(\psi + 4\pi/3) \end{bmatrix} \begin{bmatrix} -\sin\psi \\ -\sin(\psi + 2\pi/3) \\ -\sin(\psi + 4\pi/3) \end{bmatrix} \\ &= \Omega \begin{bmatrix} 0 \\ 0 \\ 1-1 \end{bmatrix} = \begin{bmatrix} 0 \\ 0 \\ 0 \end{bmatrix}. \end{aligned} \tag{3.195}$$

The simpler definition of the transformed velocity gives

$$\begin{aligned} \mathbf{v}^{\psi} = \mathbf{T}_B^{\psi} \frac{d}{dt}\begin{bmatrix} q_1 \\ q_2 \\ q_3 \end{bmatrix} &= \Omega \begin{bmatrix} \frac{1}{3} & \frac{1}{3} & \frac{1}{3} \\ \frac{2}{3}\cos\psi & \frac{2}{3}\cos(\psi + 2\pi/3) & \frac{2}{3}\cos(\psi + 4\pi/3) \\ \frac{2}{3}\sin\psi & \frac{2}{3}\sin(\psi + 2\pi/3) & \frac{2}{3}\sin(\psi + 4\pi/3) \end{bmatrix} \begin{bmatrix} -\sin\psi \\ -\sin(\psi + 2\pi/3) \\ -\sin(\psi + 4\pi/3) \end{bmatrix} \\ &= \Omega \begin{bmatrix} 0 \\ 0 \\ -1 \end{bmatrix}. \end{aligned} \tag{3.196}$$

This is understood as the velocities, expressed in multi-blade coordinates; it is not the time derivative of the multi-blade coordinate deflections. The key point, however, is that Equation

3.185 also eliminates azimuth-dependence from the equations, and is thus also an effective means to make the state-space matrices time-invariant.

4 Manipulation and Solution of the State Equations

Equations 3.185 and 3.186 are combined with the aerodynamic state equations into a unified state space, in the form of Equation 1.3. This is thereafter reduced, via Equation 1.4, to the form of Equation 1.2. A complete list of states, inputs, and intermediate variables (considered to be outputs) is given in Section 1.5.

The coupling of the aerodynamic and structural equations is, on the one hand, by way of the aerodynamic forces on the blade degrees-of-freedom, and on the other hand, by the structural displacements and velocities of the blade elements, which are fed back to the aerodynamic equations.

Equation 1.2 can be solved in a variety of ways. For instance, in the time domain, the equations can be integrated numerically, or a solution can be written as [23]

$$\mathbf{x}(t) = \exp[\mathbf{L}^{-1}\mathbf{A}(t-t_0)]\,\mathbf{x}(t_0) + \int_{t_0}^{t} \exp[\mathbf{L}^{-1}\mathbf{A}(t-\tau)]\,\mathbf{L}^{-1}\mathbf{B}\,\mathbf{u}(\tau)\,d\tau\,. \tag{4.1}$$

In the frequency domain, stability and damping properties can be evalutated and transfer functions can be computed between quantities of interest.

4.1 Augmenting the State Space

The expansion of the state-space matrices to accommodate other functions, such as controls, is illustrated by two examples. First, an induction generator response is added to a wind turbine with a free driveshaft degree-of-freedom. This illustrates how to interface with the applied force entries in the **u** vector, and the procedure is applicable to other actuator loads, wave loads, and so forth. Next, a blade pitch controller is implemented, where the pitch angle degrees-of-freedom are driven directly. Rather than modelling the actuator forces, which would be identical to the case of the generator torque, directly driving degrees-of-freedom requires that the state matrices be restructured.

4.1.1 Generator Torque

In this example we wish to implement the relationship

$$T = K_g \Omega\,, \tag{4.2}$$

where T is the generator torque and K_g is a characteristic stiffness. The torque is defined such that a positive torque will tend to resist rotation of the driveshaft and rotor. A torque across the air gap is equivalent to a moment

$$(\mathbf{M}^d)_Z = -K_g \frac{d(\boldsymbol{\Theta}^d_{1,d/n})_Z}{dt} \tag{4.3}$$

applied to the driveshaft reference node, and the reaction

$$\mathbf{M}^y = \mathbf{T}^y_n \mathbf{T}^n_d \begin{bmatrix} 0 \\ 0 \\ K_g\, d(\boldsymbol{\Theta}^d_{1,d/n})_Z \,/ dt \end{bmatrix} \tag{4.4}$$

applied to the $(\boldsymbol{\theta}^y_{m/s})_Z$ nodal degree-of-freedom on the nacelle master node. The nacelle is not represented by nodal degrees-of-freedom, these having been transformed to a modal representation, however the conversion to modal coordinates is contained in the **B** matrix, derived from Equation 3.179.

Consider the vectors of nodal forces $\mathbf{F}^B$ and nodal velocities $d\mathbf{q}^B/dt$. By adding zeros, Equations 4.3 and 4.4 can be expanded to fill these vectors, taking the form of a new (or alternatively augmented) output equation

$$\mathbf{F}^B = \mathbf{C}\mathbf{x}, \tag{4.5}$$

where **C** then contains K_g and the transform matrices. The state equation is augmented by partitioning the columns of **B** as

$$\mathbf{L}\frac{d\mathbf{x}}{dt} = \mathbf{A}\mathbf{x} + \mathbf{B}_u\mathbf{u} + \mathbf{B}_y\mathbf{F}^B. \tag{4.6}$$

Equations 4.5 and 4.6 are reduced to the standard state-space form, by use of Equation 1.4. This results in redefined state matrices which include the effects of the generator torque response.

4.1.2 Direct Specification of Blade Pitch Angle

Suppose that one wishes to implement a simplified model of blade pitch control, such as that described by Jonkman *et al.* [16], which ignores the details of the actuator dynamics, and simply prescribes a blade pitch angle. This in effect reassigns the blade pitch degrees-of-freedom from states to inputs. The state equations can then be partitioned like

$$\begin{bmatrix}\mathbf{L}_{11} & \mathbf{L}_{12}\\ \mathbf{L}_{21} & \mathbf{L}_{22}\end{bmatrix}\frac{d}{dt}\begin{bmatrix}\mathbf{x}_1\\ \mathbf{u}_2\end{bmatrix} = \begin{bmatrix}\mathbf{A}_{11} & \mathbf{A}_{12}\\ \mathbf{A}_{21} & \mathbf{A}_{22}\end{bmatrix}\begin{bmatrix}\mathbf{x}_1\\ \mathbf{u}_2\end{bmatrix} + \begin{bmatrix}\mathbf{B}_1\\ \mathbf{B}_2\end{bmatrix}\mathbf{u}_1, \tag{4.7}$$

resulting in the modified state equation, for frequency-domain analysis, of

$$\mathbf{L}_{11}\frac{d\mathbf{x}_1}{dt} = \mathbf{A}_{11}\mathbf{x}_1 + \begin{bmatrix}\mathbf{B}_1 & \mathbf{A}_{12} - i\omega\mathbf{L}_{12}\end{bmatrix}\begin{bmatrix}\mathbf{u}_1\\ \mathbf{u}_2\end{bmatrix}. \tag{4.8}$$

(Time domain analysis would retain $d\mathbf{u}_2/dt$ as an additional input.) The output equation becomes

$$\mathbf{y} = \mathbf{C}_1\mathbf{x}_1 + \begin{bmatrix}\mathbf{D} & \mathbf{C}_2\end{bmatrix}\begin{bmatrix}\mathbf{u}_1\\ \mathbf{u}_2\end{bmatrix}. \tag{4.9}$$

With Equations 4.8 and 4.9 as a starting point, the control is implemented in the manner of Section 4.1.1, albeit with the prescribed pitch angles instead of forces.

4.2 Natural Modes, Damping, and Transfer Functions

To obtain frequency transfer functions, one can substitute

$$\mathbf{x} = \mathbf{x}_0\exp(i\omega t),\ \mathbf{y} = \mathbf{y}_0\exp(i\omega t), \text{ and } \mathbf{u} = \mathbf{u}_0\exp(i\omega t) \tag{4.10}$$

into Equation 1.2 to obtain

$$(i\omega\mathbf{L} - \mathbf{A})\mathbf{x}_0 = \mathbf{B}\mathbf{u}_0. \tag{4.11}$$

Selecting desired inputs by setting elements of $\mathbf{u}_0$ to one – or, in effect, picking columns of **B** – gives transfer functions between these inputs and the states

$$(i\omega\mathbf{L} - \mathbf{A})\mathbf{X}_0 = \mathbf{B}. \tag{4.12}$$

Here $\mathbf{X}_0$ is solved numerically as a system of linear equations; $(i\omega\mathbf{L} - \mathbf{A})$ is, in the present case, sparse, while its inverse is nearly full. Transfer functions between outputs and inputs follow from

$$\mathbf{Y}_0 = \mathbf{C}\mathbf{X}_0 + \mathbf{D}, \tag{4.13}$$

where, if only a subset of the transfer functions is desired, **Y**, **C**, and **D** may be reduced by picking rows, and **D** again reduced by picking the same columns as **B**.

Natural modes and damping ratios can be computed by setting the input to zero and solving Equation 4.11 as an eigenvalue problem

$$\mathbf{A}\mathbf{x}_0 = i\omega\mathbf{L}\mathbf{x}_0 . \tag{4.14}$$

5 Verification

Where possible, the simple functions in the STAS program have been double-checked and verified by hand. The more complex, higher-level calculations are verified by comparison against other programs.

5.1 Aerodynamics

The aerodynamic modules have been verified by comparison against the nonlinear quasi-steady BEM method, and nonlinear time-domain simulations using the FAST software [17].

5.1.1 Mean Aerodynamic Loads

The mean aerodynamic loads are computed by a script, called speedyBEM.m, implementing the quasi-steady blade-element momentum method. This script was derived from the Fortran subroutine speedyBEM.f90, which was implemented by Merz [20], and extensively validated. As an illustration, Table II compares the rotor power and thrust obtained from speedyBEM.m against the same values obtained from the BEM method in HAWCStab2, as reported by Bak *et al*. [2]. The agreement is not perfect, especially at high windspeeds. This is to be expected, as above the rated windspeed the aerodynamic loads are very sensitive to the blade pitch angle, and details of the airfoil modelling; a small change in the pitch angle brings the results in line. For instance, at 25 m/s, changing the pitch angle from the nominal 22.98° to 22.63° results in speedyBEM.m output of 10.66 MW power and 576 kN thrust.

Table II: A comparison of power and thrust obtained from two different BEM analyses.

V_∞ (m/s)	P (W)		F_T (N)	
	speedyBEM	Bak *et al*.	speedyBEM	Bak *et al*.
5	8.130E+05	7.991E+05	3.400E+05	3.515E+05
7	2.549E+06	2.506E+06	6.307E+05	6.434E+05
9	5.434E+06	5.312E+06	9.945E+05	1.009E+06
11	9.921E+06	9.698E+06	1.486E+06	1.507E+06
13	1.047E+07	1.065E+07	1.052E+06	1.082E+06
15	1.018E+07	1.068E+07	8.497E+05	8.908E+05
17	9.891E+06	1.064E+07	7.274E+05	7.740E+05
19	9.736E+06	1.065E+07	6.501E+05	6.984E+05
21	9.583E+06	1.064E+07	5.934E+05	6.421E+05
23	9.426E+06	1.064E+07	5.504E+05	5.998E+05
25	9.230E+06	1.064E+07	5.158E+05	5.672E+05

5.1.2 Fluctuating Aerodynamic Loads

The aerodynamic portion of the STAS linearized state equations was isolated, effectively making the structure rigid, and deactivating all control actions. The aerodynamic properties were defined based upon the DTU 10 MW Reference Wind Turbine [2]. Frequency transfer functions were computed by Equation 4.12; transfer functions were computed for the sensitivity of the axial and tangential aerodynamic forces, with respect to axial and tangential turbulence, at a radius of 80.8 m (where the blade tip is at a radius of 89.2 m). These are shown as solid lines in Figure 11, for mean windspeeds of 7, 11, 15, and 19 m/s. The turbine was given a rotational speed and blade pitch angle corresponding to the nominal operating schedule at each windspeed.

Using speedyBEM.m, the force/turbulence sensitivities were computed using a two-sided finite-difference scheme. The speedyBEM.m script performs a quasi-steady analysis, and thus represents the limit at zero frequency. The results are shown in Figure 11 as white dots, and agree with the linearized blade-element momentum equations at the zero-frequency limit.

In order to verify the linear model at higher frequencies, nonlinear time-domain simulations were performed using the FAST/AeroDyn program [17]. AeroDyn, the aerodynamics module, employs a quasi-steady blade-element momentum method at windspeeds below 8 m/s, and a generalized dynamic wake (also known as acceleration potential [5]) method at windspeeds above 8 m/s. This latter method solves for the pressure drop across the rotorplane, as a function of radial and azimuthal coordinates, based upon a linearization of the Euler equations of inviscid fluid flow; it is thus more advanced (though not necessarily more accurate) than the basic blade-element momentum analysis.

The FAST/Aerodyn simulations were run with a spatially-uniform, time-varying wind field input. The wind was given a sinusoidal fluctuation about a mean windspeed. The frequency of the oscillation was set to 0.005, 0.2, or 1.0 Hz. For each frequency, three simulations were run, with different amplitudes. The smallest amplitude was set to 1% of the mean windspeed, and represents a perturbation about the mean value. The next amplitude was set to 10% of the mean windspeed, which is in the vicinity of the standard deviation due to turbulence. Finally, the amplitude was set to 50% of the mean windspeed, which represents a severe gust, being more than three standard deviations above and below the mean.

The results indicate that the linearized state equations give a reasonable estimate of the fluctuation in aerodynamic forces, even for windspeeds which depart significantly from the point of linearization. An important caveat is that the comparisons in Figure 11 do not include pitch control actions, nor the elastic response of the structure.

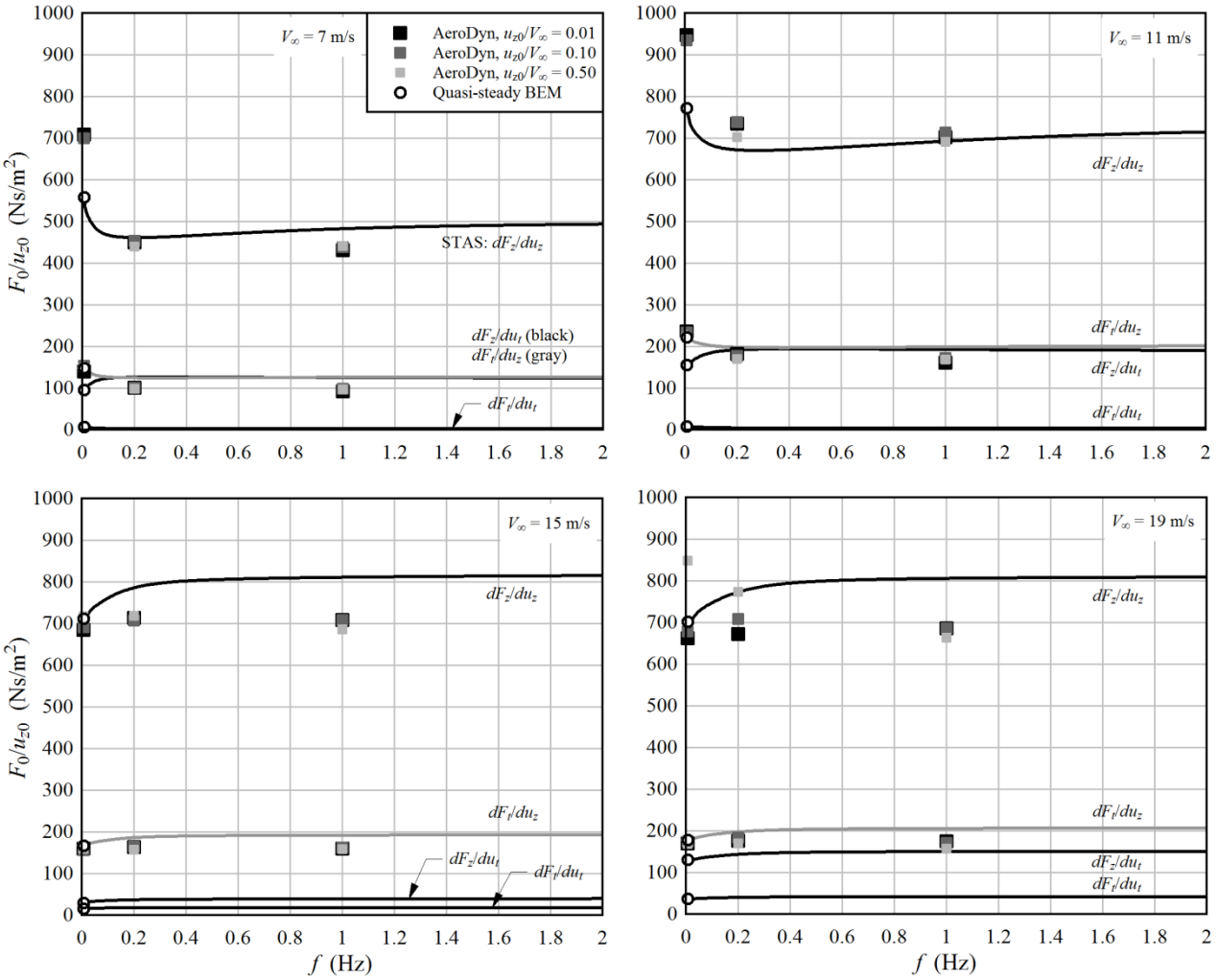

Figure 11: The magnitude of the sensitivity of aerodynamic forces (per unit spanwise length) with respect to sinusoidal fluctuations in the incoming axial and tangential components of the windspeed. Lines show the results for the linearized state space representation of the aerodynamics in the STAS program. These are compared with a nonlinear quasi-steady BEM calculation (speedyBEM.m) and, for the axial velocity component, nonlinear time-domain analyses using FAST/AeroDyn.

5.2 Structural Dynamics

The structural dynamic analysis has been verified by comparing with the Fedem finite element analysis program, as well as published results obtained with the FAST, Adams, and HAWCStab2 programs.

5.2.1 Parked Condition

A static analysis was conducted in order to compare the displacements obtained using the full set of degrees-of-freedom against those obtained with modal reduction. A force of 100 kN in the Z^p direction was applied to each of the three blades at the 6th node from the hub. The modal analysis employed 20 modes for the tower, 8 for the nacelle, 18 for the driveshaft/hub, and 20 for each blade. The full model had 575 degrees-of-freedom, while the reduced model had 100. Displacements were observed to be nearly identical.

Natural frequencies obtained with the present analysis were compared with those from the Fedem finite-element analysis program, for the DTU 10 MW wind turbine, and from Jonkman *et al.* [16], for the NREL 5 MW wind turbine. The results are shown in Table III and Table IV. A

brief description of each mode is given; the higher modes become more complicated and difficult to identify.

In Table III, the Fedem and STAS models were nominally of the same turbine geometry, to the extent that this is specified by Bak *et al.* [2]. The specification of the foundation was also the same. However, the models were created independently by different analysts, and no effort was made to equalize them, for example, by using an identical element distribution. It is suspected that some of the details of modelling, especially of the driveshaft, monopile, and seabed properties, are responsible for the observed differences. The same can be said for the comparison in Table IV. Overall, the results indicate that there are no gross errors in the structural portion of the model.

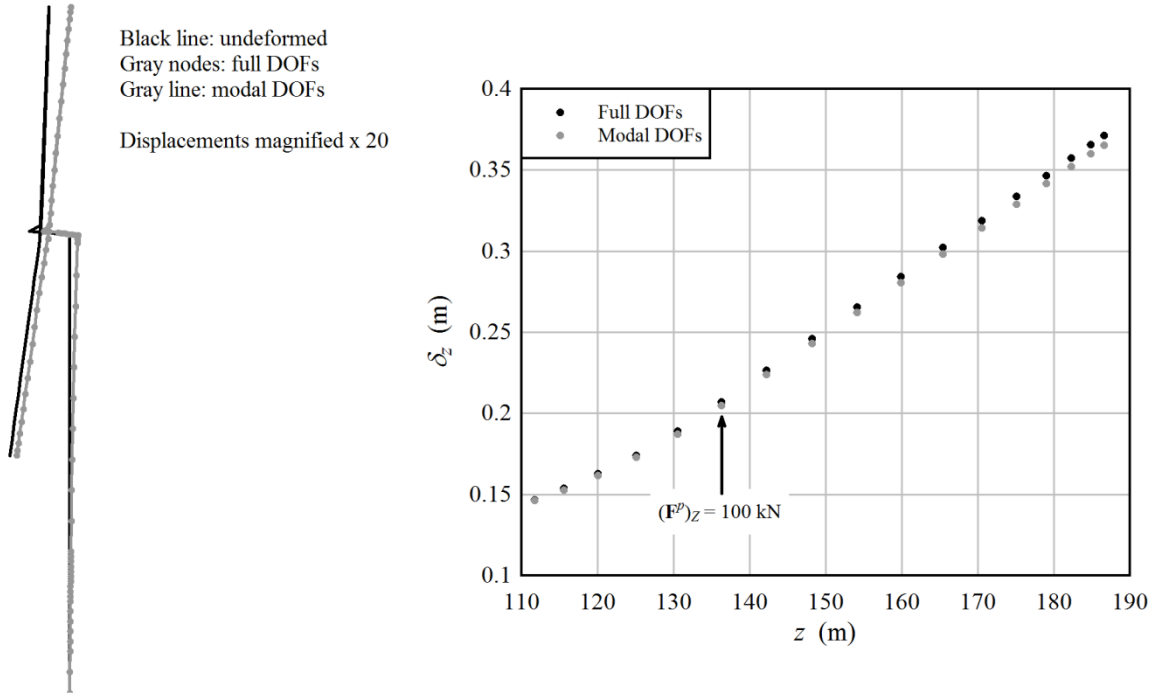

Figure 12: A comparison of full and reduced models under static thrust loading of the rotor. At left: the (exaggerated) displaced shape relative to the undeformed position, looking at the turbine from the side. At right: a plot of blade 2 flapwise displacements (relative to the global coordinate system, and with blade pitch set to zero) versus z^g coordinate; the location of the applied load is shown.

Table III: A comparion of natural frequencies obtained with the present program, with full and reduced degrees-of-freedom, with those from the Fedem finite element program. Results for Fedem and the present analysis were obtained for the DTU 10 MW wind turbine, installed atop an offshore monopile foundation in 30 m water depth. Selected

frequencies, published by DTU for a land-based turbine, are also shown. Fedem results courtesy of L. Eliassen, NTNU.

	f (Hz)				
	Fedem	DTU	Full DOFs	Modal DOFs	Description
1	0.212		0.237	0.237	1st tower side-to-side
2	0.212		0.238	0.238	1st tower fore-aft
3		0.502	0.504	0.505	1st driveshaft torsion
4	0.582	0.547	0.562	0.562	1st rotor flapwise yaw
5	0.604	0.590	0.584	0.584	1st rotor flapwise tilt
6	0.634	0.634	0.632	0.632	1st rotor collective flapwise
7	0.952	0.922	0.909	0.909	1st rotor asymmetric edgewise 1
8	0.962	0.936	0.913	0.913	1st rotor asymmetric edgewise 2
9	1.003		0.959	0.959	2nd tower fore-aft/rotor tilt
10	1.077		0.989	0.988	2nd tower side-to-side
11	1.519	1.376	1.477	1.477	2nd rotor flapwise yaw
12	1.730	1.550	1.615	1.615	2nd rotor flapwise tilt
13	1.820	1.763	1.810	1.810	2nd rotor collective flapwise
14	2.337		2.068	2.068	Rotor edgewise
15	2.605		2.538	2.540	Rotor flapwise
16	2.734		2.590	2.592	Rotor flapwise/edgewise
17	2.961		2.875	2.879	3rd rotor asymmetric edgewise
18	3.016		2.897	2.900	Rotor flapwise/edgewise
19	3.060		3.006	3.008	3rd rotor flapwise tilt
20	3.665		3.328	3.368	3rd tower fore-aft/rotor flapwise

Table IV: A comparison of natural frequencies obtained with the present program against those published by Jonkman *et al*. [16] for the NREL 5 MW wind turbine.

	f (Hz)			
	FAST	ADAMS	(Present)	Description
1	0.324	0.319	0.304	1st tower fore-aft
2	0.312	0.316	0.301	1st tower side-to-side
3	0.621	0.609	0.617	1st driveshaft torsion
4	0.666	0.630	0.643	1st rotor flapwise yaw
5	0.668	0.669	0.675	1st rotor flapwise tilt
6	0.699	0.702	0.723	1st rotor collective flapwise
7	1.079	1.074	1.112	1st rotor asymmetric edgewise 1
8	1.090	1.088	1.128	1st rotor asymmetric edgewise 2
9	1.934	1.651	1.736	2nd rotor flapwise yaw
10	1.922	1.856	1.857	2nd rotor flapwise tilt
11	2.021	1.960	2.052	2nd rotor collective flapwise
12	2.900	2.859	2.721	2nd tower fore-aft/rotor tilt
13	2.936	2.941	2.703	2nd tower side-to-side/rotor edgewise

5.2.2 Operating Conditions

Analysis under operating conditions includes the coupling between aerodynamic and structural loads, as well as the multi-blade coordinate transformation, and is therefore far more demanding than analysis under parked conditions.

Table V lists the natural frequencies and damping ratios of the NREL 5 MW wind turbine, when rotating at its operating speed, at a windspeed of 19 m/s. The values are open-loop, including no generator torque or blade pitch response. The windspeed of 19 m/s was chosen as this is directly between the operating conditions for which Stol [25] and Sønderby [26] reported natural frequencies and damping ratios.

Table V: A comparison of natural frequencies and damping ratios while operating at a high windspeed. Results are shown with and without the gyroscopic and centrifugal terms in the equations of motion. The calculations are performed "open-loop", that is, with no control system, a free driveshaft, and locked pitch and yaw bearings. The damping of driveshaft torsion is low, as the present model does not consider the rather high damping associated with a geared drivetrain; in reality this mode will be even more highly damped by the generator torque. (*) The specification of the NREL 5 MW turbine does not include the bending properties of the driveshaft. The present driveshaft was given reasonable dimensions, but these should not be interpreted as final values for the driveshaft modes.

	f (Hz)				ζ				
	Sønderby (20 m/s)	Stol (18 m/s)	(Present) (19 m/s)	No $\mathbf{G}c, \mathbf{G}k$ (19 m/s)	Sønderby	Stol	(Present)	No $\mathbf{G}c, \mathbf{G}k$	Description
1	0.320	0.320	0.308	0.307	0.006	0.006	0.010	0.008	Tower side-to-side
2	0.330	0.330	0.312	0.312	0.080	0.081	0.099	0.101	Tower fore-aft
3	0.630	0.290	0.798	0.804	0.800	0.873	0.825	0.824	1st rotor flapwise regressive
4	0.800	0.880	0.908	0.925	0.006	0.013	0.013	0.012	1st rotor edgewise regressive
5	0.840	0.520	1.001	1.003	0.714	0.702	0.761	0.761	1st rotor flapwise collective
6	1.010	0.700	1.202	1.189	0.652	0.607	0.693	0.694	1st rotor flapwise progressive
7	1.200	1.150	1.284	1.303	0.008	0.009	0.015	0.012	1st rotor edgewise progressive
8	1.530	1.720	1.678	1.668	0.217	0.217	0.267	0.260	2nd rotor flapwise regressive
9	1.620	1.680	1.710	1.721	0.031	0.025	0.007	0.006	First driveshaft torsion (free-free)
10	1.940	2.120	1.939	1.986	0.163	0.174	0.203	0.222	2nd rotor flapwise progressive
11	1.930	2.000	2.086	2.086	0.166	0.178	0.212	0.212	2nd rotor flapwise collective
12			2.216	2.222			0.048	0.048	Driveshaft bending (*)
13			2.217	2.222			0.048	0.048	Driveshaft bending (*)
14	2.620	2.890	2.711	2.709	0.021	0.019	0.039	0.022	2nd tower fore-aft
15	2.850	2.940	2.729	2.737	0.006	0.012	0.019	0.026	2nd tower side-to-side
16	2.730		3.222	3.230	0.039		0.019	0.018	2nd driveshaft torsion
17	2.750	6.080	3.676	3.700	0.037	0.045	0.038	0.036	1st tower yaw

It is observed that the centrifugal and gyroscopic terms make little contribution to the response. (The effects of centrifugal stiffening are included in both cases.)

Figure 13 shows the open-loop transfer function between the collective rotor-average windspeed and the driveshaft rotational speed. This was obtained by setting the collective amplitudes (in multi-blade coordinates) of u_z velocity inputs to 1, at all the blade elements. Two sets of results were generated: one using the baseline structural damping expected for a gearless drivetrain, and the other using a weak induction-generator-type reaction of the driveshaft torsion, to match the damping of the first torsional mode assumed by Sønderby [26]. The equivalent transfer function obtained by Sønderby, using the HAWCStab2 program, is also shown. The transfer function matches closely in the range between 0.25 Hz and 1.75 Hz. Above this frequency, the results diverge due to differences in the driveshaft model, as evident in the different frequencies obtained for the second driveshaft torsional mode. (The specification of the NREL 5 MW turbine, Jonkman *et al*. [16], does not include the driveshaft design, so it is not surprising that different modelling assumptions were made.) Differences in the low-frequency response approaching 0 Hz are also evident. The reason for the discrepancy at low frequencies is not known; it was found not to be related to the model of dynamic inflow, nor is it related to the gyroscopic or centrifugal terms. It is noted that a linear model might not give meaningful results for the open-loop response of a rotor to low-frequency fluctuations in the wind, which could lead to large variations in speed. In reality, the generator torque response would govern the dynamics at low frequencies.

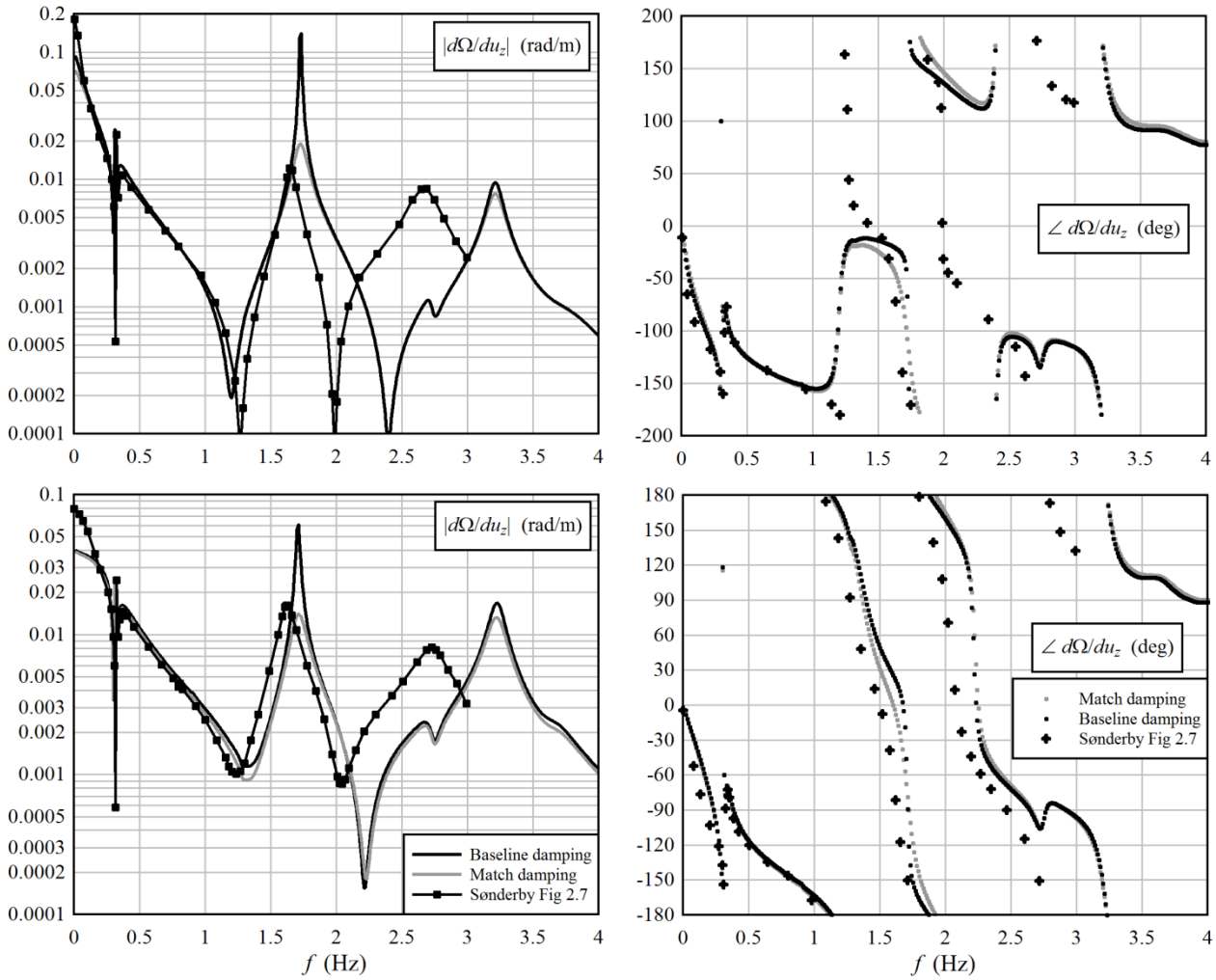

Figure 13: The open-loop transfer function between collective rotor-average windspeed and driveshaft speed, compared with values from the HAWCStab2 program, published by Sønderby [26]. Upper row: windspeed of 14 m/s, lower row: windspeed of 20 m/s. NREL 5 MW turbine. Results are shown for the baseline damping, representative of a direct-drive generator, and a damping value which approximates that used by Sønderby for the first drivetrain torsion mode.

6 Conclusions

A set of Matlab/Octave scripts have been developed, which output the state matrices describing a linear aeroelastic model of an offshore wind turbine. The model is open-loop; controls, actuator models, and environmental loads can be added by augmenting the given matrices.

The model has been verified by comparing natural frequencies, damping ratios, and frequency transfer functions against results obtained from other programs. It appears to give adequate results for the design and analysis of control systems for offshore wind turbines. The model is intended to be incorporated into the STAS wind power plant analysis program, as the basis for evaluating the turbines' dynamic response under actions of the local and supervisory control systems.

In future work, the model could be improved in several ways. To increase the speed of computation, the aerodynamic modes could be reduced, following Sønderby [26]. Center-of-gravity and shear-center effects could be accounted for in the blade element cross-sections, which would allow the model to be used to predict flutter instability. The present model is fully linear; if combined with a nonlinear quasi-static solution, the model could be linearized about the deformed

position of the turbine structures. There is a need to develop a version of the multi-blade coordinate transform that can account for a first-order perturbation or a stochastic fluctuation in the rotational speed. The response at low frequencies should be verified against nonlinear time-domain simulations. Finally, the computation of the $\mathbf{G}_c$ and $\mathbf{G}_k$ terms should be revisited, as it was observed that many of these evaluate to zero, and thus could be eliminated from the computation.

References

[1] Ackermann T (editor). *Wind Power in Power Systems*. Second Edition, Wiley, 2012.

[2] Bak C, *et al*. Description of the DTU 10 MW Reference Wind Turbine. DTU Wind Energy Report-I-0092, Technical University of Denmark, 2013.

[3] Bir G. Multiblade coordinate transformation and its application to wind turbine analysis. Paper NREL/CP-500-42553, National Renewable Energy Laboratory, 2008. Presented at the ASME Wind Energy Symposium, Reno, NV, USA, January 7-10, 2008.

[4] Blevins RD. *Flow-Induced Vibration*. Second Edition, Van Nostrand Reinhold, 1990.

[5] Burton T, *et al*. *Wind Energy Handbook*. Wiley, 2001.

[6] Coleman RP, Feingold AM. Theory of self-excited mechanical oscillations of helicopter rotors with hinged blades. Report NACA-TR-1351, National Advisory Committee for Aeronautics, 1958.

[7] Cook RD, *et al*. *Concepts and Applications of Finite Element Analysis*. Third Edition, Wiley, 1989.

[8] Craig Jr. RR, Bampton MCC. Coupling of substructures for dynamic analyses. AIAA Journal 6 (1968) 1313-1319.

[9] Ellis A, *et al*. A Generic Wind Power Plant Model. Chapter 35 of [1].

[10] Hansen MH. Improved modal dynamics of wind turbines to avoid stall-induced vibrations. Wind Energy 6 (2003) 179-195.

[11] Hansen MH. Aeroelastic stability analysis of wind turbines using an eigenvalue approach. Wind Energy 7 (2004) 133-143.

[12] Hansen MH, *et al*. A Beddoes-Leishman type dynamic stall model in state-space and indicial formulations. Report Risø-R-1354(EN), Risø National Laboratory (DTU), Denmark, 2004.

[13] Hansen MH, Henriksen LC. Basic DTU Wind Energy Controller. Report DTU Wind Energy E-0028, Technical University of Denmark, 2013.

[14] Hansen MOL. *Aerodynamics of Wind Turbines*. Second Edition, Earthscan, 2008.

[15] Johnson W. *Helicopter Theory*. Dover, 1994.

[16] Jonkman JM, *et al*. Definition of a 5-MW Reference Wind Turbine for Offshore System Development. Report NREL/TP-500-38060, National Renewable Energy Laboratory, 2009.

[17] Jonkman JM, Buhl Jr. ML. FAST User's Guide. Report NREL/EL-500-38230, National Renewable Energy Laboratory, 2005.

[18] Leishman JG. Challenges in modelling the unsteady aerodynamics of wind turbines. Wind Energy 5 (2002) 85-132.

[19] Leithead W, Connor B. Control of variable speed wind turbines: dynamic models. International Journal of Control 73 (2000) 1173-1188.

[20] Merz KO. *Conceptual design of a stall-regulated rotor for a deepwater offshore wind turbine*. Doctoral theses at NTNU, 2011:191, Norwegian University of Science and Technology, 2011.

[21] Merz KO. Rapid optimization of stall-regulated wind turbine blades using a frequency-domain method: Part 1, loads analysis. Wind Energy (2014).

[22] Øye S. Dynamic stall, simulated as a time lag of separation. McAnulty KF (editor), Proceedings of the Fourth IEA Symposium on the Aerodynamics of Wind Turbines, ETSU-N-118, 1991.

[23] Schultz DG, Melsa JL. *State Functions and Linear Control Systems*. McGraw-Hill, 1967.

[24] Shabana AA. *Dynamics of Multibody Systems*. Fourth Edition, Cambridge University Press, 2013.
[25] Stol KA, *et al*. A comparison of multi-blade coordinates transformation and direct periodic techniques for wind turbine control design. AIAA 2009-479, 47th AIAA Aerospace Sciences Meeting, Orlando, FL, USA, January 5-8, 2009.
[26] Sønderby IB. *Low-order aeroelastic models of wind turbines for controller design*. PhD Thesis, Technical University of Denmark, 2013.
[27] Sønderby I, Hansen MH. Open-loop frequency response analysis of a wind turbine using a high-order linear aeroelastic model. Wind Energy 17 (2014) 1147-1167.
[28] Sørensen P. Frequency domain modelling of wind turbine structures. Report Risø-R-749(EN), Risø National Laboratory (DTU), Denmark, 1994.
[29] Sørensen P, *et al*. A complex frequency domain model of wind turbine structures. Journal of Solar Energy Engineering 117 (1995) 311-317.
[30] van Engelen TG, Braam H. TURBU Offshore, Computer Program for Frequency Domain Analysis of Horizontal Axis Offshore Wind Turbines. Report ECN-C--04-079, Energy Research Centre of the Netherlands, 2004.
[31] Young JT (editor). Primer on the Craig-Bampton Method. http://femci.gsfc.nasa.gov , 2000. (Accessed October 2014.)

Technology for a better society

www.sintef.no